LIBRARY
TECHNICAL REPORT SECTION
NAVAL POSTGRADUATE SCHOOL
MONTEREY, CALIFORNIA 93940

NPS-52MV70091A

UNITED STATES
NAVAL POSTGRADUATE SCHOOL

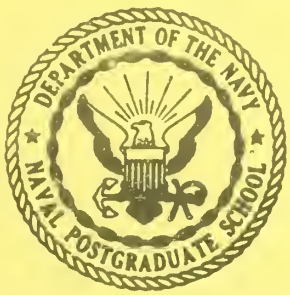

THEORY AND PERFORMANCE OF A MATCHED-FILTER DOPPLER DIRECTION-FINDING SYSTEM

by

Henry Orejuela

and

Glen A. Myers

September 1970

This document has been approved for public release and sale; its distribution is unlimited.

FEDDOCS
D 208.14/2:NPS-52MV70091A

NAVAL POSTGRADUATE SCHOOL
Monterey, California

Rear Admiral R. W. McNitt, USN
Superintendent

Milton Clauser
Academic Dean

ABSTRACT:

A new radio direction-finding (DF) technique which applies matched-filter theory to the DF problem is presented. The new technique, called Matched-Filter Doppler Direction Finding (MFD DF) is based on the doppler DF principle in which a rotating antenna, or its equivalent, superimposes periodic frequency modulation on the received carrier. The phase of the induced modulation contains information on the angle of arrival. It is shown that a bandpass filtering operation, which satisfies the phase-matching requirement of a matched filter, converts the frequency-modulated signal to an amplitude-modulated signal whose envelope is a periodic narrow pulse with no sidelobes. The relative time of occurrence of the pulse is a measure of angle of arrival.

Included is the description of and results obtained with an experimental system used to confirm the analytical results, to study the effects of noise, and to explore alternatives available in the design of an operating system. Encouraging results were obtained using this same experimental system with a conventional operating doppler DF set.

This task was supported by: Naval Ship Systems Command (Code 6050)

ABSTRACT

A new radio direction-finding (DF) technique which applies matched-filter theory to the DF problem is presented. The new technique, called Matched-Filter Doppler Direction Finding (MFD DF) is based on the doppler DF principle in which a rotating antenna, or its equivalent, superimposes periodic frequency modulation on the received carrier. The phase of the induced modulation contains information on the angle of arrival. It is shown that a bandpass filtering operation, which satisfies the phase-matching requirement of a matched filter, converts the frequency-modulated signal to an amplitude-modulated signal whose envelope is a periodic narrow pulse with no side-lobes. The relative time of occurrence of the pulse is a measure of angle of arrival.

Included is the description of and results obtained with an experimental system used to confirm the analytical results, to study the effects of noise, and to explore alternatives available in the design of an operating system. Encouraging results were obtained using this same experimental system with a conventional operating doppler DF set.

TABLE OF CONTENTS

I. INTRODUCTION ---------- 17

A. BACKGROUND ---------- 17

B. CONTENTS AND SUMMARY ---------- 19

C. PLAN OF THE REPORT ---------- 24

II. THE MATCHED-FILTER DOPPLER DF TECHNIQUE ------- 26

A. THE DOPPLER DF PRINCIPLE ---------- 26

B. CONVENTIONAL DOPPLER DF SYSTEMS ---------- 28

C. THE MATCHED-FILTER DOPPLER DF SYSTEM ------ 30

1. Matched-Filter Concepts ---------- 30

2. Spectral Representation of FM by a Sinusoid ---------- 31

3. Determining Angle of Arrival ---------- 38

4. Dependence of DF Accuracy on System Parameters ---------- 47

5. Increased β by Frequency Multiplication ---------- 55

III. RADIO DIRECTION FINDING WITH ROTATING ANTENNAS ---------- 58

A. THEORY OF ROTATING ANTENNAS ---------- 59

1. Basic Formulation ---------- 59

2. Fourier Transform Representation ------ 61

3. Time Domain Processing ---------- 67

4. Conversion of ζ frequencies to Real Frequencies ---------- 70

B. ONE ROTATING ELEMENT ---------- 71

IV. HARDWARE SIMULATION AND PERFORMANCE OF A MATCHED-FILTER DOPPLER DF SYSTEM ---------- 75

A. SYSTEM DESCRIPTION ---------- 75

B. CONFIRMATION OF THEORY ---------- 78

1. Processing Without Frequency Multiplication ---------- 78

2. Spectral Symmetry ---------- 83

3. Processing With Frequency Multiplication ---------- 85

C. IMPERFECT FILTERING EFFECTS ---------- 87

D. NOISE EFFECTS ---------- 96

1. Equipment ---------- 101

2. Processing Without Frequency Multiplication ---------- 104

3. Processing With Frequency Multiplication ---------- 127

E. EXPERIMENT USING A CONVENTIONAL DOPPLER DF SYSTEM ---------- 145

1. Description of Equipment ---------- 145

2. Results ---------- 146

V. THE TWO SIGNAL CASE ---------- 157

A. THEORY ---------- 157

B. RESOLUTION ---------- 164

C. INFLUENCE OF ELEVATION ANGLE ---------- 165

VI. SUMMARY AND RECOMMENDATIONS ---------- 170

A. SUMMARY ---------- 170

B. RECOMMENDATIONS ---------- 173

APPENDIX A: COMPUTATION OF THE RESPONSE OF AN IDEAL MATCHED-FILTER DOPPLER DF SYSTEM ---------- 174

APPENDIX B: COMPUTATION OF IDEAL MFD DF SYSTEM TWO-SIGNAL RESPONSE ---------- 176

APPENDIX C: MODIFICATION OF MFD DF TO PROCESS MODULATED SIGNALS ---------- 179

LIST OF REFERENCES ---------- 181

INITIAL DISTRIBUTION LIST ---------- 183

FORM DD 1473 ---------- 185

LIST OF TABLES

I. Effect of Noise on the Performance of a Matched Filter Doppler DF System ---------- 109

II. Effect of Noise on the Performance of a Matched Filter Doppler DF System ---------- 116

III. Effect of Noise on the Performance of a Matched Filter Doppler DF System ---------- 122

IV. Effect of Noise on the Performance of a Matched Filter Doppler DF System ---------- 132

V. Effect of Noise on the Performance of a Matched Filter Doppler DF System ---------- 137

VI. Effect of Noise on the Performance of a Matched Filter Doppler DF System ---------- 141

VII. Performance of an Experimental MFD DF System used with a Conventional Doppler DF Set ---------- 147

LIST OF DRAWINGS

1. Photograph of the Typical Output of a MFD DF System ---------- 19

2. Block Diagram of a MFD DF System ---------- 23

3. Plan View of a Rotating Antenna Element ---------- 27

4. Block Diagram of a Conventional Doppler DF System ---------- 29

5. Spectrum of FM by a Sinusoid when $\beta = 25$ ---------- 33

6. Spectrum of FM by a Sinusoid when $\beta = 25$ ---------- 37

7. Envelope of One Cycle of the Periodic Output of a Filter Matched to a Carrier FM by a Sinusoid ---------- 39

8. Spectrum of FM by a Sinusoid Showing the In-phase Group of Interest ---------- 41

9. Envelope of the Isolated In-phase Group of Frequency Components Shown in Fig. 8 ---------- 43

10. Computed Envelope of an Equal-amplitude, In-phase Frequency Group ---------- 45

11. Phasor Diagrams ---------- 46

12. Spectra of FM by a Sinusoid ---------- 49

13. Computed Envelopes of the Output of an Ideal MFD DF System as β Increases ---------- 50

14. Output of the Experimental MFD DF System when $\beta = 100$ ---------- 54

15. Graph of the 3-dB Pulse Width and the Number of Significant Components in the In-phase Group vs β ---------- 56

16. One-dimensional Aperture and Related Geometry ---------- 62

17. Block Diagram of a Frequency-processing Receiving System ---------- 68

18. Plan View of the Rotatable Element ---------- 72

19. Block Diagram of the Experimental MFD DF System ---------- 76

20. Circuit Diagram of the Frequency Doubler --------- 77

21. Amplitude- and Phase-vs-Frequency Characteristics of the 10-kHz Ceramic Bandpass Filter ---------- 79

22. Amplitude- and Phase-vs-Frequency Characteristics of the 4-kHz Ceramic Bandpass Filter ---------- 80

23. Photographs of the Response of the Experimental MFD DF System ---------- 82

24. Computed Envelope of the Response of an Ideal MFD DF System ---------- 81

25. Photographs of the Response of the Experimental MFD DF System as β Increases ------ 84

26. Photograph of the Response of the Experimental MFD DF System to the In-phase Group of Frequency Components Below the Carrier Frequency ---------- 85

27. Photograph of the Response of the Experimental MFD DF System which Includes Frequency Multiplication by a Factor of Four ---------- 86

28. Partial Spectrum of FM by a Sinusoid ---------- 89

29. Computed Envelope of the Response of an Ideal MFD DF System ---------- 88

30. Theoretical Response of a MFD DF System as Undesired Frequency Components are Processed ---------- 90

31. Response of the Experimental MFD DF System as Undesired Frequency Components are Processed ---------- 93

32. Response of the Experimental MFD DF System as Undesired Frequency Components are Processed ---------- 94

33. Response of the Experimental MFD DF System as Undesired Frequency Components are Processed ---------- 95

34. Theoretical Response of a MFD DF System as Some Desired Frequency Components are Not Processed ---------- 97

35. Response of the Experimental MFD DF System as Desired Frequency Components are not Processed ---------- 98

36. Response of the Experimental MFD DF System as Desired Frequency Components are not Processed ---------- 99

37. Response of the Experimental MFD DF System as Desired Frequency Components are not Processed ---------- 100

38. Block Diagram of the Experimental MFD DF System used to Study Noise Effects ---------- 102

39. Amplitude-vs-Frequency Characteristics of Bandpass Noise Filters ---------- 103

40. Graph of the SNR Improvement I_1 vs β ---------- 105

41. Graph of the SNR Improvement I_2 vs β ---------- 107

42. Photographs of the Response of the Experimental MFD DF System for Various Values of Input SNR ---------- 110

43. Photographs of the Response of the Experimental MFD DF System for Various Values of Input SNR ---------- 117

44. Photographs of the Response of the Experimental MFD DF System for Various Values of Input SNR ---------- 123

45. Photographs of the Response of the Experimental MFD DF System for Various Values of Input SNR ---------- 133

46. Photographs of the Response of the Experimental MFD DF System for Various Values of Input SNR ---------- 138

47. Photographs of the Response of the Experimental MFD DF System for Various Values of Input SNR ---------- 142

48. Block Diagram of the Experimental MFD DF System Interfaced with a Conventional Doppler DF System ---------- 148

49. Photographs of the Response of the MFD-AN/TRD-15 DF System ---------- 150

50. Photographs of the Response of the MFD-AN/TRD-15 DF System ---------- 151

51. Photograph of the Envelope of the Response of the MFD-AN/TRD-15 DF System ---------- 152

52. Photographs of the Envelope of the Response of the MFD-AN/TRD-15 DF System ---------- 153

53. Photographs of the Envelope of the Response of the MFD-AN/TRD-15 DF System ---------- 155

54. Plan View of a Rotating Antenna Element Showing the Reception of Two Like-Frequency Simultaneous Signals ---------- 158

55. Computed Envelope of the Response of an Ideal MFD DF System to Two Simultaneous Signals ---------- 159

56. Computed Envelopes of the Response of an Ideal MFD DF System to Two Simultaneous Signals ---------- 161

57. Computed Envelopes of the Response of an Ideal MFD DF System to Two Simultaneous Signals ---------- 162

58. Computed Envelope of the Response of an Ideal MFD DF System to Two Simultaneous Signals ---------- 164

59. Graph of the Theoretical R solution and Bearing Error of the MFD DF System vs the Ratio of the Amplitudes of Two Like-frequency Simultaneous Signals ---------- 166

60. Graph of the Theoretical Resolution of the MFD DF System vs the Difference ψ_1 in Phase of the Two Like-Frequency Simultaneous Signals ---------- 167

61. Graph of the Theoretical Resolution of the MFD DF System vs the Modulation Index β--------- 168

LIST OF SYMBOLS

$b = K_2/K_1$	Ratio of signal amplitudes (two-signal case)
d	Fractional part of the total bandwidth of a carrier, frequency modulated by a sinusoid
d'	Fractional part of the total signal energy contained in d
f	Frequency in Hertz
f_c	Carrier frequency in Hertz
f_r	Antenna rotation (modulation) frequency in Hertz
g(u)	Antenna pattern
h(t)	Inverse Fourier transform of H(f)
ℓ	Radius of rotation in meters
p(t)	Output voltage of a rotating antenna element (two-signal case)
$p_1(t)$	Output voltage of a matched-filter doppler DF system (two-signal case)
s(t)	Output voltage of a rotating antenna element (single-signal case)
$s_1(t)$	Output voltage of a matched-filter doppler DF system (single-signal case)
$s_n(t)$	Output voltage of a frequency multiplier whose input is s(t)
t	Time, seconds
$t' = t-\pi/\omega_r$	Time, seconds
$u = \sin\theta$	
v(t)	Antenna output voltage as a time function (γ fixed)
$v(\gamma)$	Antenna output voltage as a function of rotation angle γ
$v_1(\gamma)$	Truncated version of $v(\gamma)$

$w(t)$	Output voltage of antenna processor
x	Distance, meters
$y(\theta)$	Antenna pattern in the azimuthal plane
$y_1(\theta)$	Truncated version of $y(\theta)$
$z(\theta)$	Far field source distribution in the azimuthal plane
$D(x/\lambda)$	Aperture excitation along the normalized x axis
$E(t)$	Amplitude modulation factor of $s_1(t)$
$F(t)$	Amplitude modulation factor of $p_1(t)$
$G(\eta)$	Fourier transform of $g(u)$
$H(f)$	Transfer function of antenna processor
I_1	Signal-to-noise ratio improvement term due to bandpass filtering, in dB
I_2	Signal-to-noise ratio improvement term due to pulse compression, in dB
$J_k(\beta)$	Bessel function of the first kind of order k and argument β
$V_1(\zeta)$	Fourier transform of $v_1(\theta)$
$W(f)$	Fourier transform of $w(t)$
$Y_1(\zeta)$	Fourier transform of $y_1(\theta)$
$Z(\zeta)$	Fourier transform of $z(\theta)$
α	Angle of elevation from the horizontal plane
β	Modulation index or peak phase deviation of an angle modulated signal
γ	Angle of rotation in the azimuthal plane in radians
$\delta(\theta)$	Dirac delta function
$\varepsilon(\theta)$	Angular measurement error (Processing without multiplication)

$\varepsilon'(\theta)$	Angular measurement error (Processing with multiplication)
ζ	Counterpart Fourier transform variable associated with θ
η	Spatial frequency (counterpart Fourier transform variable associated with μ)
θ	Azimuthal angle, radians
θ_k	Azimuthal angle of arrival of a radio wave ($k = 0, 1 \ldots$)
λ	Wavelength in meters
λ_c	Carrier wavelength in meters
$\rho(t)$	Equal-amplitude frequency
τ	Time delay in seconds
$\phi(t)$	Phase modulation term of $s_1(t)$
ψ_1	Constant phase difference between two like-frequency signals at the center of rotation of a rotating antenna element
$\omega = 2\pi f$	Radian frequency
$\omega_c = 2\pi f_c$	Radian carrier frequency
$\omega_r = 2\pi f_r$	Radian rotation frequency
Γ_i	Signal-to-noise ratio at the input of a frequency doubler
Γ_o	Signal-to-noise ratio at the output of a frequency doubler
Θ_B	Half-power width of the output pulse of a MFD DF system with no frequency multiplication
Θ'_B	Half-power width of the output pulse of a MFD DF system using a frequency doubler
$\Phi(t)$	Phase modulation term of $p_1(t)$

ACKNOWLEDGEMENTS

The authors are pleased to acknowledge the support of Naval Ship Systems Command (Code 6050) in this study.

We also wish to thank Mr. Douglas N. Travers and his colleagues at the Southwest Research Institute, San Antonio, Texas for use of their facilities and for their assistance with an experiment conducted at that institution.

I. INTRODUCTION

This report is concerned with radio direction finding (DF), namely the ability to determine the direction of arrival of a radio wave. The direction of arrival includes azimuth angle (0-360 degrees) and elevation angle (0-90 degrees); however, this paper deals almost exclusively with the azimuth angle of arrival (AOA). In addition, an underlying assumption is that the receiver is far enough from the transmitter so that the arriving wavefront is essentially planar.

A. BACKGROUND

As early as 1899 it was recognized that electromagnetic waves could be aimed or beamed in a specific direction by the use of antennas such as loops or spaced dipoles. For receiving purposes this meant that the direction of arrival of a radio wave could be determined by moving or steering a directive antenna beam in azimuth until a maximum signal was obtained. The beam could be steered by physically moving an antenna or by appropriately summing the outputs of the individual elements of an array.

The science of radio direction finding has been the subject of much study since the early 1900's as reflected, for example, in the extensive bibliography by Travers and Hixon [1] which contains over 5000 entries. Among the inventors of some of the first radio direction finders were such pioneers as Marconi and de Forrest [2].

A major improvement over early DF systems came with the development in the 1920-1940 era of the Adcock DF system employing four or more spaced elements with an overall aperture of one-half wavelength or less. The Adcock system achieves an instrumental accuracy of about five degrees [3].

Since the end of World War II there has been a trend toward larger aperture systems. For example, doppler DF systems, in which frequency modulation (FM) by a sinusoid is induced on the received signal by a rotating antenna or its equivalent, usually range in size from one-half to five wavelengths and are capable of accuracies of two degrees or less [3].

The Wullenweber DF system which was developed in Germany in the early 1940's consists of a large circular array on the order of 10 wavelengths in diameter [4]. At any instant of time only one segment of the array is used, and with proper phasing of the elements in use, this segment is made equivalent to a planar array. By commutation the planar array is in essence caused to move in a circle. An accuracy of one-half degree or less is possible with this system [3].

At microwave frequencies, antennas having aperture sizes of several wavelengths and with extremely directive patterns can be physically rotated to give accurate AOA information. An alternate method which is very accurate for large values of signal-to-noise ratio (SNR) is the amplitude-sensing monopulse technique in which two identical directive antennas are placed some distance apart [5]. The pattern

produced by subtracting the output of one antenna from the other has a sharp null when the pair is aimed at the arriving signal.

B. CONTENTS AND SUMMARY

In this report the DF problem is considered as a signal-processing problem. In any scanning DF system an ideal waveform for determining AOA is a narrow pulse whose location along some time (azimuth) scale varies directly with the AOA. Figure 1 is an example of the processed output of the DF system considered in this report. In that figure, the horizontal axis is calibrated to show AOA. It should be noted that the accuracy with which the location of the

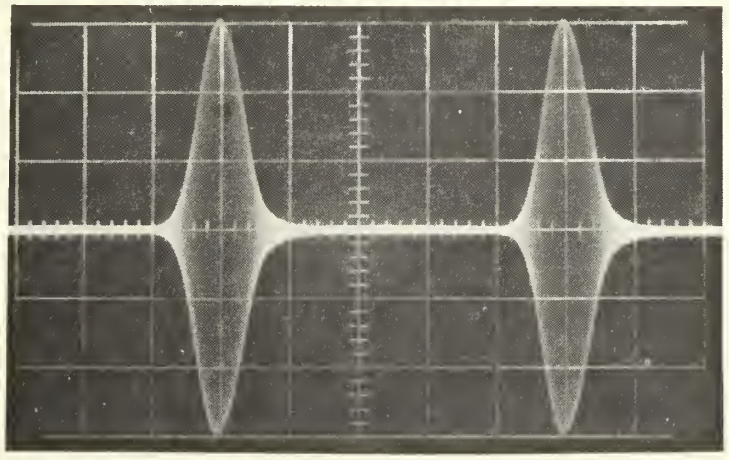

FIG. 1. PHOTOGRAPH OF THE TYPICAL OUTPUT OF A MFD DF SYSTEM

peak of any pulse can be determined is limited only by noise. In the presence of noise, Skolnik [6, p. 476-478] shows that measurement accuracy is directly proportional to the SNR and inversely proportional to the width of the pulse. From the well known inverse relationship between a time function and its frequency representation as expressed in the Fourier transform, it is clear that the narrower a pulse in the time domain the larger its bandwidth [7]. This basic principle, which underlies the theory of pulse compression, is applied here to the DF problem.

To generate a narrow (short duration) pulse by signal processing, a useful spreading of the spectrum of the received signal is necessary. One way to broaden the signal spectrum is to pass the signal through a nonlinear device. This is the basis for the DF technique suggested by Ierukhimovich [8] in which the summed output of two antennas is applied to an nth-order nonlinear device to create higher harmonics. The harmonics are amplified individually and then summed to produce a desired periodic train of narrow radio-frequency pulses. This particular technique has apparently received little attention.

Another way of spreading the spectrum of an incoming signal is through use of the doppler principle. If a radio wave is received by an antenna element which rotates at a fixed rate about a central point, and if the antenna is omnidirectional in the plane of rotation, the instantaneous

frequency of the received signal varies in a sinusoidal manner. It can be recognized from the doppler principle that the maximum positive frequency deviation occurs when the antenna is moving perpendicularly toward the incoming wavefront; thus, there is a direct relationship between the position of the antenna and the time of maximum instantaneous frequency. The periodic FM signal produced in this manner not only has a spectrum whose bandwidth is proportional to the radius of rotation, but the phase of each of its discrete spectral components is directly related to AOA.

Since a large bandwidth is only a necessary but not a sufficient condition for the generation of a short-duration pulse, other processing may be required. Processing the output of an antenna to improve its directivity or some other parameter is not a new concept. In fact, Ksienski [9] surveys a number of signal-processing antennas. However, a DF system is specialized in that there is one particular desired output -- an accurate indication of the AOA. For this reason the design of a DF system may have fewer restrictions than the design of a directional receiving system. That is, a DF system need not improve gain nor optimize any other parameter of reception; it must only provide accurate AOA information. For example, a null in an antenna pattern can be used to obtain an accurate bearing, but it is of no use in signal reception.

A principal result of this research is the development of a Matched-Filter Doppler DF (MFD DF) technique which is a simple means of processing the output of a rotating antenna to obtain the AOA of a radio wave. An MFD DF system, shown in general form in Fig. 2, extracts the AOA information from the periodic FM signal by a linear filtering operation which yields a periodic amplitude-modulated signal consisting of a single recurring pulse with no sidelobes as shown in Fig. 1. The position of the voltage pulse relative to a reference time scale gives the AOA of the signal. Because the portion of the spectrum which is filtered satisfies the phase-matching requirement of a matched filter the new technique is called the Matched-Filter Doppler DF technique.

Consideration is given to the use of frequency multiplication which in the absence of noise improves the ability to measure AOA accurately. The MFD DF concept is simulated on a digital computer for modulation indexes which correspond to a range of aperture diameters from eight to 1000 wavelengths.

To demonstrate the feasibility of the MFD DF principle and to investigate design alternatives in developing a practical system, an analog simulation was conducted using conventional electronic hardware. The same hardware is used in conjunction with a conventional doppler DF system to confirm the basic characteristics of the MFD DF technique under operating conditions.

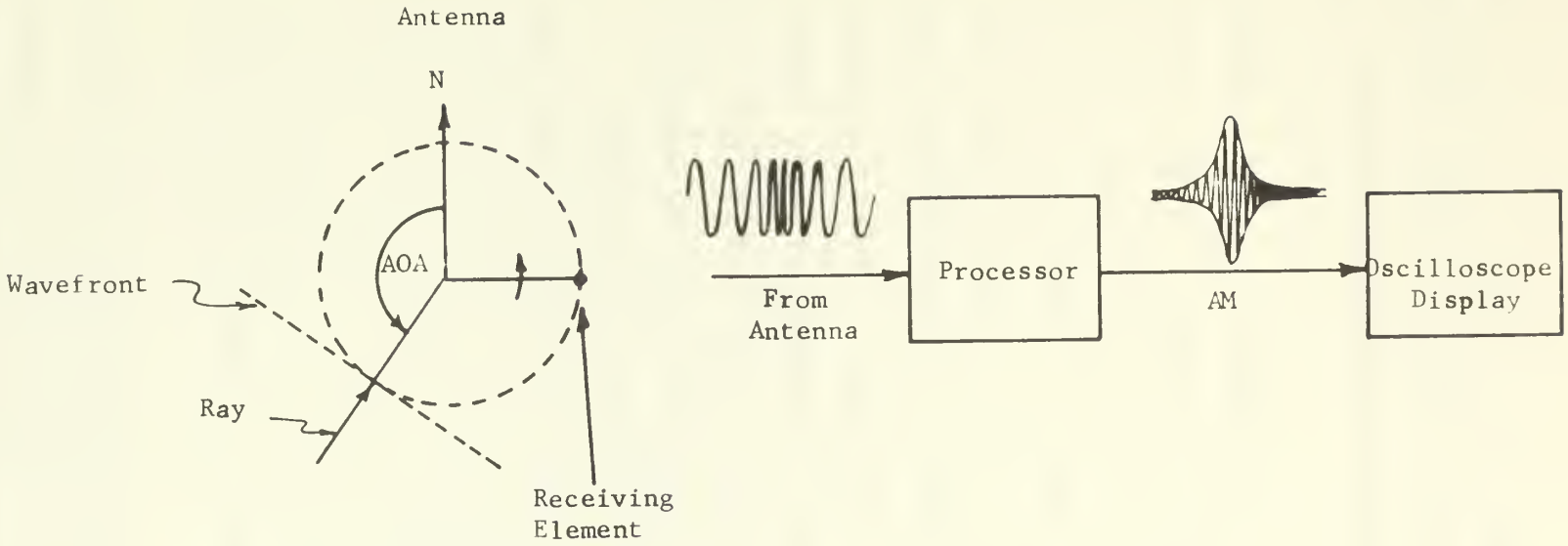

(a) Antenna geometry

(b) Processing and display system

FIG. 2. BLOCK DIAGRAM OF A MFD DF SYSTEM

C. PLAN OF THE REPORT

Chapter II reviews the familiar doppler DF principle [10][11][12], and develops in detail the theory of the new MFD DF technique.

In order to apply time-domain signal-processing techniques, such as matched filtering, to obtain spatial information, such as direction of arrival, the receiving antenna must convert spatial information to temporal form. As shown in Chapter III this is exactly what occurs when a linear antenna (or array) is rotated about a central point. In addition, this chapter unifies a number of previously known results of antenna theory, applies them to rotating antennas, and, for the first time, extends the results to rotating signal-processing DF antennas in general, and the MFD DF system in particular.

Chapter IV demonstrates the physical realizability of the MFD DF scheme by presenting results obtained with a hardware simulation system. Physical limitations are considered as well as the effect of noise. The last section in this chapter gives the results of an experiment in which the simulation hardware is interfaced with a conventional doppler DF set.

Chapter V is a theoretical study of the effect on a MFD DF system produced by the simultaneous reception of two signals of the same frequency at different azimuth angles.

Chapter VI is a summary of the report and lists recommendations for future work. Appendices A, B, and C support results presented in the report. A list of references is provided.

II. THE MATCHED-FILTER DOPPLER DF TECHNIQUE

This chapter reviews the doppler DF principle and then introduces the matched-filter doppler DF technique in which the AOA of a radio wave is extracted from a frequency-modulated carrier by a linear filtering process. The technique relies on the fact that modulation is imposed on the received radio wave by the motion of the receiving element. The periodic frequency-modulated signal at the antenna output is converted to a periodic amplitude-modulated signal consisting of a narrow voltage pulse with no sidelobes. The position of the pulse relative to a fixed reference time is directly related to the AOA.

A. THE DOPPLER DF PRINCIPLE

Consider a radio wave of carrier frequency f_c received by an antenna element which rotates at a constant rate f_r about a central point and which is omnidirectional in the plane of rotation as shown in Fig. 3. For simplicity the radio wave is assumed to lie in the plane of rotation. If the azimuthal AOA is θ_o, the output of the antenna is given by [Ref. 13]

$$s(t) = C\cos[\omega_c t + \beta(\sin\omega_r t - \theta_o)] \qquad (1)$$

where C is a constant, $\omega_c = 2\pi f_c = 2\pi/\lambda_c$, $\omega_r = 2\pi f_r$ and the modulation index or peak phase deviation is

$$\beta = 2\pi\ell/\lambda_c \qquad (2)$$

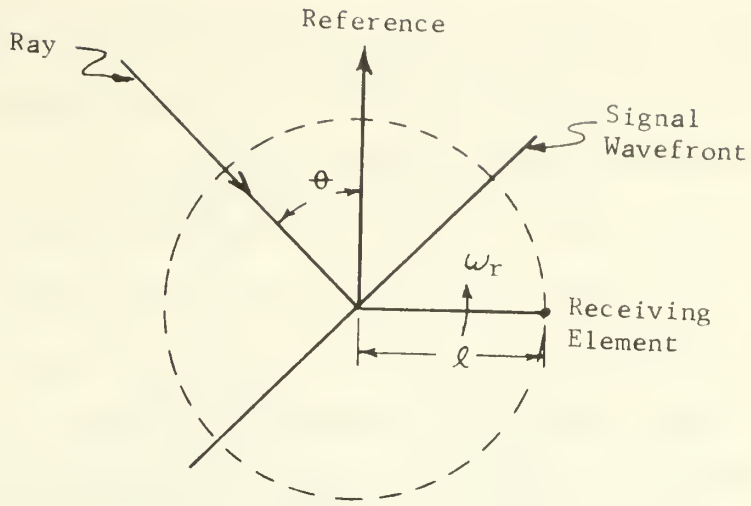

FIG. 3. PLAN VIEW OF A ROTATING ANTENNA ELEMENT

where ℓ is the radius of the circular antenna path.[1] The same doppler effect can be achieved with a circular array of receiving elements sampled sequentially.

Equation (1) is in the familiar form of frequency or phase modulation by a sinusoid. As the antenna rotates the instantaneous frequency of the antenna output varies due to the doppler effect. As the receiving element travels towards and then away from the incoming wavefront the received signal is frequency modulated in a sinusoidal fashion. This doppler effect can be viewed as phase

---

[1] If the signal is not traveling in the horizontal plane of rotation and arrives at an angle of elevation α the only effect of interest here is to make the modulation index $\beta = 2\pi\ell(\cos\alpha)/\lambda_c$.

modulation by noting that as the antenna travels around the circle, the path length between the transmitter and the receiving element changes. This causes the phase of the received signal to vary sinusoidally relative to the phase of the signal at the center of the circular path. The peak phase deviation β is therefore quite naturally equal to the radius of rotation in radians as given by (2). More importantly, for DF purposes, regardless of whether the antenna output is considered frequency modulation or phase modulation, the relative phase of the modulating sinusoid is directly related to the AOA of the signal. This doppler effect is the basis for conventional doppler DF systems, and it is also the basis for the matched-filter doppler DF technique presented in this report.

B. CONVENTIONAL DOPPLER DF SYSTEMS

Conventional doppler DF systems were first proposed in the late 1940's by Budenbom [10] and Boulet [11] in this country and by Earp and Godfrey [12] in Great Britain.

The block diagram of a typical conventional doppler DF system is given in Fig. 4. The output of a rotating antenna or an equivalent commutated array is frequency demodulated yielding a sinusoidal voltage

$$s_d(t) \propto \beta\omega_r \cos(\omega_r t - \theta_o) \ . \qquad (3)$$

The phase of $s_d(t)$ is compared with the phase of a like-frequency reference sinusoid which is associated with a

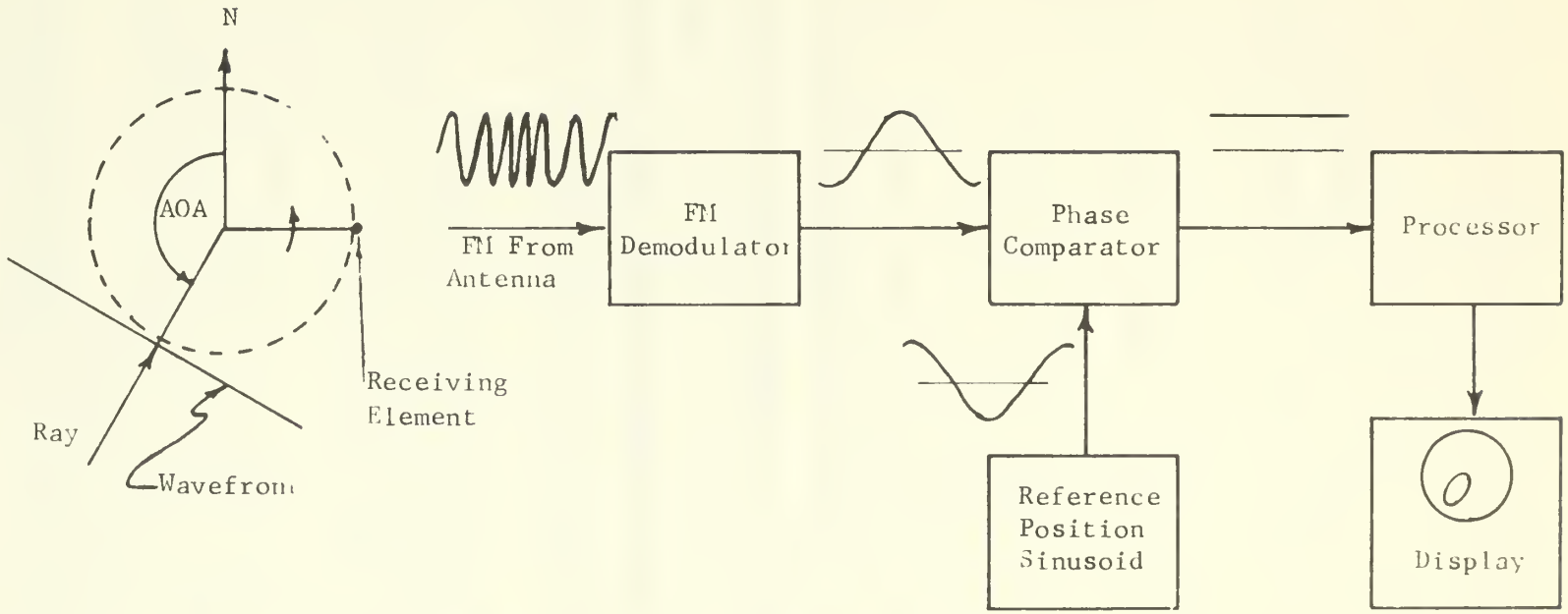

(a) Geometry (b) Receiver

FIG. 4. BLOCK DIAGRAM OF A CONVENTIONAL DOPPLER DF SYSTEM

fixed direction, typically true north. As shown in Fig. 4, the dc voltage level out of the phase comparator is a linear measure of the AOA. Conventional doppler DF sets are usually of medium-aperture size (circular path diameter of one-half to five wavelengths), and their performance in terms of accuracy is reported to be two degrees or better [3]. Conventional doppler systems cannot measure the AOA of weak signals in the presence of strong signals or noise due to the capture effect or small-signal suppression effect of FM receivers [4][14].

The matched-filter doppler DF technique presented in the next section requires no frequency or phase demodulators (nonlinear devices). The MFD DF system is completely linear, easily realizable, and from Figs. 1 and 2 it is seen that the MFD DF system provides AOA information in a simple and useful form suitable for direct display.

C. THE MATCHED-FILTER DOPPLER DF SYSTEM

In a scanning DF system, a repetitive narrow pulse whose occurrence time (phase) varies linearly with AOA is a useful waveform. In this section matched-filter processing is considered as a means of obtaining such a pulse from a carrier frequency modulated by a sinusoid.

1. Matched-Filter Concepts

It is useful here to review the properties of matched filters [15]. If a function v(t) has a Fourier transform V(f) given by

$$V(f) = \int_{-\infty}^{\infty} v(t)e^{-j2\pi ft}dt = |V(f)|e^{j\Psi(f)} \qquad (4)$$

where $\Psi(f)$ is the argument of the complex frequency function, then the transfer function of a filter matched to v(t) is given by

$$K_1|V(f)|e^{-j\Psi(f)}\ e^{-j2\pi f\tau} \qquad (5)$$

where K_1 is a constant and τ is a fixed time delay experienced by the signal when passed through the filter. The matched filter is also called a conjugate filter because, except for the delay and amplitude factors, the filter transfer function is the conjugate of V(f); therefore, a matched filter:

(1) Scales the magnitude of each spectral component of v(t) by the factor $|V(f)|$ (amplitude matching) and,

(2) Places all of the spectral components of v(t) in phase at $t = \tau$ due to the conjugate property (phase matching).

To use these fundamental properties of matched filters to provide DF information, the spectral representation of FM by a sinusoid is now considered.

2. Spectral Representation of FM by a Sinusoid

The function s(t) given in (1) is periodic with period $2\pi/\omega_r$ and hence can be expanded in a Fourier series as [16, p. 125-130],

$$s(t) = J_o(\beta)\cos\omega_c t + \sum_{k=1}^{\infty} J_k(\beta)\cos[(\omega_c + k\omega_r)t - k\theta_o]$$

$$+ \sum_{k=1}^{\infty} (-1)^k J_k(\beta)\cos[(\omega_c - k\omega_r)t + k\theta_o] \quad (6)$$

where $J_k(\beta)$ is the Bessel function of the first kind of order k and argument β. In (6) and equations following, C has been set equal to one. It is assumed throughout the following development that $f_r << f_c$.

Equation (6) shows that FM by a sinusoid can be represented by a carrier-frequency term and an infinite number of side-frequency terms, each separated from its neighbor by a frequency increment equal to f_r Hz. Corresponding upper and lower side frequencies have the same magnitude. Bessel functions also have the property that beyond the value of order k equal to the argument β, the magnitude of the Bessel function and hence of the corresponding frequency component decreases rapidly and asymptotically to zero [17]. This means that although the series is infinite, there are a finite number of significant frequency components.

When considered as phasors, the frequency components given in (6) have relative phase-angle relationships which vary with time; however, there are specific instants of time when all of the phasors have either a zero or 180-degree relative phase angle. These instants are important here because they are directly related to the AOA of the received signal. For example, Fig. 5 shows the magnitudes of the

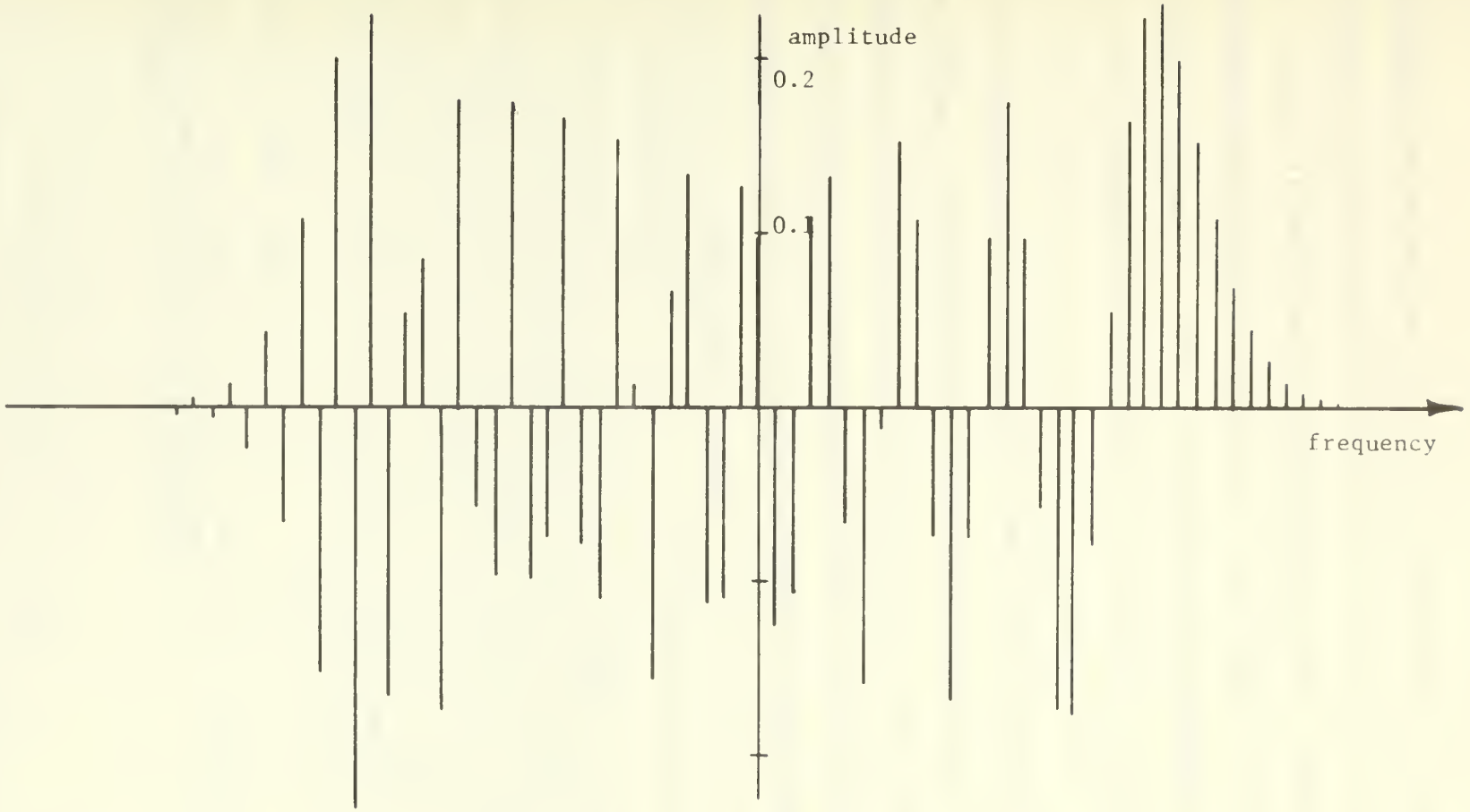

FIG. 5. SPECTRUM OF FM BY A SINUSOID WHEN $\beta = 25$.
Reference time $t_o = \theta_o/\omega_r$.

coefficients of the Fourier series components of s(t) when $\beta = 25$. (A value of β of 25 corresponds in Fig. 3 to a radius of about four wavelengths.) The sign of each coefficient is indicated by its projection above (positive) or below (negative) the frequency axis. Conventionally, such a diagram as Fig. 5 is called the spectrum of the signal.

Because the series which represents s(t) consists solely of cosine functions and since all of the coefficients (Bessel functions) are real, Fig. 5 can be used to convey information about the relative phase angles between the various frequency components (phasors). However, since each phasor rotates at a different rate, Fig. 5 only gives valid phase-angle relationships when the principal value of the argument of <u>every</u> cosine function in (6) is the same. The first instant at which this happens is $t = 0$ if the cosine terms have no initial phase angle ($\theta_o = 0$). Since s(t) has a phase lag of θ_o radians, the instant at which the relative phase angle relationships of Fig. 5 exist is $t_o = \theta_o/\omega_r$. At $t_o = \theta_o/\omega_r$

$$s(\theta_o/\omega_r) = J_o(\beta)\cos\omega_c(\theta_o/\omega_r) + \sum_{k=1}^{\infty} J_k(\beta)\cos\omega_c(\theta_o/\omega_r)$$

$$+ \sum_{k=1}^{\infty} (-1)^k J_k(\beta)\cos\omega_c(\theta_o/\omega_r) , \qquad (7)$$

and all of the spectral components (phasors) with positive coefficients (above the frequency axis) have a zero-degree

phase angle relative to each other, while those spectral components with negative coefficients (below the frequency axis) have a 180-degree relative phase angle. As seen from the second term of (6) and (7), the spectral components of frequency greater than the carrier frequency have a positive or negative coefficient according to the sign of the Bessel function with which each is associated. When $\beta = 25$, all Bessel functions of order 20 or more are positive; hence, all frequency components of value $f_c + 20f_r$ or more are in relative phase conjunction at $t_o = \theta_o/\omega_r$. Because s(t) has a period of $2\pi/\omega_r$, the same relative phase-angle relationships shown in Fig. 5 recur at instants

$$t_m = \frac{\theta_o + 2m\pi}{\omega_r} \qquad m = 0, 1, \ldots n. \qquad (8)$$

The preceding analysis was concerned primarily with the characteristics of the frequency components above the carrier frequency. The reason for this is now given. Each side frequency below the carrier is equal in magnitude to its counterpart above the carrier and differs only in relative phase angle at $t = \theta_o/\omega_r$ because of the $(-1)^k$ factor in the third term of (6) and (7). However, if a new reference time t' is selected where

$$t' = t - \pi/\omega_r,$$

which corresponds to a displacement of one-half of a rotation cycle of the antenna of Fig. 3, then the antenna output can be expressed as

$$s(t-\frac{\pi}{\omega_r}) = J_o(\beta)\cos\omega_c(t-\frac{\pi}{\omega_r}) + \sum_{k=1}^{\infty}(-1)^k J_k(\beta)\cos[\omega_c(t-\frac{\pi}{\omega_r})+k\omega_r t-k\theta_o]$$

$$+ \sum_{k=1}^{\infty} J_k(\beta)\cos[\omega_c(t-\frac{\pi}{\omega_r})-k\omega_r t+k\theta_o] \qquad (9)$$

The spectrum of (9) is given in Fig. 6 and it reflects the change in location of the $(-1)^k$ factor from the third term in (6) to the second term in (9). By similarity with the argument presented for s(t) as represented in Fig. 5, Fig. 6 gives the relative phase angles (zero or 180 degrees) between the spectral components of s(t') at time $t_o' = \theta_o/\omega_r$. At t_o', which corresponds to $t = t_o + \pi/\omega_r$

$$s(\frac{\theta_o+\pi}{\omega_r}) = J_o(\beta)\cos\omega_c(\frac{\theta_o+\pi}{\omega_r}) + \sum_{k=1}^{\infty}(-1)^k J_k(\beta)\cos\omega_c(\frac{\theta_o+\pi}{\omega_r})$$

$$+ \sum_{k=1}^{\infty} J_k(\beta)\cos\omega_c(\frac{\theta_o+\pi}{\omega_r}) \qquad (10)$$

It is clear that the relative phase angle relationships among the phasors (frequency components) above the carrier frequency at t_o(Fig. 5), are transposed to the frequency components below the carrier frequency at $t_o + \pi/\omega_r$ (Fig. 6). The significance of this result is that there are only two instants during each rotation or scanning cycle (θ_o/ω_r and $(\theta_o+\pi)/\omega_r$ during the first cycle) when all of the spectral components of the antenna output have either a zero or a 180-degree relative phase angle; these two instants are directly related to the AOA of the signal.

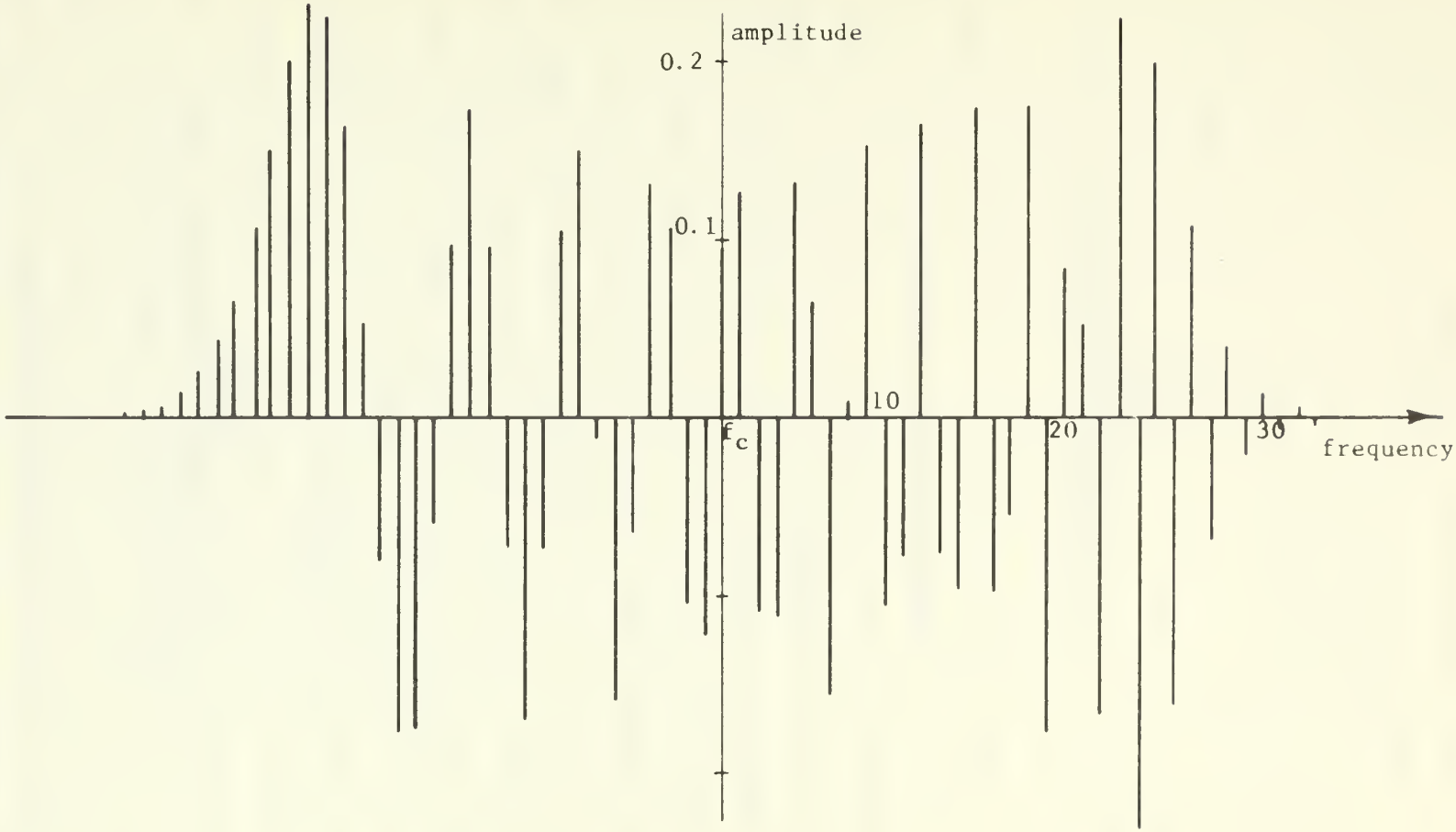

FIG. 6. SPECTRUM OF FM BY A SINUSOID WHEN β = 25

3. Determining Angle of Arrival

Having reviewed matched-filter theory and investigated the spectral characteristics of FM by a sinusoid, this section describes a realizable filter which is phase matched to part of the spectrum of the antenna output voltage. The filter output can be used directly -- no further processing required -- to obtain the AOA of a radio wave.

Consider first the output of a filter matched to s(t) of (1). The matched-filter output is easy to calculate mathematically by multiplying each coefficient of the Fourier series expansion of s(t) given in (6) by itself. This operation yields a function which satisfies both the amplitude-matching and phase-matching requirements of a matched filter. The computed envelope of one cycle of the filter output is shown in Fig. 7-a for $\beta = 25$. This envelope can be used to determine AOA directly since it consists of a narrow main lobe whose position along the time axis depends on the AOA of the signal. That is, the time axis can be graduated in degrees of azimuth for DF purposes. The voltage of Fig. 7-a repeats once for each rotation cycle of the antenna. It is interesting to note that the 3-db width of the main lobe is 5.04 degrees (considering one scanning cycle equivalent to 360 degrees), which is nearly two degrees narrower than the calculated main lobe of an antenna pattern produced by a uniformly excited linear antenna of the same aperture.

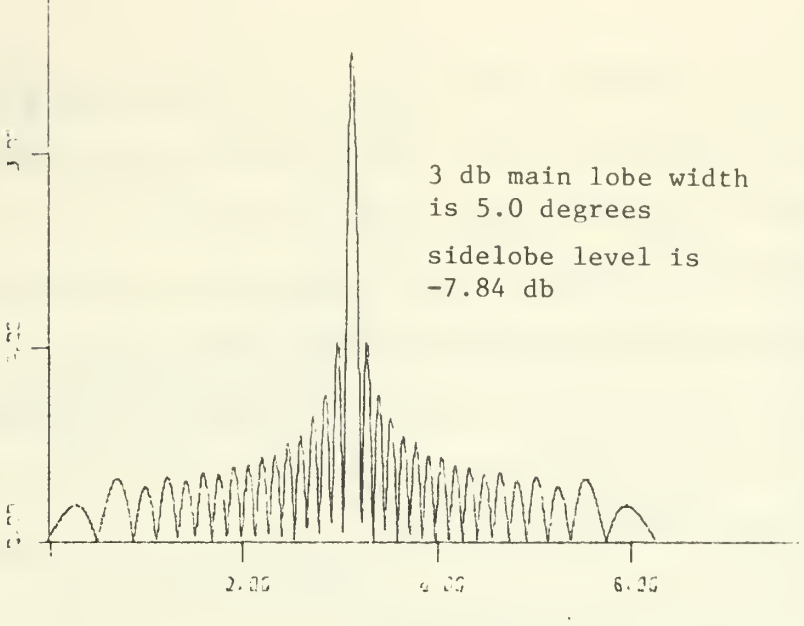

(a) Amplitude and phase matching

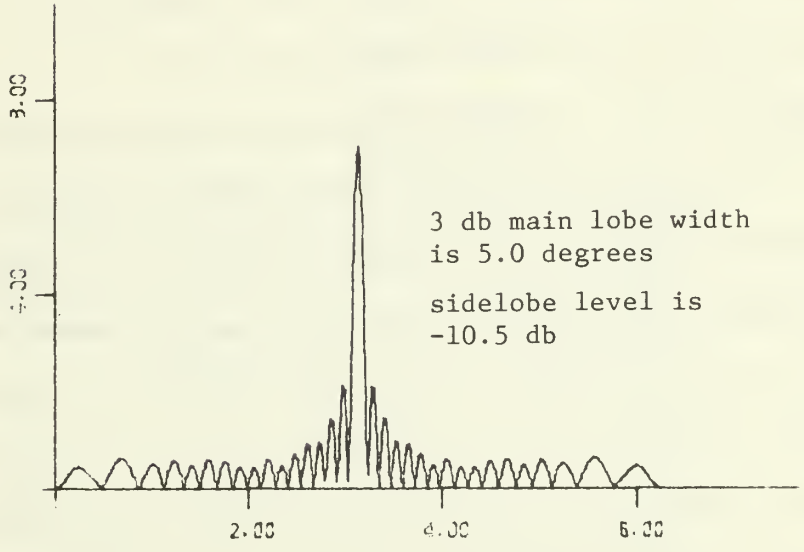

(b) Phase matching only

FIG. 7. ENVELOPE OF ONE CYCLE OF THE PERIODIC OUTPUT OF A FILTER MATCHED TO A CARRIER FM BY A SINUSOID. β is 25.

It is observed from Fig. 5 that various adjacent frequency components of s(t) have phase angles which differ by π radians; therefore any filter matched to s(t) must also introduce π-radian phase changes in a similar manner due to the phase-matching property. The realization of such a filter is impractical. Phase matching is in general more important in the generation of narrow pulses than is amplitude matching. This is shown in Fig. 7-b which displays the calculated envelope of one cycle of the output of a phase-matched rectangular bandpass filter for $\beta = 25$. For DF purposes the waveform of Fig. 7-b is just as useful as that of Fig. 7-a. However, in both cases the presentation may be undesirable because of the number and magnitude of sidelobes present.

Difficulty in realizing a filter matched to the spectrum of Fig. 5 and the sidelobe structure of the matched-filter output (Fig. 7) prompts consideration of compromise solutions. When $\beta > 10$ the spectrum of FM by a sinusoid always contains one large contiguous group of components (phasors) which have the same relative phase angle at the instant $t_o = \theta_o/\omega_r$. When $\beta = 25$ these like-phase components appear as the group shown isolated in Fig. 8. A portion of the spectrum, therefore, already satisfies the phase-matching requirement of a matched-filter output. If these components are removed as a group from the rest of the spectrum, the resulting waveform should display some of the properties frequently seen in matched-filter waveforms -- a large

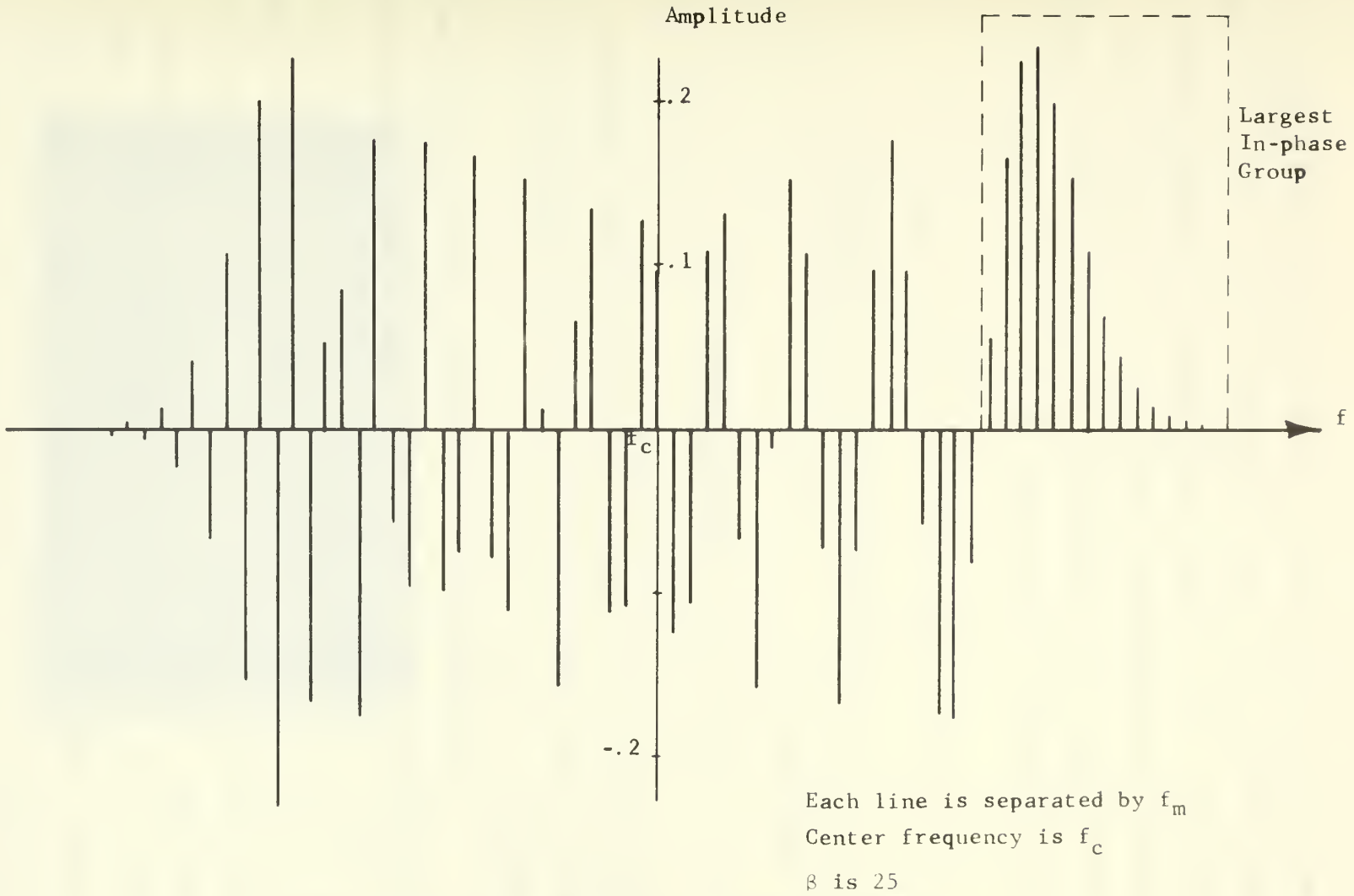

FIG. 8. SPECTRUM OF FM BY A SINUSOID SHOWING THE IN-PHASE GROUP OF INTEREST

amplitude at one instant of time with relatively smaller amplitudes at all other times during each cycle of antenna rotation. The in-phase group having the largest number of significant components, which for $\beta = 25$ consist of the 20th through 31st harmonics of f_r above f_c, can be selected with a bandpass filter whose output is given from (6) as

$$s_1(t) = \sum_{k=20}^{31} J_k(\beta)\cos[(\omega_c+k\omega_r)t - k\theta_o]. \quad (11)$$

[2]

By the use of trigonometric identities $s_1(t)$ can be expressed as

$$s_1(t) = E(t)\cos[\omega_c t + \phi(t)] \quad (12)$$

where $E(t)$ is the amplitude-modulation factor (envelope) and $\phi(t)$ is a phase modulation term (see Appendix A for details).

The waveform $E(t)$ of interest, shown in Fig. 9-a for one scanning cycle, not only has a main peak corresponding in time to the AOA of the signal (180° in this case), but it is also a smooth pulse free of sidelobes. As the transmitter azimuth changes the pulse position moves along the time axis. Figure 9-b is a photograph of the undetected output of an experimental system used to simulate the MFD DF system. Experimental results are presented in detail in Chapter IV.

---

[2] In this and other examples the last significant component is the last component that has any discernable effect on the calculated waveform $s_1(t)$.

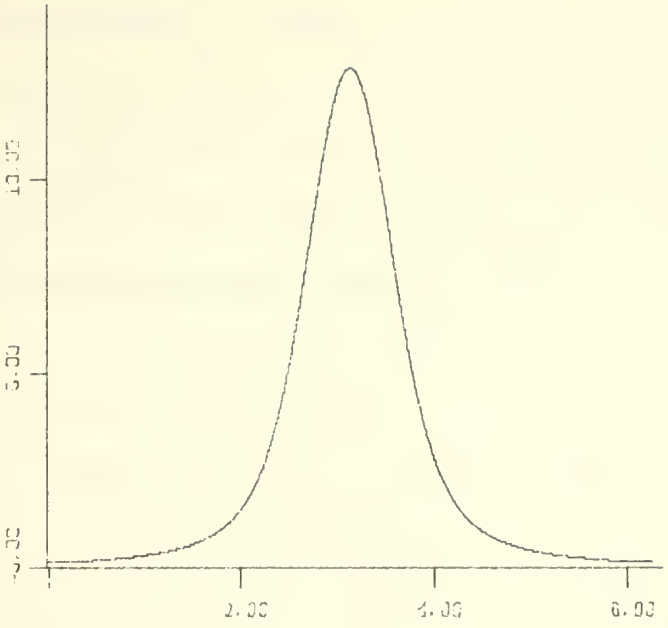

(a) Computed envelope.

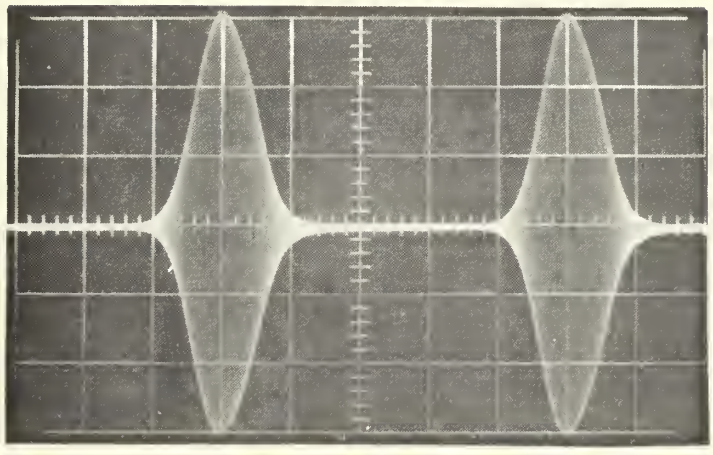

(b) Undetected output of experimental system. Two scanning cycles are displayed.

FIG. 9. ENVELOPE OF THE ISOLATED IN-PHASE GROUP OF FREQUENCY COMPONENTS SHOWN IN FIG. 8

Because of the spectral symmetry discussed in section 2 and shown in Fig. 6, there is a corresponding group of frequencies <u>below</u> f_c which are also in phase relative to each other once per cycle but at a later time corresponding to an additional half-cycle of antenna rotation. Obviously this lower-frequency group can be bandpass filtered to produce a waveform identical to that shown in Fig. 9, except for the fixed time delay of π/ω_r seconds. Computations and experimental results verify this conclusion.

It is instructive to consider the in-phase spectral components as a group of sinusoids which are added. Guillemin [18] calls waveforms such as $s_1(t)$ in (11) frequency groups. These particular groups have uniformly spaced discrete-frequency components and all frequency components are in phase at some reference time. Guillemin explores some of the properties of frequency groups, particularly the envelopes of groups with equal-amplitude components because they can be expressed mathematically in closed form with easily predictable behavior. For example, a group of 12 sinusoids of equal amplitude separated by Δf H_z and with a median frequency f_c much greater than Δf can be expressed as

$$\rho(t) = \frac{\sin[\frac{12(2\pi\Delta f)}{2}t]}{\sin[\frac{2\pi\Delta f}{2}t]} \cdot \cos 2\pi f_c t \qquad (13)$$

The envelope of $\rho(t)$ as shown in Fig. 10 has a principal maximum of width $1/(6\Delta f)$ which repeats every $1/(\Delta f)$ seconds. Minima occur every $1/(12\Delta f)$ seconds except when this corresponds to a multiple of $1/(\Delta f)$. Secondary maxima (sidelobes) appear about halfway between the secondary minima.

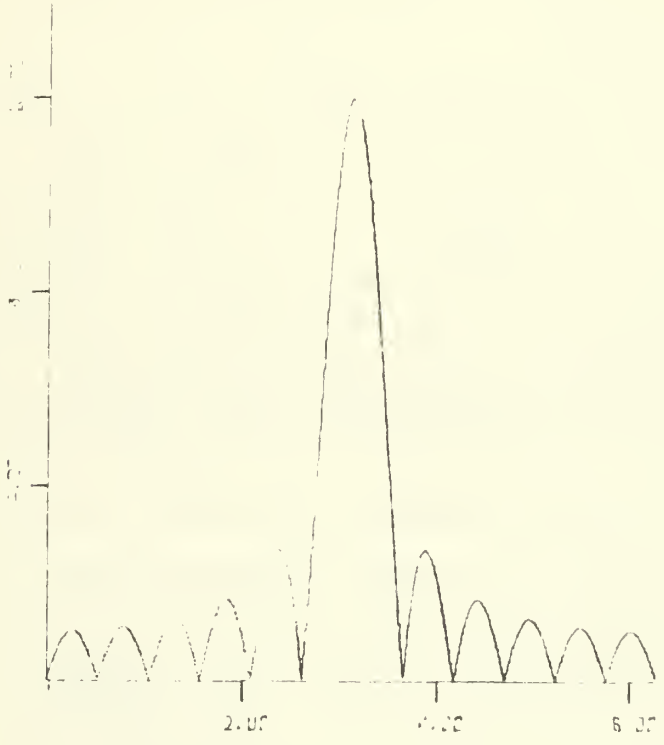

FIG. 10. COMPUTED ENVELOPE OF AN EQUAL-AMPLITUDE, IN-PHASE FREQUENCY GROUP

Unfortunately, groups such as those encountered in the spectrum of Fig. 5 which have members of unequal magnitudes can not be so simply expressed as (13), and their envelopes are not as readily predicted from their series form (11) or closed form (12). For example, as shown previously, the group of 12 in-phase spectral components associated with FM by a sinusoid when β is 25 (Fig. 8) is expressed as the series of (11).

The envelope E(t) of this group as given in (12) has a maximum at multiples of $1/f_r$, but other specific details are not obvious unless the envelope is plotted. Despite the differences between equal-amplitude frequency groups and those of interest here, Guillemin's results can be used to obtain insight into general envelope properties of frequency groups.

The phasor diagram is also a useful tool to gain insight into the behavior of a frequency group. In phasor form, a group such as $s_1(t)$ of (11) adds together in the complex plane to form a resultant phasor of magnitude E(t) and phase angle $\phi(t)$. To illustrate this, Fig. 11 shows a typical group of five phasors at two instants of time.

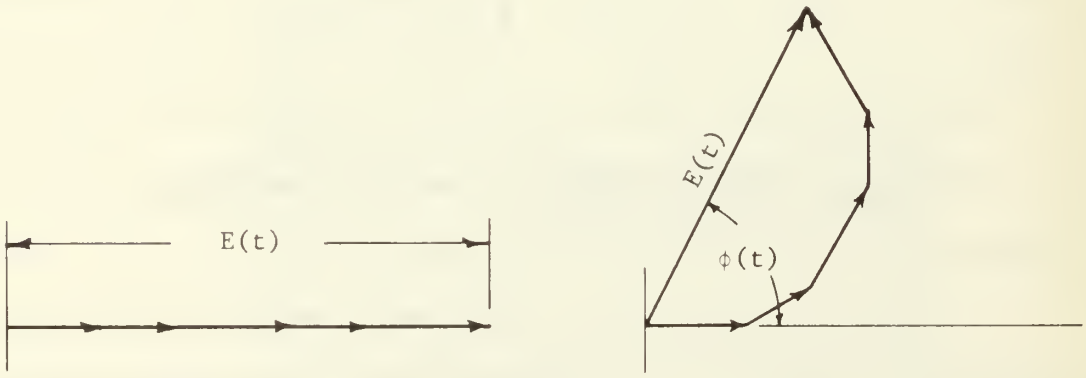

FIG. 11. PHASOR DIAGRAMS

Because $s_1(t)$ is an in-phase group and because the frequency components which form $s_1(t)$ differ from each other by f_r Hz, once and only once every $1/f_r$ seconds all of the phasors add constructively to form the large pulse shown in Fig. 9. It is interesting to note that there are no times when smaller groups among the frequency components of $s_1(t)$ constructively interfere to form sidelobes.

In summary, it has been shown that a rotating antenna element superimposes sinusoidal FM on a received carrier. The simple process of bandpass filtering a group of in-phase spectral components of the FM signal produces a periodic AM waveform with no discernable sidelobes. The peak of the lobe occurs at a time linearly related to the AOA of the signal. Since the in-phase group of frequencies satisfies the phase-matching property of a matched-filter output, the new technique is called Matched-Filter Doppler Direction Finding (MFD DF). These theoretical results are supported by results obtained with an experimental MFD DF system. These experimental results are presented in Chapter IV.

4. Dependence of DF Accuracy on System Parameters

In the absence of noise the time of occurrence of the peak of a pulse can be measured in theory with unlimited accuracy. However, the ease with which this value can be ascertained, particularly by an operator, is dependent on the shape of the pulse. Furthermore, Skolnik [6, p. 462-478] shows that the measurement error in the presence of noise

(at a high SNR) is inversely proportional to the square root of the SNR and directly proportional to the half-power width of the pulse. In the limit as the SNR becomes very large, the error becomes negligible. This section explores the properties of FM by a sinusoid and the matched-filter technique, particularly the effect of those parameters which affect the shape of the output pulse of a MFD DF system.

The two parameters of s(t) of (1) that can be controlled at the receiving site are scanning rate f_r and modulation index β. As will be shown later, the value of f_r affects system design, but its only effect on the spectrum of s(t) is to change the separation between the frequency components. The value of modulation index β given by (2) has a marked effect on the spectrum. As β increases the total number of significant sidebands increases. For β greater than 50, approximately 2β significant sidebands exist [17]. Figure 12 shows the spectrum of s(t) for values of β of 50 and 100 (only components above f_c are shown). The characteristic of primary importance here is that the number of components in the last group of in-phase members and hence the bandwidth of that group increases with β. It is also interesting that the difference in magnitudes of adjacent components in that group decreases with β.

As expected from Guillemin's results and as shown in Fig. 13, obtained by evaluating equations similar to

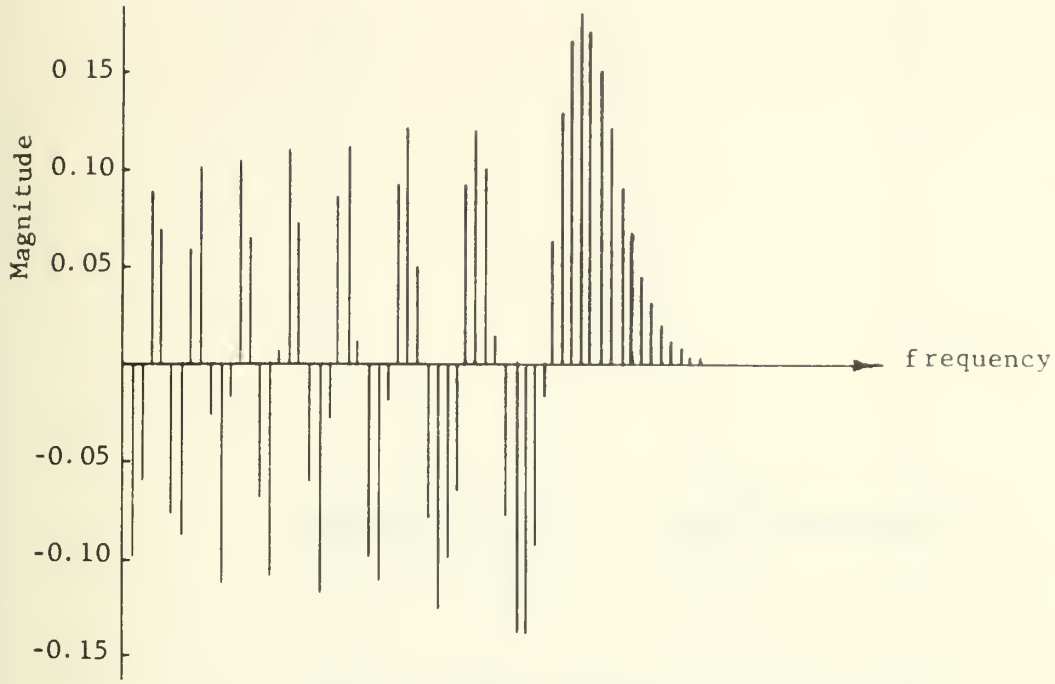

(a) $\beta = 50$

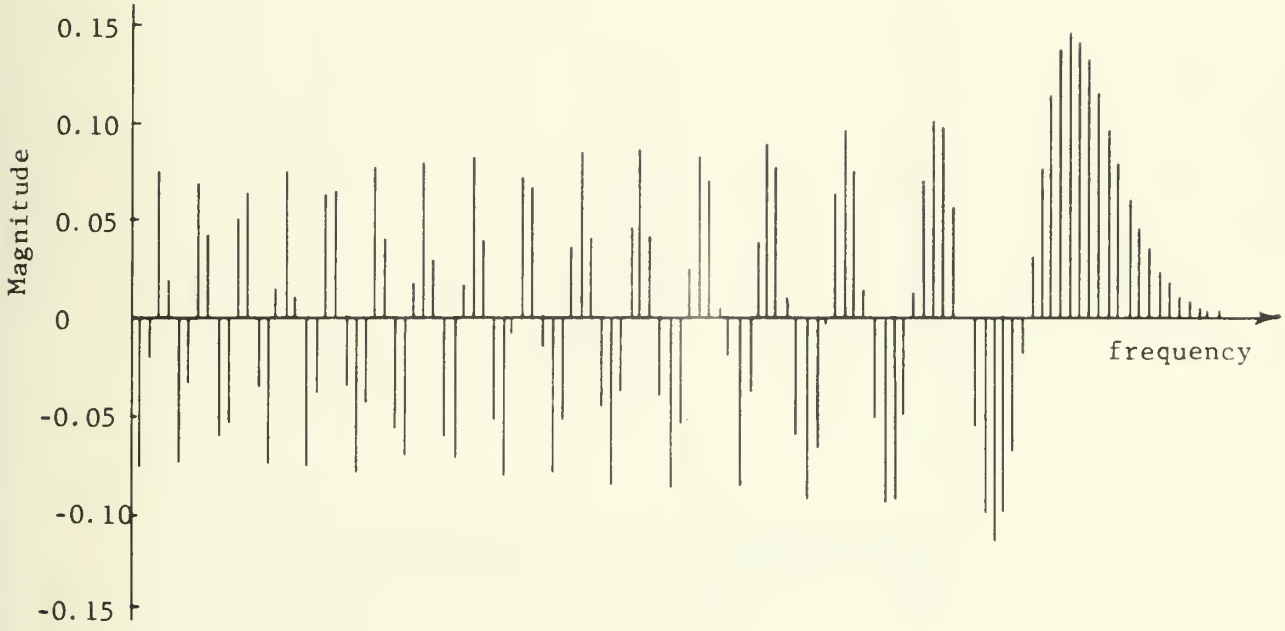

(b) $\beta = 100$

FIG. 12. SPECTRA OF FM BY A SINUSOID

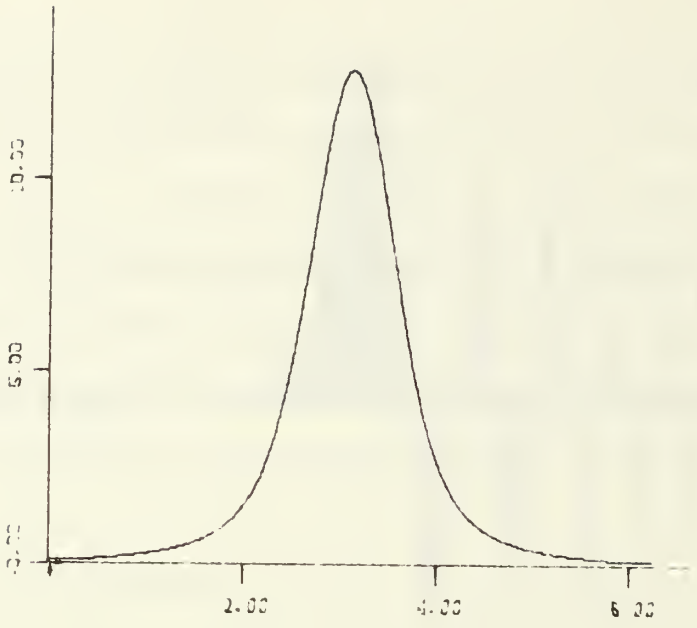

(a) β = 25, Half-power width = 43.5°

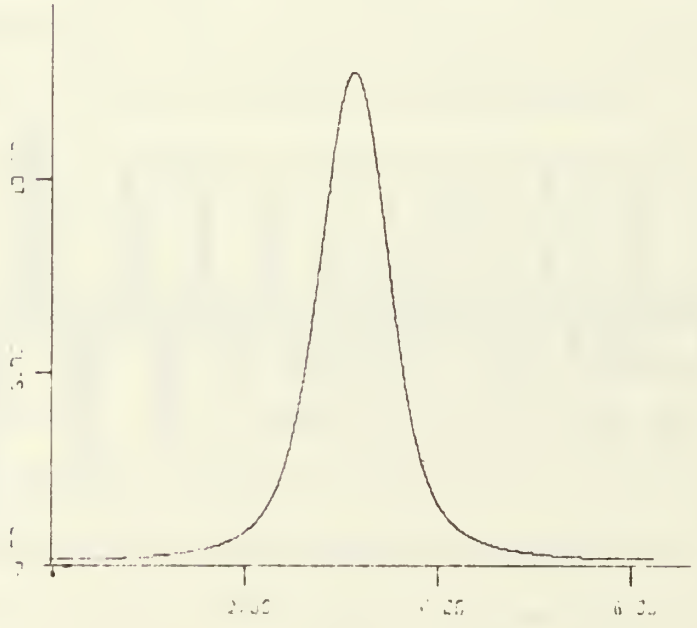

(b) β = 50, Half-power width = 33.8°

FIG. 13. COMPUTED ENVELOPES OF THE OUTPUT OF AN IDEAL MFD DF SYSTEM AS β INCREASES

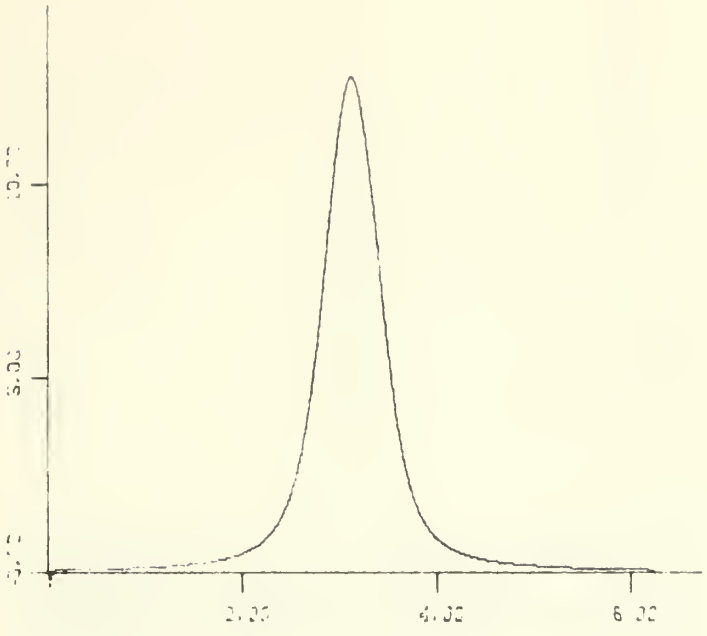

(c) β = 100, Half-power width = 27.5°

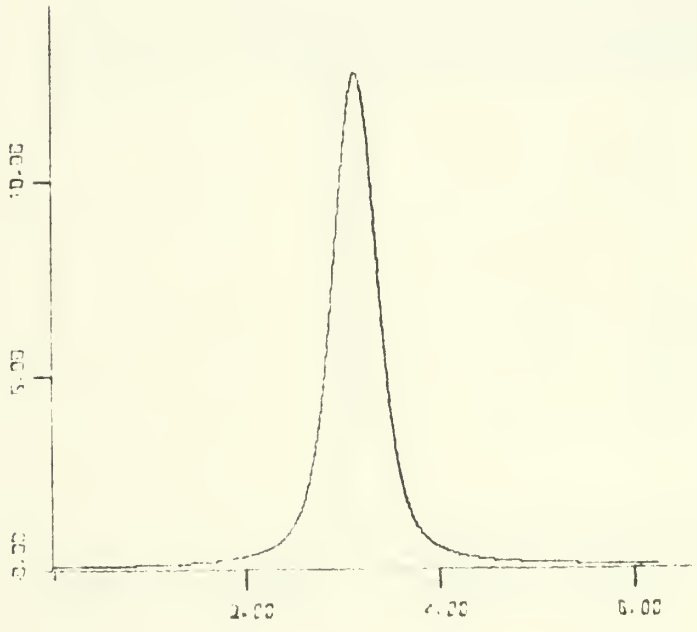

(d) β = 200, Half-power width = 21.8°

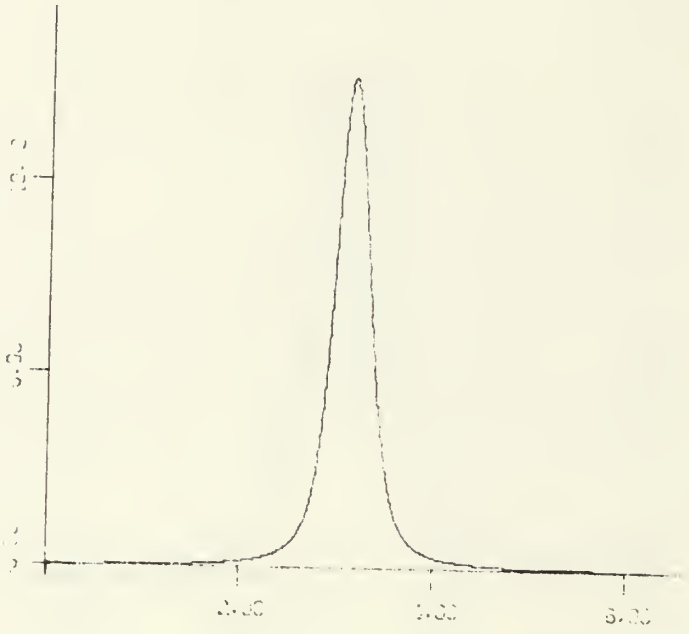

(e) β = 400, Half-power width = 17.20°

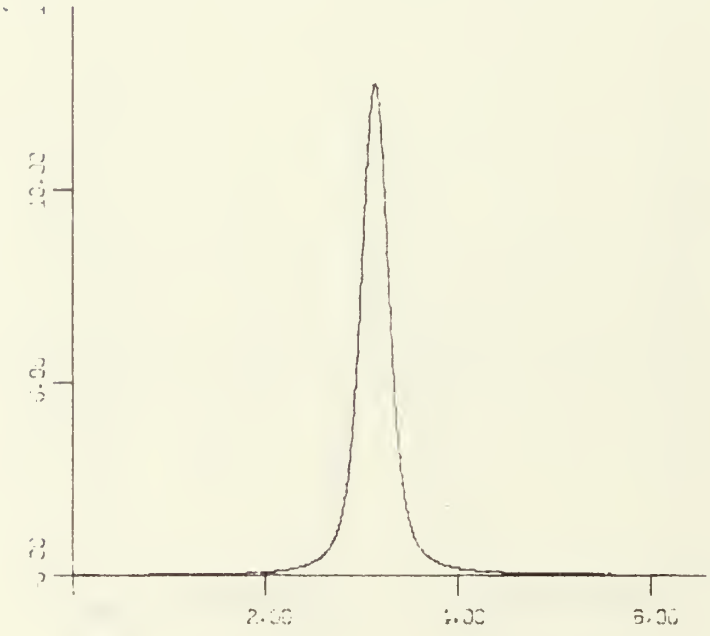

(f) β = 800, Half-power width = 13.8°

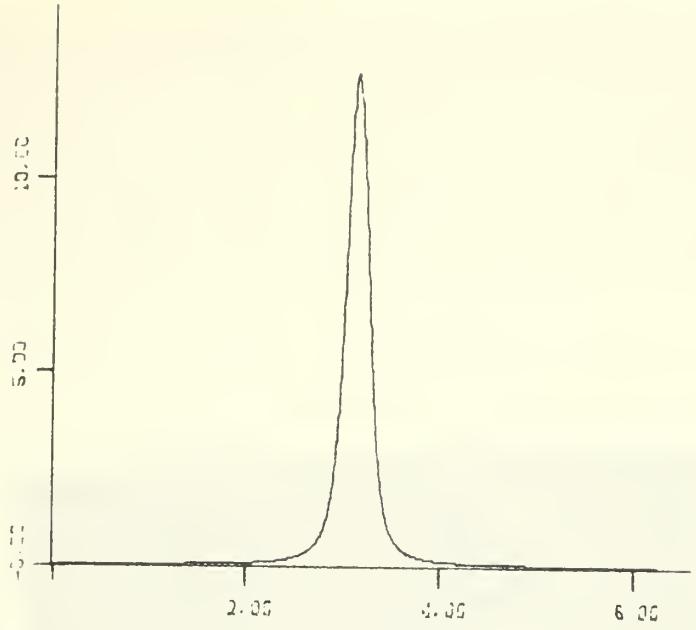

(g) β = 1600, Half-power width = 11.5°

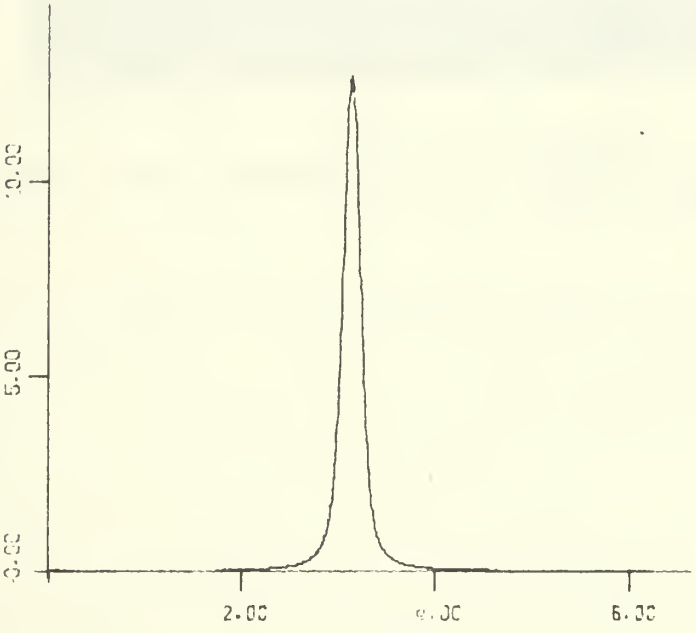

(h) β = 3200, Half-power width = 8.2°

(11) with the aid of a digital computer, the main lobe of the envelopes of the in-phase frequency groups narrows with increasing β and no discernable sidelobes appear. Experimental results confirm this as seen in Fig. 14 which shows

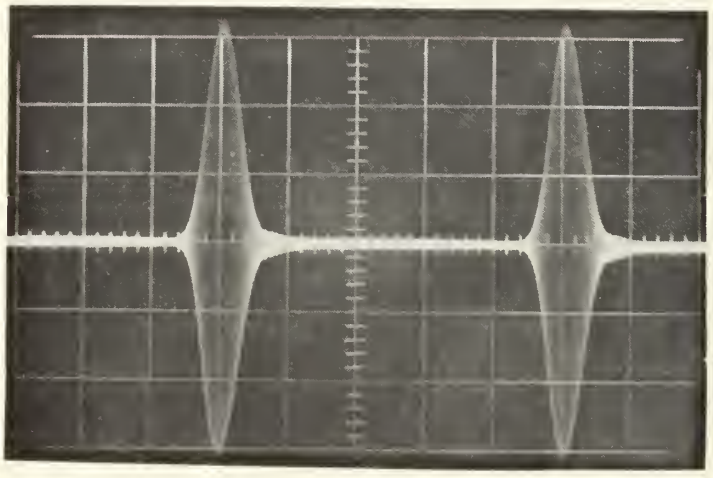

FIG. 14. OUTPUT OF THE EXPERIMENTAL MFD DF SYSTEM WHEN β = 100

the output of an experimental MFD DF system when β is 100 (Chapter IV gives details). Figure 15 summarizes these results by simultaneously displaying the 3-db widths of the main lobe of the envelopes as well as the number of members in the in-phase group as a function of β. It is concluded then that as β increases, the width of the output pulse of the MFD DF system narrows which is desireable for measurement purposes because the time at which the pulse occurs is more discernable to an operator.

5. Increased β by Frequency Multiplication

For a given carrier wavelength λ_c, β is linearly related to the radius of the path of the rotating antenna or equivalent array [Eq. (2)]. Practical limits are soon reached in attempting to increase the value of β by increasing the array diameter. However, frequency multiplication [16, p. 132-134] provides a means of increasing β without increasing the size of the antenna aperture.

For a carrier frequency modulated by a sinusoid given by

$$s(t) = C\cos[\omega_c t + \beta\sin(\omega_r t - \theta_o)] \ , \qquad (1)$$

frequency multiplication by a factor n produces

$$s_n(t) = C\cos[n\omega_c t + n\beta(\sin\omega_r t - \theta_o)] \ . \qquad (14)$$

The carrier frequency is increased by the factor n, but the spectral components of $s_n(t)$ are still separated by f_r Hz. More importantly, the modulation index is now nβ and the relative phase of the modulating signal, which corresponds to the AOA, is preserved. Frequency multiplication for the application of interest has the same effect as increasing the size of the receiving aperture.

The effect of noise on the technique of frequency multiplication will be covered in Chapter IV; however, even in the absense of noise, Fig. 15 shows that the envelope 3-dB width decreases at a rather slow rate with increasing β so that practically there is undoubtedly a limited number of useful stages of frequency multiplication.

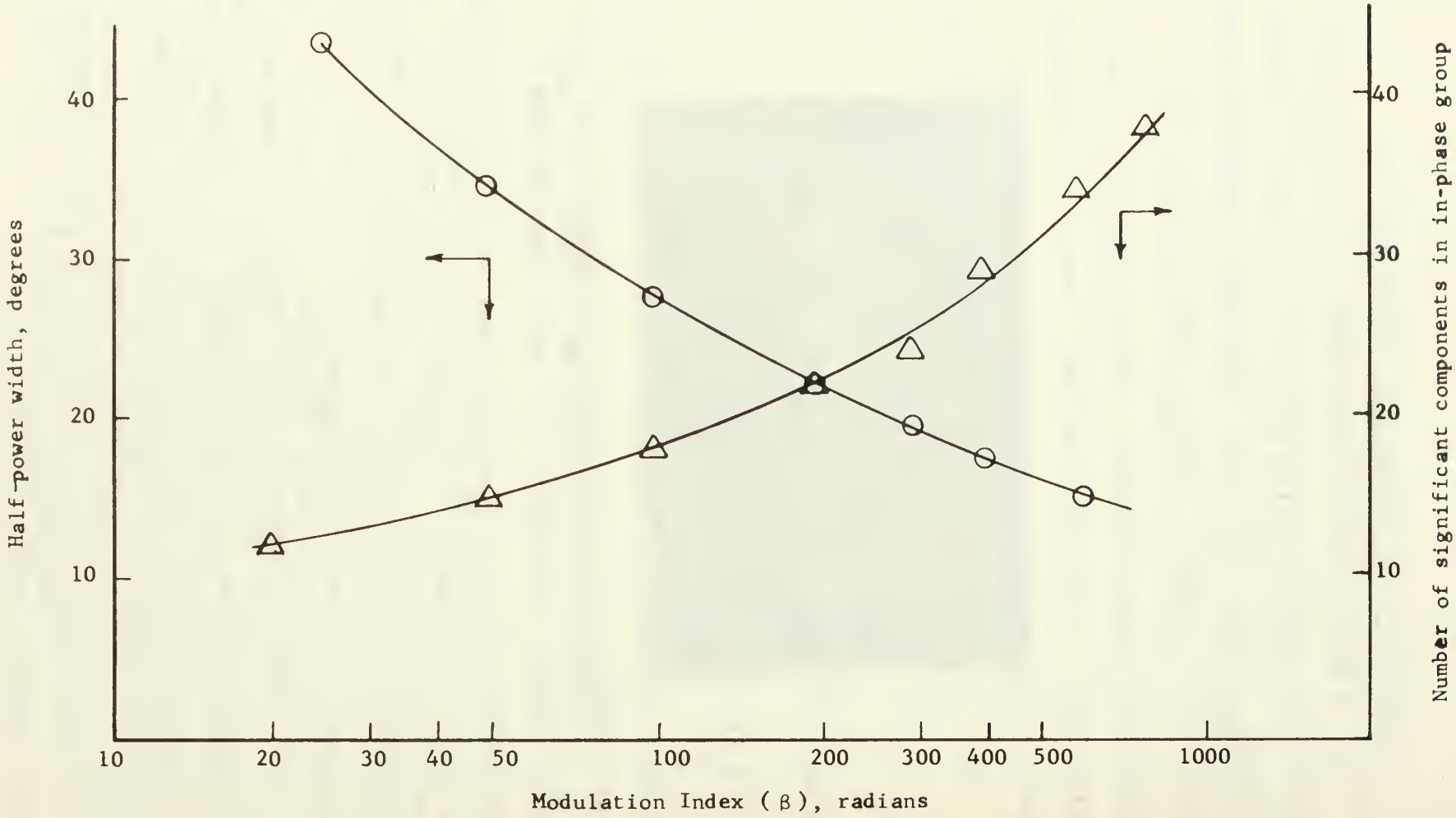

FIG. 15. GRAPH OF THE 3-dB PULSE WIDTH AND THE NUMBER OF SIGNIFICANT COMPONENTS IN THE IN-PHASE GROUP VS β

There is no theoretical limit to the value of β possible and hence to the width of the output pulse (after bandpass filtering the in-phase group). This can be interpreted, for DF purposes at least, as corresponding to superdirectivity in the time domain. The term superdirectivity is used in the sense that, given a signal from a finite-aperture antenna, a waveform can in theory be produced which has a main pulse of duration less than the duration of a pulse formed by the scanning beamwidth of the antenna pattern produced by a uniformly excited aperture of the same size. This corresponds to the broad definition of superdirectivity given by Tucker [19]. The concept of superdirectivity will be considered in Chapter III with regard to the processing of the output of rotating antennas.

III. RADIO DIRECTION FINDING WITH ROTATING ANTENNAS

A single rotating receiving element, used to this point to explain the MFD DF technique, is but one of many possible forms of rotating antennas. This chapter considers rotating antennas in general, with emphasis on their direction-finding capabilities. The purpose of the chapter is

1. To unify a number of previously known results of antenna theory and to apply these results to rotating antennas.

2. To extend these results to include signal processing of the output of rotating antennas, and

3. To apply these results to the specific case of MFD DF.

Antennas which rotate at a constant rate convert spatial information to temporal information. Once this conversion has occurred, signal processing techniques can be applied to produce a waveform from which desired spatial information, such as the bearing of a radio source, can be accurately extracted. In the analysis of rotating antennas it proves useful to consider a Fourier transform representation of the azimuthal distribution of far-field sources. In the transform domain, antennas are shown to act as "filters" to the far-field sources.

The general theory of rotating antennas is applied to the case of a single rotating element and it is argued that the output of such an antenna, by virtue of its spectral

characteristics, contains as much directional information as the pattern of a highly directive array of the same aperture size. This is confirmed by the results of Chapter II.

A. THEORY OF ROTATING ANTENNAS

1. Basic Formulation

Consider a one-dimensional aperture or an antenna array with a far-field pattern $y(\theta)$. For a receiving antenna this means that its output $v(t)$ due to a point source radiating a sinusoid of frequency f_c and located at an azimuth θ_o is given in phasor notation by

$$v(t) = \int_{-\pi}^{\pi} y(\theta)\phi(\theta - \theta_o)e^{j\omega_c t}\, d\theta \qquad (15\text{-a})$$

where $\delta(\theta - \theta_o)$ is the ordinary Dirac delta function. From the property of delta functions, (15-a) becomes

$$v(t) = y(\theta_o)e^{j(\omega_c t)} \qquad (15\text{-b})$$

Although frequently not considered, $y(\theta)$ may have a phase characteristic as well as an amplitude characteristic. We observe from (15-b) that v experiences a sinusoidal time variation. In the following development, this time variation is implied when writing v as a function of azimuthal angle.

If the antenna is pivoted at its center and may be rotated, an additional variable, angle γ of rotation, is

is introduced and the antenna pattern as a function of two variables becomes $y(\theta - \gamma)$.

In the general case, which includes distributed far-field sources given by $z(\theta)$, (15-a) becomes

$$v(\gamma) = \int_{-\pi}^{\pi} y(\theta - \gamma) z(\theta) d\theta \tag{16}$$

where $v(\gamma)$ and $z(\gamma)$ are understood to be sinusoidal time functions [20].

If $y(\theta)$ is assumed to be an even function, (16) can be written as

$$v(\gamma) = \int_{-\pi}^{\pi} y(\gamma - \theta) z(\theta) d\theta \tag{17}$$

The right-hand member is in the form of a convolution integral except for the finite limits of integration. In (17) $v(\gamma)$ is a periodic function because $y(\gamma-\theta)$ is periodic in γ and $v(\gamma)$ can therefore be expanded in a Fourier series which has a Fourier transform consisting of discrete components. However, for the following development it is useful to define a modified function, $v_1(\gamma)$ having a continuous Fourier transform. The results are then related to the periodic case. To establish $v_1(\gamma)$ the function $y_1(\theta)$ is introduced such that

$$y_1(\theta) = \begin{cases} y(\theta) & -\pi \leq \theta \leq +\pi \\ 0 & \text{elsewhere.}^3 \end{cases} \tag{18}$$

---

[3] A single exception is the case where $y(\theta)$ is constant. In this case $y_1(\theta) = y(\theta)$.

Equation (17) can then be rewritten with extended limits of integration as

$$v_1(\gamma) = \int_{-\infty}^{\infty} y_1(\gamma - \theta) z(\theta) d\theta \ . \tag{19}$$

This formulation is similar though somewhat more general than that given by Bracewell and Roberts [20]. Since the modified variables $y_1(\theta)$ and $v_1(\gamma)$ as well as $z(\theta)$ have continuous Fourier transforms, it proves useful to examine their Fourier transform representation.

2. Fourier Transform Representation

Consider the Fourier transform of a function of θ (or γ) such as $z(\theta)$,

$$Z(\zeta) = \int_{-\infty}^{\infty} z(\theta) e^{-j2\pi\zeta\theta} d\theta \ . \tag{20}$$

By analogy to the Fourier transform of a time function, ζ may be considered a frequency variable. It has no physical significance comparable with the physical meaning associated with frequencies arising from the Fourier transform of a time function.

The variable ζ is related to spatial frequency η which arises when the Fourier transform of an antenna pattern, expressed as a function of $u = \sin\theta$, is taken as

$$G(\eta) = \int_{-\infty}^{\infty} g(u) e^{-j2\pi u\eta} du \ . \tag{21}$$

It must be emphasized that the variables ζ and η are not linearly related except when $\theta \simeq \sin\theta$. Therefore, in the antenna literature, results given in terms of spatial frequency η are not, in general, directly applicable to the ζ-frequency representation [21]. One well-known result concerning spatial frequency comes from the fact that the far-field pattern g(u) of a one-dimensional unidirectional antenna oriented along the x-axis is proportional to the Fourier transform of the aperture excitation function $D(x/\lambda)$,

$$g(u) \alpha \int_{-\infty}^{\infty} D(x/\lambda) e^{-j2\pi u(x/\lambda)} \, d(x/\lambda) \qquad (22)$$

where θ is measured from a perpendicular to the x-axis as shown in Fig. 16 [22].

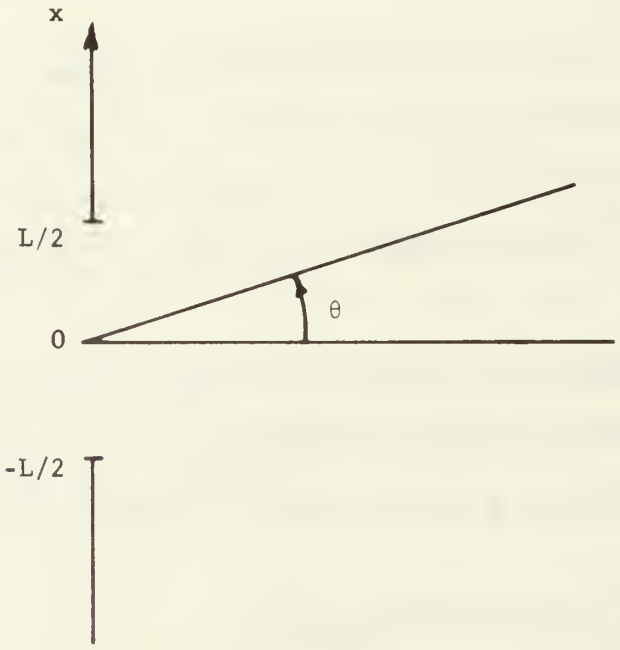

FIG. 16. ONE-DIMENSIONAL APERTURE AND RELATED GEOMETRY

The inverse transform is given by

$$D(x/\lambda) \propto \int_{-\infty}^{\infty} g(u) e^{j2\pi u(x/\lambda)}\, du \tag{23}$$

Because this integral includes a region of u which is physically meaningless, that is $|u|>1$, the following result is meaningful only for directive antennas for which $g(u)\to 0$ when $|u|\to 1$.

By noting the similarity between (21) and (23) it is seen that directive antennas have spatial frequency functions $G(\eta)$ which are proportional to the spatial excitation $D(x/\lambda)$ of the aperture. Because the aperture is absolutely limited in extent, the spatial frequencies are absolutely limited also [21]. It must be emphasized that this result applies to the ζ-frequency representation only in cases where $g(u)$ approaches zero while $\sin\theta$ and θ are interchangeable.

Having defined the Fourier transform of a function of azimuth angle, (19) can be considered again. The Fourier transform of $v_1(\theta)$ in (19) is given from the convolution theorem by

$$V_1(\zeta) = Y_1(\zeta) \cdot Z(\zeta) \tag{24}$$

If the antenna excitation is considered a linear process then the antenna itself may be considered a "filter" $Y_1(\zeta)$ acting upon the ζ-spectral characteristics of the far field, $Z(\zeta)$. The "filter" characteristics can be controlled to

some extent by the designer, so it is important to determine what characteristics are desirable in a DF system.

In order to obtain an exact azimuth bearing and perfect resolution, an ideal antenna pattern is a delta function

$$y_1(\theta-\gamma) = \delta(\theta-\gamma) \ . \tag{25}$$

In the ζ domain this gives

$$Y_1(\zeta) = e^{-j2\pi\zeta\gamma} \tag{26-a}$$

from which

$$|y_1(\zeta)| = 1 \ . \tag{26-b}$$

Correspondingly, a point source at azimuth θ_o is described by

$$z(\theta) = \delta(\theta-\theta_o) \tag{27}$$

and in the ζ domain,

$$Z(\zeta) = e^{-j2\pi\theta_o} \tag{28-a}$$

and

$$|Z(\zeta)| = 1 \ . \tag{28-b}$$

The ideal point source therefore has ζ-frequency components extending over the entire ζ spectrum and the transfer function of the ideal DF antenna preserves all these components. This results in a delta function for

the output $v_1(\theta)$ which gives the azimuth angle of the source precisely.

Consider by means of an example what occurs in the case of a real antenna. Suppose the antenna pattern is given by

$$y_1(\theta) = \frac{K}{\sqrt{2\pi\sigma}} e^{-\theta^2/2\sigma^2} \tag{29}$$

where σ is such that $y_1(\theta)$ is very small when $|\theta| \geq \pi/2$.

The transform of (29) is given by

$$Y_1(\zeta) = Ke^{-2\pi^2\sigma^2\zeta^2} \ . \tag{30}$$

If we consider for simplicity a point source at zero degrees of azimuth then,

$$z(\theta) = \delta(\theta) \tag{31}$$

The antenna output is given in the ζ domain by

$$V_1(\zeta) = Y_1(\zeta) \cdot Z(\zeta) \ , \tag{32-a}$$

$$V_1(\zeta) = Ke^{-2\pi^2\sigma^2\zeta^2} \cdot 1 \ . \tag{32-b}$$

Comparing this result with the ideal case it can be seen that a real antenna has a "filter" characteristic which attenuates ζ-spectral components of the far-field source in proportion to ζ. Obviously, as the antenna pattern $y_1(\theta)$ gets narrower (σ decreases) the corresponding transfer function $Y_1(\zeta)$ becomes broader. Conventionally, the directivity of an antenna pattern is increased by making

the antenna larger in aperture which has, of course, practical limitations. Since real antennas have patterns which extend over a finite range of θ their transfer functions in the ζ domain are never all-pass as in the ideal case but taper off in magnitude with ζ in some fashion, depending on the specific antenna. This contrasts with the spatial frequency approach in which the spatial frequency representation of an antenna pattern is absolutly limited along the η-axis. The example just given in (29)-(32) shows that the ζ-frequency transform of an antenna pattern does <u>not</u> have absolute limits though its magnitude does decrease directly with ζ. Davies and Longstaff [23] arrived at this same basic result for the case of a rotating linear array.

As mentioned previously, an antenna pattern ideal for DF is one with an arbitrarily narrow beamwidth. The quest for unlimited directivity leads to consideration of superdirective antennas which are broadly defined as antennas which exceed the directivity of a uniformly excited antenna of the same size [19]. The theory of superdirective (or supergain) antennas shows that there is no limit to the directivity that can be achieved with a finite aperture antenna; however, supergain is difficult to achieve in practice [24].

Ksienski [21] has shown that superdirective antennas cannot be characterized in terms of spatial frequency u because the simple Fourier transform relationship between

the antenna excitation function and the far field pattern given by (22) and (23) loses its physical connotation. That is, classical superdirective antennas have far-field patterns which have finite theoretical values, outside of the range of real angles ($|u|>1$). Hence, the assumption which allowed use of limits of $\pm\infty$ in (23) does not hold. On the other hand Davies and Longstaff [23] showed by means of an example which is directly applicable to ζ frequencies that conventional techniques for designing supergain arrays have the effect of attenuating the lower ζ components to make them comparable in amplitude to the higher ζ components or in effect broadening the "filter" passband by emphasizing the higher ζ frequencies. Consequently, this suggests an alternate definition of supergain as any technique which increases the directivity of an antenna beyond that of an equivalent uniformly excited antenna by increasing its ζ-spectrum passband without increasing its aperture.

3. Time-Domain Processing

In the preceding paragraphs antennas have been considered in terms of their ζ-frequency characteristics. If it were possible to convert ζ frequencies to real frequencies, the converted output of an antenna could be processed to achieve an overall transfer function including the antenna and the processor which produces in the time domain a waveform with good directional characteristics, perhaps even superdirectivity. Assuming that the conversion to the

real frequency domain is possible, as will be demonstrated, such a system is shown in block diagram form as Fig. 17.

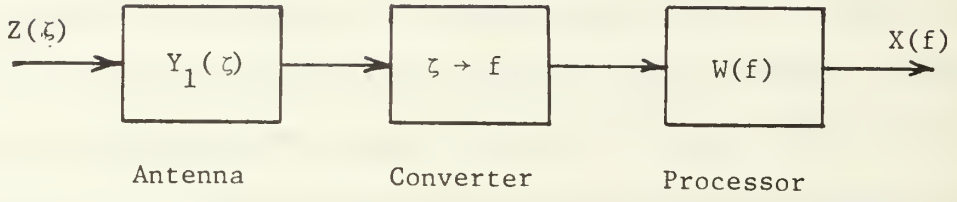

FIG. 17. BLOCK DIAGRAM OF A FREQUENCY-PROCESSING RECEIVING SYSTEM

From basic transform algebra, for a linear system,

$$W(f) = H(f)\, Y_1(f)\, Z(f) \tag{33}$$

As discussed previously, it is desirable that W(f) equal Z(f), so that w(t) is a delta function. This requires that

$$1 = H(f)\, Y_1(f) \tag{34-a}$$

from which

$$H(f) = 1/Y_1(f) \; . \tag{34-b}$$

This makes H(f) the inverse filter of $Y_1(f)$. In a similar context, Davies and Longstaff [23] refer to the inverse filter implicitly in proposing a filter that equalizes all frequency components to the same magnitude. For the example given previously by (29)-(32),

$$Y_1(f) = Ke^{-2\pi^2\sigma^2 f^2} \quad . \tag{35}$$

Therefore, from (34-b)

$$H(f) = \frac{e^{2\pi^2\sigma^2 f^2}}{K} \quad . \tag{36}$$

H(f) is a perfectly acceptable processor transfer function in a noiseless environment and the processor output w(t) corresponds to an arbitrarily narrow voltage pulse; however, in the presence of white noise, the inverse filter for functions such as $Y_1(f)$ accentuates the noise spectrum indefinitely at high frequencies and is thus not practical. Qualitatively, it should be noted that the inverse filter broadens the input spectrum by accentuating the higher frequencies and hence satisfies the alternate definition of supergain proposed in section A.2 of this chapter.

The best known compromise to the inverse filter is the matched filter which for a given signal maximizes the SNR at the filter output at some instant of time based on knowledge of the noise spectral density [15]. Usually, additive white gaussian noise is assumed.

It is necessary at this point to digress briefly to relate the results obtained using $y_1(\theta)$, a truncated version of the actual antenna pattern $y(\theta)$, to the actual situation. By using $y_1(\theta)$ it was possible to make the preceding ζ-frequency development by means of continuous Fourier transforms and basic transfer-function algebra.

Since $y(\gamma)$ and the antenna output $v(\gamma)$ are periodic functions of the rotation angle γ, they can be expanded in a Fourier series having a spectrum of discrete components in the ζ-frequency domain. The envelope of these discrete spectral components corresponds to the hypothetical $V_1(\zeta)$ or $Y_1(\zeta)$, just as the envelope of the Fourier transform of a rectangular pulse train corresponds to the transform of a single pulse. With this distinction in mond the conclusions arrived at in the preceding sections are applicable.

4. Conversion of ζ frequencies to Real Frequencies

The process of converting ζ frequencies to real frequencies is straightforward. When a linear antenna or array rotates at a constant rate ω_r, its output is given from (17) by

$$v(\omega_r t) = \int_{-\pi}^{\pi} y(\omega_r t-\theta)z(\theta)d\theta \qquad (37)$$

What previously was a function of γ becomes a function of time which repeats every $2\pi/\omega_r$ seconds.[4] The Fourier transform of the output is no longer in the ζ-frequency domain but rather in the real-frequency domain. Uniform rotation of the antenna can be thought of as producing a transformation of variable from ζ to f. As discussed previously the antenna output can then be processed as desired.

---

[4] The repetition period is only π/ω_r seconds for linear arrays which are usually bidirectional in their pattern.

B. ONE ROTATING ELEMENT

This section applies the general theory of rotating antennas to the specific case of a single rotating element which is omnidirectional in the plane of propagation. It is shown that the output of such an antenna contains directional information which, of course, confirms the results obtained in Chapter II using a different approach.

A single, fixed vertical dipole has a horizontal antenna pattern given by

$$y_1(\theta) = K \tag{38}$$

In the ζ domain this becomes

$$Y_1(\zeta) = K\,\delta(\zeta) \tag{39}$$

As a filter to the ζ-spectrum of a far-field point source this antenna has an extremely narrow bandpass. Since directive antennas have been associated with broad ζ-spectral bandpasses, one would expect the fixed dipole on this basis to have little directivity in the horizontal plane. The output of the dipole due to a point source at $\theta_o = 0$ is, in phasor notation

$$v(t) = Ke^{j\omega_c t} \tag{40}$$

As expected, neither the envelope nor the phase of the output voltage contains information about the signal AOA.

However, if a dipole which is omnidirectional in the plane of the circle of Fig. 18 is placed a distance ℓ from

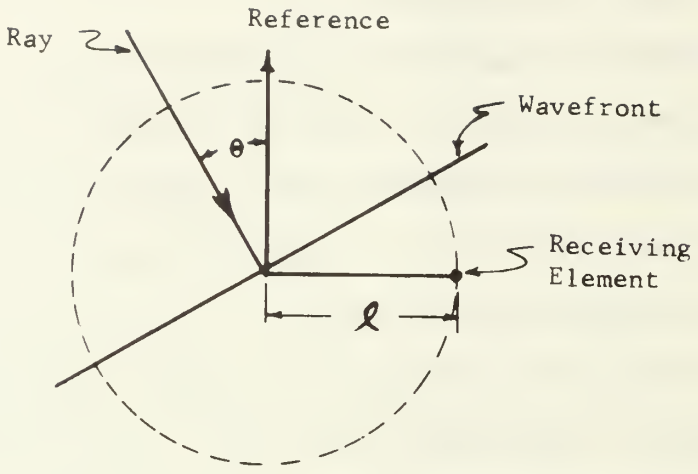

FIG. 18. PLAN VIEW OF THE ROTATABLE ELEMENT

a central reference point and oriented initially in azimuth as shown, its excitation pattern is given in phasor notation as

$$y(\theta) = Ke^{-j\frac{2\pi\ell}{\lambda_c}\sin\theta} \tag{41}$$

where the phase is measured relative to that of the voltage measured at the center of rotation in Fig. 18. If the element is displaced γ radians counter-clockwise around the circle, the pattern becomes

$$y(\theta-\gamma) = Ke^{j\frac{2\pi\ell}{\lambda_c}\sin(\gamma-\theta)} . \tag{42}$$

If the element rotates at a constant rate f_r, the pattern becomes a function of time and azimuth,

$$y(\theta-\omega_r t) = Ke^{j\frac{2\pi\ell}{\lambda_c}\sin(\omega_r t-\theta)} . \qquad (43)$$

The Fourier transform of $y(\theta,\omega_r t)$ is

$$Y(f) = K \sum_{k=-\infty}^{\infty} J_k(\frac{2\pi\ell}{\lambda_c})e^{-jk\theta}\delta(f-kf_r) . \qquad (33)$$

The bandwidth Ω of $Y(f)$ is proportional to the size of the aperture diameter of rotation in wavelengths ($\Omega \simeq \frac{4\pi\ell f_r}{\lambda_c}$). Since, from Fourier transform theory, pulse duration is proportional to the inverse of bandwidth, then the minimum pulse duration obtainable from the response of this antenna to a far-field point source is approximately $\frac{\lambda_c}{4\pi\ell f_r}$ seconds. The pulse repeats every $1/f_r$ seconds, which corresponds to one 360-degree scan in azimuth, so the minimum width of the pulse in radians is given by

$$2\pi \frac{\frac{\lambda_c}{4\pi\ell f_r}}{\frac{1}{f_r}} = \frac{\lambda_c}{2\ell}$$

As pointed out by Davies and Longstaff, who were considering the outer elements of a rotating array, this corresponds roughly to the common rule of thumb for the pattern of a directive linear array, namely, that the beamwidth in radians is approximately equal to the wavelength λ_c divided by the array length, 2ℓ,

$$\text{beamwidth} = \frac{\text{wavelength}}{\text{array length}} = \frac{\lambda_c}{2\ell}$$

This suggests that the output of a single rotating element contains enough directional information to determine the AOA with at least as much accuracy as a directional array of comparable aperture.

This fact is confirmed theoretically in Fig. 7-a which shows that the output waveform of a filter matched to the output of a rotating antenna with a diameter of about eight wavelengths ($\beta = 25$) has a 3 dB width of 5.0 degrees. The calculated beamwidth of a uniformly excited linear array eight wavelengths long is 7.2 degrees.

IV. HARDWARE SIMULATION AND PERFORMANCE OF A MATCHED-FILTER DOPPLER DF SYSTEM

This chapter reports on the results of a hardware simulation of the MFD DF system. The experimental system also defines some of the limitations of the new technique arising from the use of conventional electronic hardware. A series of experiments produced data on the effect of noise on the system for both multiplicative and non-multiplicative processing. The experimental system was also used with an operational doppler DF system. The results of this test confirm the principal features of the matched-filter technique.

A. SYSTEM DESCRIPTION

The experimental system is shown in block diagram form in Fig. 19. The output of a rotating antenna (or equivalent array) is simulated by a voltage controlled oscillator (VCO) which is frequency modulated at a rate of f_r Hz corresponding to the scanning rate of an actual doppler DF system. The processing begins with an optional frequency-multiplier section capable of multiplication by a factor of two or four (Fig. 20). A balanced mixer and a variable local oscillator are used to shift the signal spectrum in order to bring any desired group of frequencies within the filter passband.

The filter output, which contains the desired AM, is available for display immediately, or if desired the RF

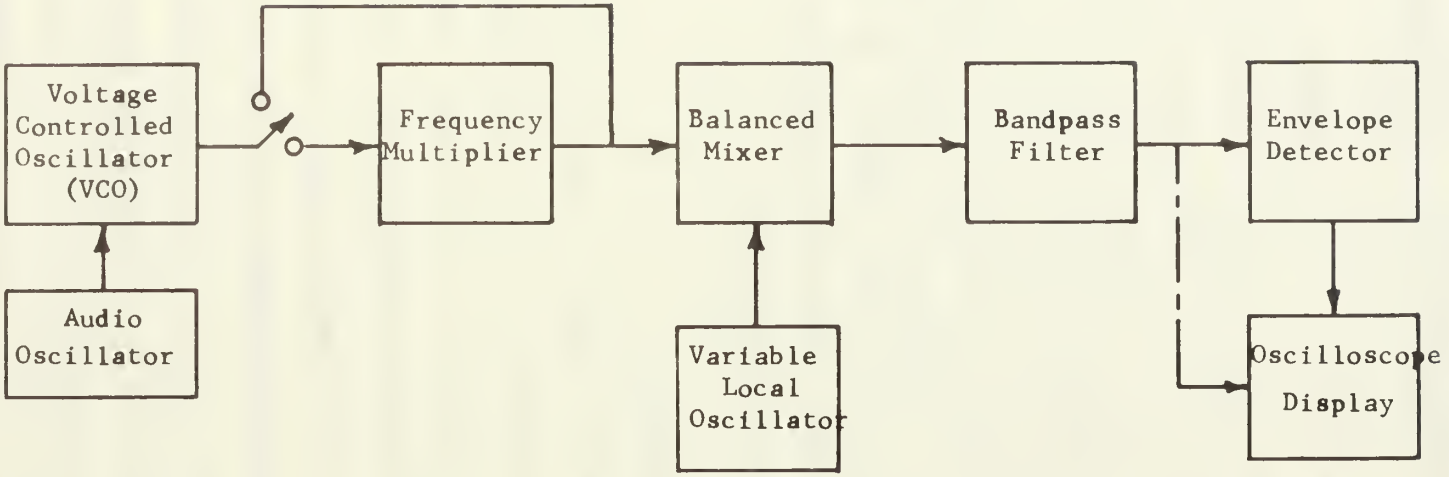

FIG. 19. BLOCK DIAGRAM OF THE EXPERIMENTAL MFD DF SYSTEM

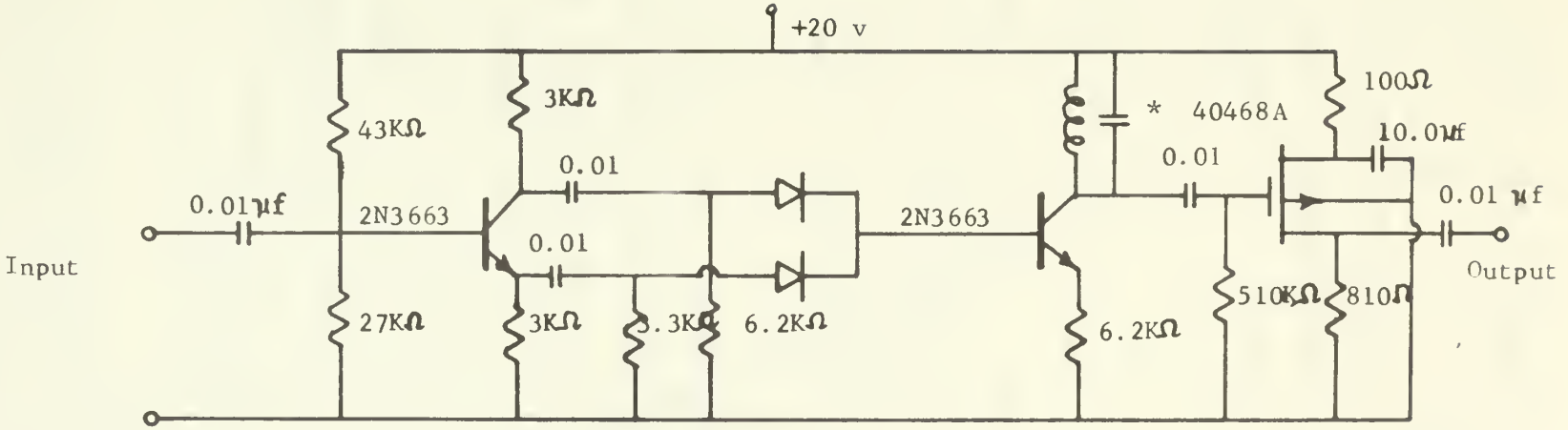

*Tank circuit tuned to the second harmonic of the input signal

FIG. 20. CIRCUIT DIAGRAM OF THE FREQUENCY DOUBLER

can be first passed to a simple diode envelope detector to obtain the AM voltage.

The critical hardware component is the bandpass filter. The filter must pass only the desired spectral components, and the filter phase characteristic must be relatively linear. The required filter bandwidth is determined by the separation of f_r Hz of the discrete frequency components and by the number of significant components in the in-phase group. This number of components depends on the modulation index (β) of the signal applied to the filter. A modulation or scanning rate of f_r = 100 Hz is used because it is comparable to the scanning rates of some conventional doppler DF systems.

After limited experimentation with tuned, ceramic, and mechanical filters, a Clevite ceramic filter (TL-10D9-20A) with a nominal passband of 10 kHz centered at 455 kHz was found to give results which most nearly approach the waveforms obtained by digital computation. The characteristics of the filter used are shown in Fig. 21. For some experiments, a Clevite filter (TL-4D8A) with a narrower passband of about 4 kHz was also used. The characteristics of the 4-kHz filter are shown in Fig. 22.

B. CONFIRMATION OF THEORY

1. Processing Without Frequency Multiplication

The important characteristics of a MFD DF system are demonstrated by the following example. The VCO of Fig. 19 generates the following signal,

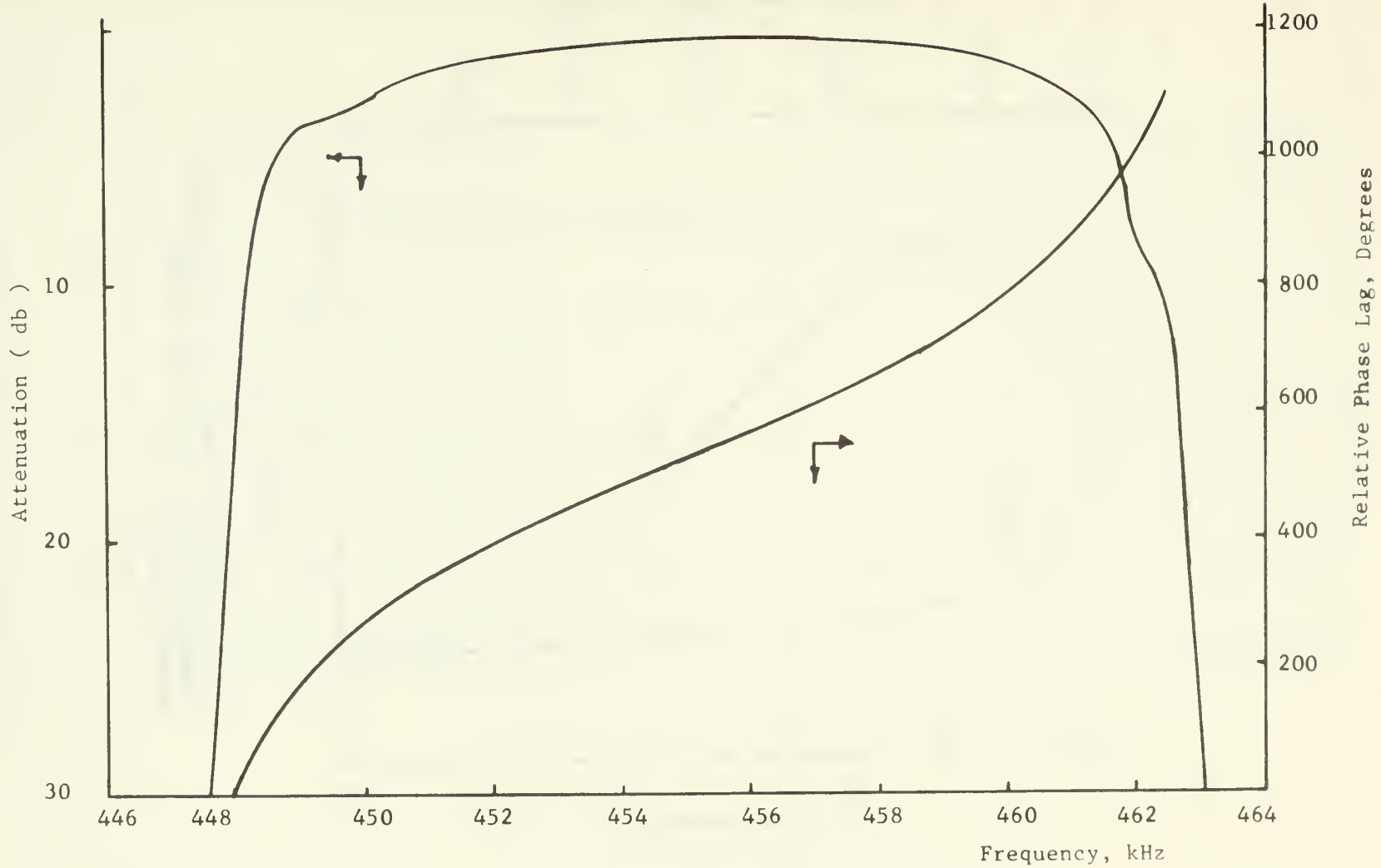

FIG. 21. AMPLITUDE AND PHASE-VS-FREQUENCY CHARACTERISTICS OF THE 10-kHz CERAMIC BANDPASS FILTER

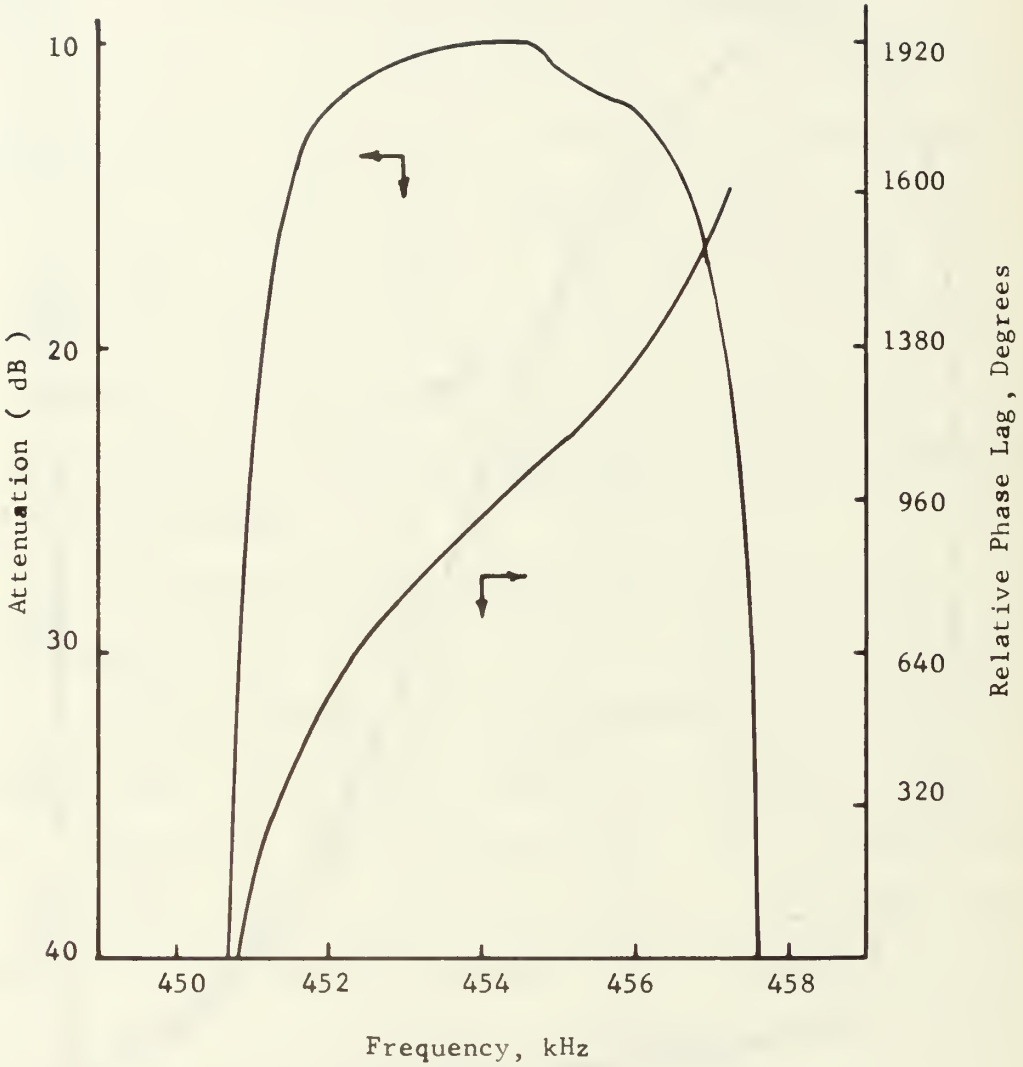

FIG. 22. AMPLITUDE AND PHASE-VS-FREQUENCY CHARACTERISTICS OF THE 4-kHz CERAMIC BANDPASS FILTER

$$s(t) = C\cos(\omega_c t + \beta \sin \omega_r t) \qquad (45)$$

where $f_c = 429$ kHz and $f_r = 100$ Hz.

By adjusting the carrier frequency the signal spectrum is shifted until the in-phase group of spectral components (Fig. 8) is in the filter passband (frequency multiplier bypassed). The resulting filter output before and after envelope detection is shown in Fig. 23. The experimental and calculated envelopes are remarkably similar as can be seen by comparing Fig. 23 with the computed output shown in Fig. 24. The 3-db width of the envelope pulse is about 50 degrees in the experimental case

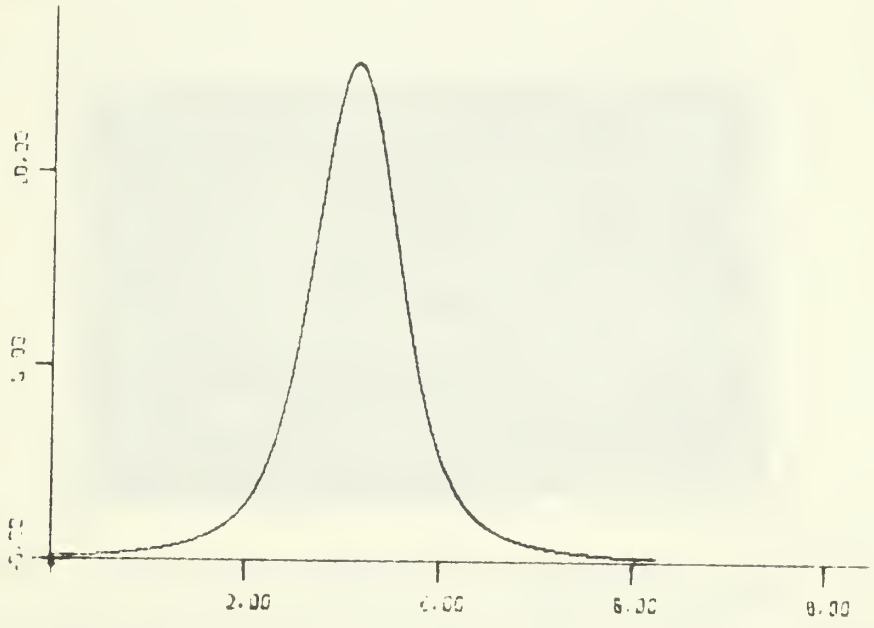

FIG. 24. COMPUTED ENVELOPE OF THE RESPONSE OF AN IDEAL MFD DF SYSTEM

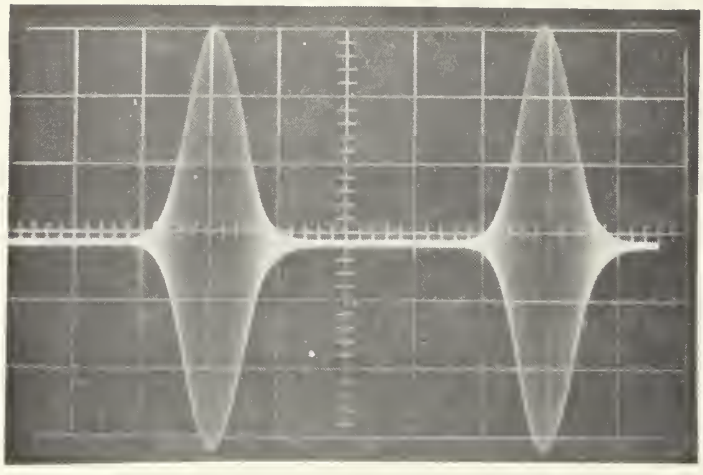

(a) Predetection envelope of bandpass filtered FM by a sinusoid. β is 25.

X Scale: 2 ms/cm

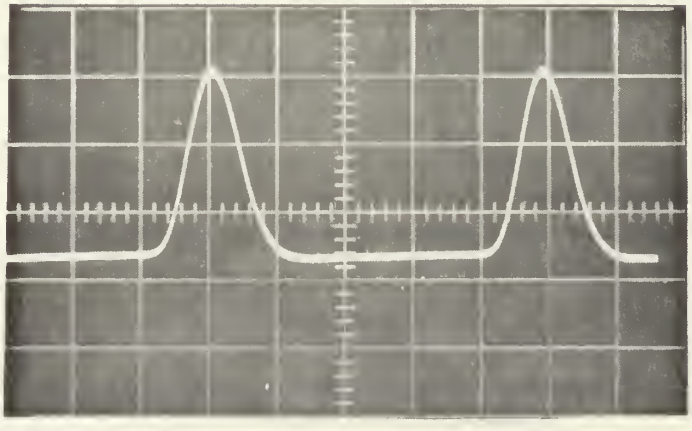

(b) Detected envelope of bandpass filtered FM by a sinusoid. β is 25.

FIG. 23. PHOTOGRAPHS OF THE RESPONSE OF THE EXPERIMENTAL MFD DF SYSTEM

as compared with 43 degrees for the calculated envelope pulse. The difference is due to two factors:

(1) In order to exclude the undesired components some of the desired frequencies are supressed due to the non-ideal "skirt" of the filter.

(2) The nonlinear phase characteristic of the ceramic filter tends to broaden the main lobe of the envelope. The narrowing of the main lobe with increasing β is seen in Fig. 25 which shows the experimental system output for β's of 50 and 100. These pulses can be compared with their calculated versions shown in Fig. 13-c and 13-d of Chapter II.

2. Spectral Symmetry

It was previously shown that the effect of filtering that group of harmonics below the carrier frequency f_r which corresponds to the in-phase group above f_r simply shifts the pulse position in time an amount corresponding to a 180-degree shift in AOA. This is clearly seen in Fig. 26 which shows the envelope of the in-phase group below the carrier frequency for the signal given in (45). The main pulse is shifted one-half of a modulation cycle or 2.5 cm to the left of the position of the pulse shown in Fig. 23. The distortion in Fig. 26 is due to the asymmetry of the ceramic-filter characteristics, i.e., the lower cutoff (filter skirt) is used to separate the in-phase components above the carrier frequency, while the upper

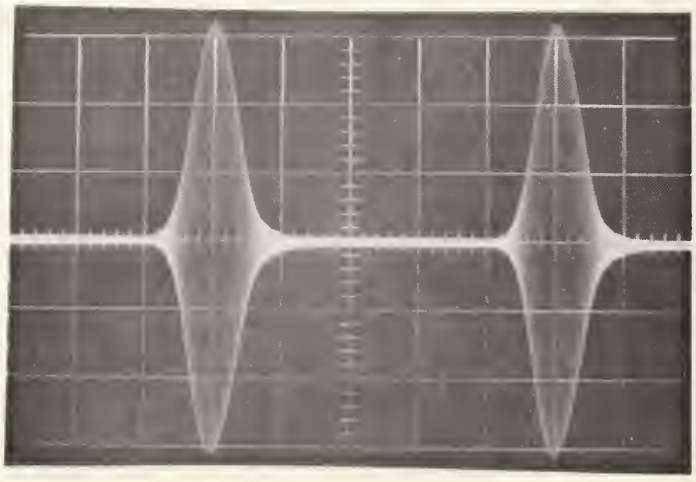

a. β is 50.

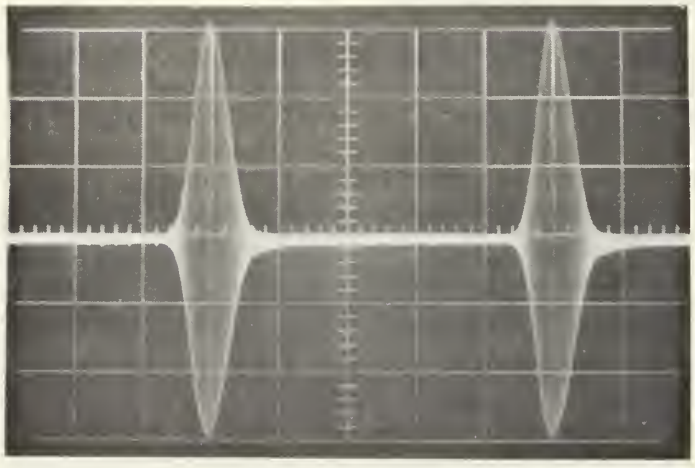

b. β is 100.

FIG. 25. PHOTOGRAPHS OF THE RESPONSE OF THE EXPERIMENTAL MFD DF SYSTEM AS β INCREASES

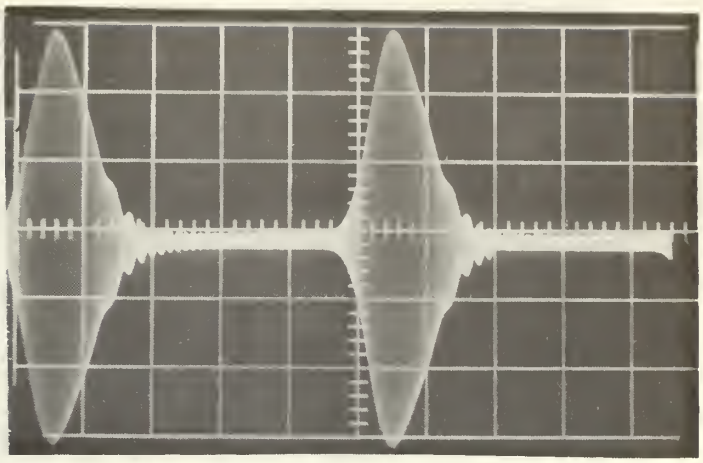

FIG. 26. PHOTOGRAPH OF THE RESPONSE OF THE EXPERIMENTAL MFD DF SYSTEM TO THE IN-PHASE GROUP OF FREQUENCY COMPONENTS BELOW THE CARRIER FREQUENCY

cutoff isolates the corresponding group below the carrier frequency.

3. Processing with Frequency Multiplication

The technique of frequency multiplication to increase β and thereby improve bearing determination by producing a narrower pulse is demonstrated by starting with a signal having a β of 25, and frequency multiplying by a factor of four to increase β to 100 prior to filtering. The filtered RF voltage shown in Fig. 27 has a 3-db width of 31 degrees compared with 50 degrees when β = 25 (Fig. 23), and 27.5 degrees in the ideal case (Fig. 13-c). As expected, the result is almost identical to that obtained by generating a signal with a β of 100 and filtering directly with no multiplication as shown in Fig. 25-b.

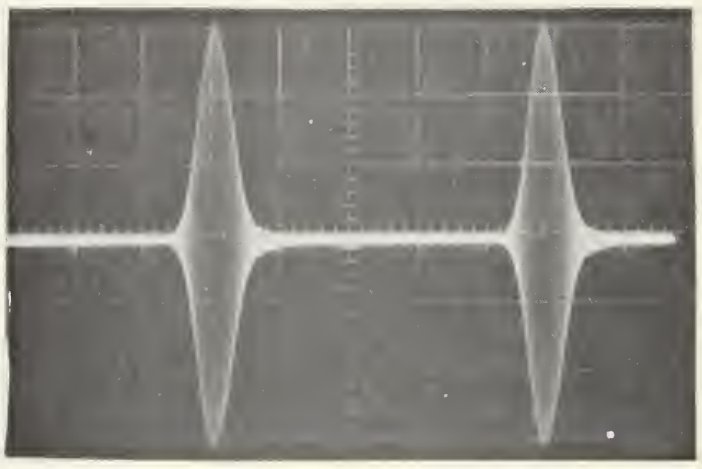

(a) Predetection envelope of bandpass filtered FM by a sinusoid after multiplication by four. β increased from 25 to 100.

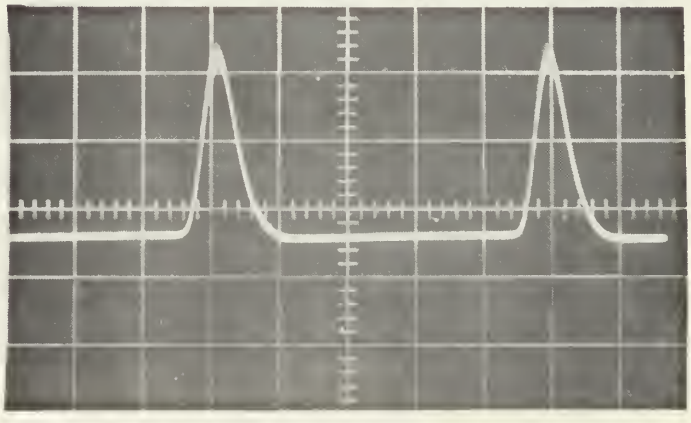

(b) Same as (a) after envelope detection.

FIG. 27. PHOTOGRAPH OF THE RESPONSE OF THE EXPERIMENTAL MFD DF SYSTEM WHICH INCLUDES FREQUENCY MULTIPLICATION BY A FACTOR OF FOUR

C. IMPERFECT FILTERING EFFECTS

In earlier sections of this report it has been shown that the last group of in-phase spectral components above (or below) the carrier frequency contains AOA information in its periodic envelope. This section examines the effect of imperfect filtering of the in-phase group from the remaining components of the spectrum of the rotating antenna output.

The inclusion in the filter passband of harmonics of lower frequency than the in-phase group is shown to produce the underirable effect of splitting the main lobe of the output envelope and reducing its amplitude. It will also be seen that the exclusion of harmonics in the in-phase group reduces the amplitude of the main lobe and broadens it, but this exclusion does not alter the position of the main lobe. Hence no error is introduced in the AOA measurement.

Imperfect filtering may occur for the following reasons:

(1) Realizable bandpass filters do not have infinite cutoff characteristics.

(2) Local oscillator mistuning can shift the spectrum presented to the bandpass filter.

Regardless of the modulation index β the spectral components of a signal which is frequency modulated by a sinusoid possess a pattern of alternating in-phase and out-of-phase groups of side frequencies as shown earlier in Figs. 5 and 6. For experimental convenience, the

investigation of the effect of imperfect filtering is carried out for the case of $\beta = 118$; but the results are generally applicable for all values of β greater than about 10.

The partial spectrum for $\beta = 118$ is shown in Fig. 28. The last in-phase group begins with the 109th harmonic of the scanning frequency f_r above the carrier frequency f_c and extends to the last significant harmonic which is the 127th. The calculated envelope of the in-phase group is shown in Fig. 29. As harmonics below the 109th are included in the filter passband they have an adverse effect on the envelope as seen in Fig. 30 because the first group of undesired harmonics (103-108) are relatively out-of-phase

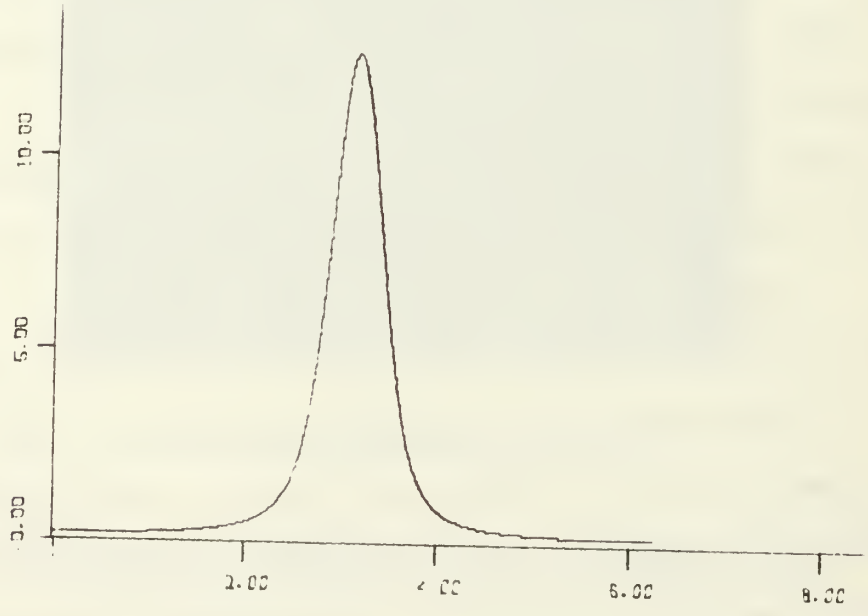

FIG. 29. COMPUTED ENVELOPE OF THE RESPONSE OF AN IDEAL MFD DF SYSTEM

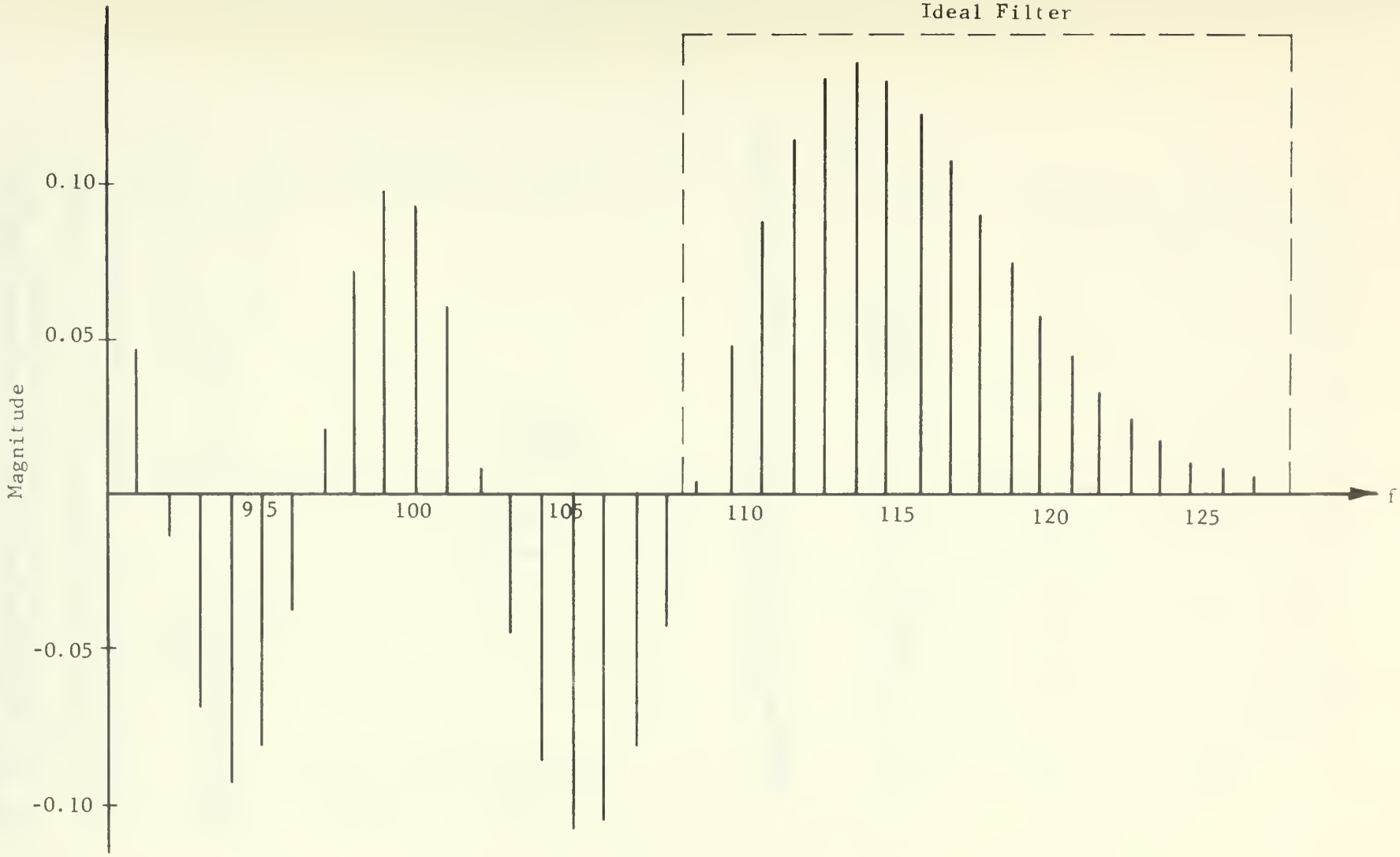

FIG. 28. PARTIAL SPECTRUM OF FM BY A SINUSOID

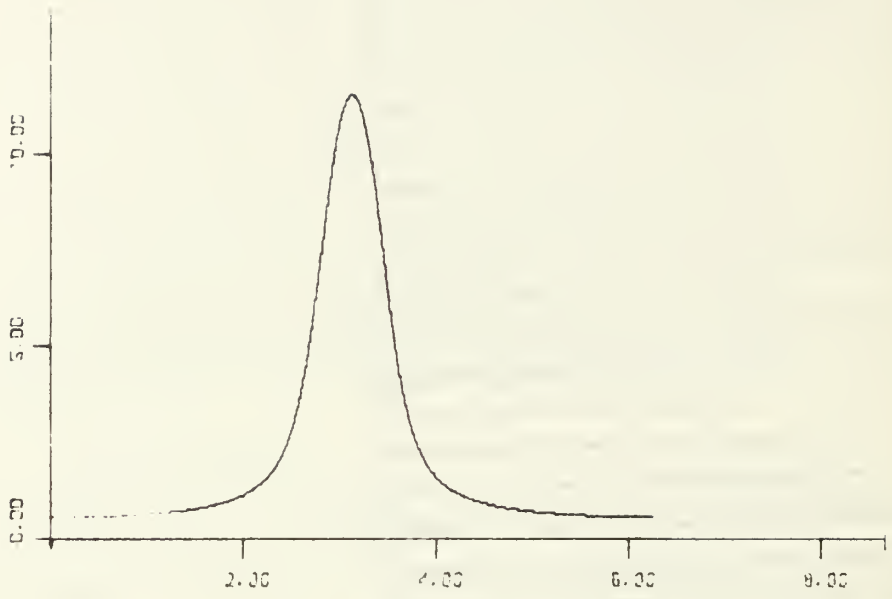

(a) Envelope when harmonics 107 and 108 are included

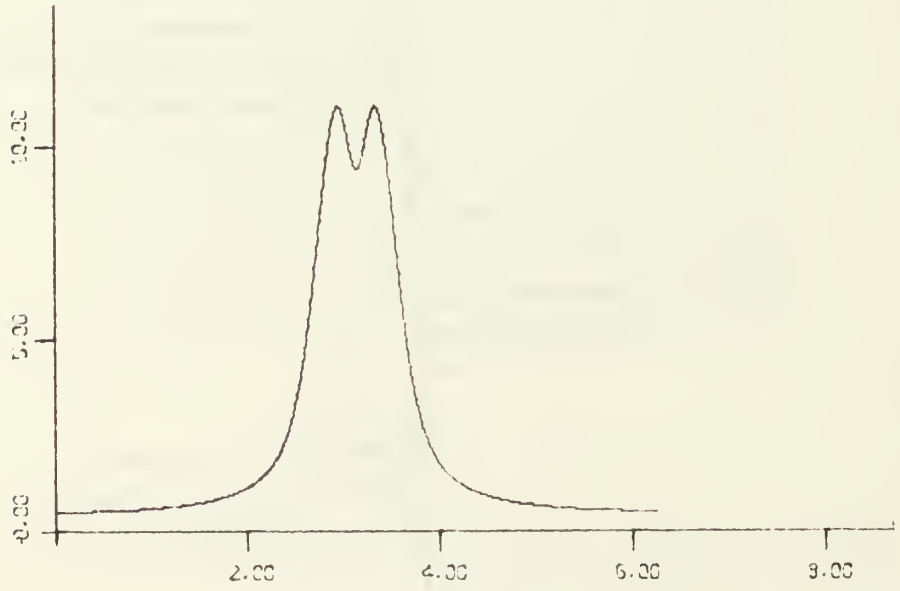

(b) Envelope when harmonics 105 - 108 are included

FIG. 30. THEORETICAL RESPONSE OF A MFD DF SYSTEM AS UNDESIRED FREQUENCY COMPONENTS ARE PROCESSED

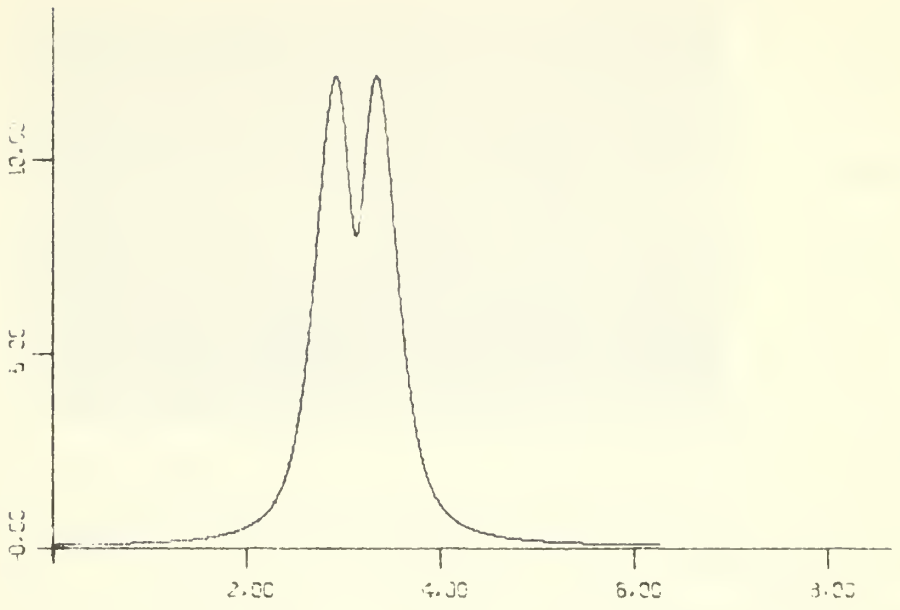

(c) Envelope when harmonics 103 - 108 are included

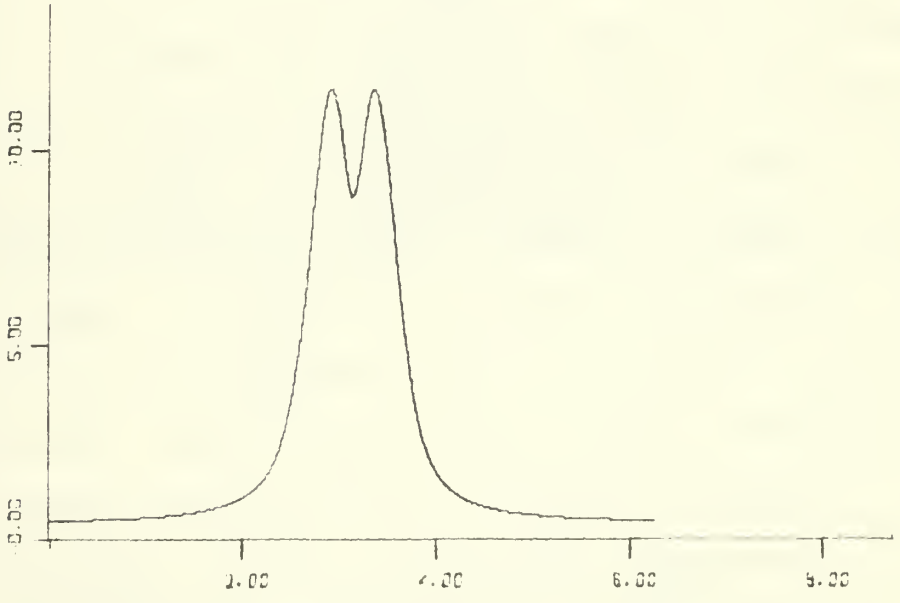

(d) Envelope when harmonics 101 - 108 are included

FIG. 30. THEORETICAL RESPONSE OF A MFD DF SYSTEM AS UNDESIRED FREQUENCY COMPONENTS ARE PROCESSED

at the instant that the in-phase group is in phase. This reduces the peak value of the envelope and, in addition, as more harmonics are included there is an interaction between the components in the in-phase and out-of-phase groups which produces a splitting of the main lobe of the envelope.

Because realizable filters have finite cutoff characteristics, it is impossible to duplicate experimentally the condition from which the computer-drawn envelopes of Fig. 30 are obtained. It is possible, however, to shift the sinusoidal FM spectrum in the experimental system described earlier in such a way as to include in the passband a number of spectral components below the 109th harmonic. The results are presented in Figs. 31-33 as undesired frequency components are brought into the filter passband. They substantially confirm the computer results. Figure 31-a shows an output closely resembling the theoretical result given as Fig. 29. Figures 32-a and 33-a show the emergence of the second peak which did not grow to the same size as the first, probably due to the nonlinearity of the phase characteristic of the 10-kHz ceramic filter. Along with each photograph is shown the spectrum which appears at the output of the filter (Figs. 31-b - 33-b). The dotted spectral lines indicate the magnitudes prior to filtering.

Of as much interest as the inclusion of undesired harmonics is the exclusion of some of the desired ones. This is explored for the ideal case in the computer-drawn

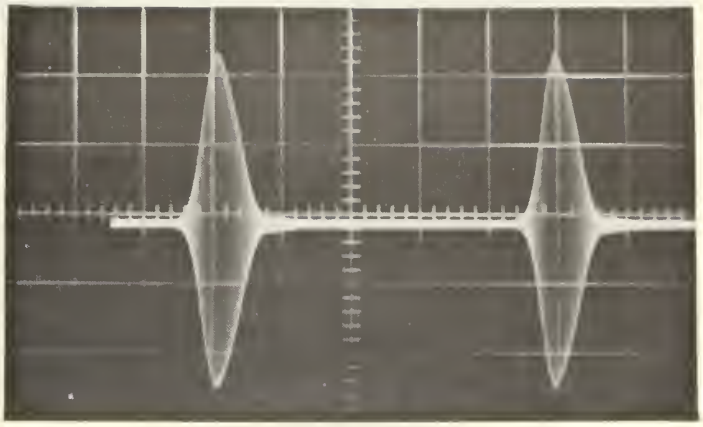

(a) Envelope of the spectrum shown in Fig. 31(b).

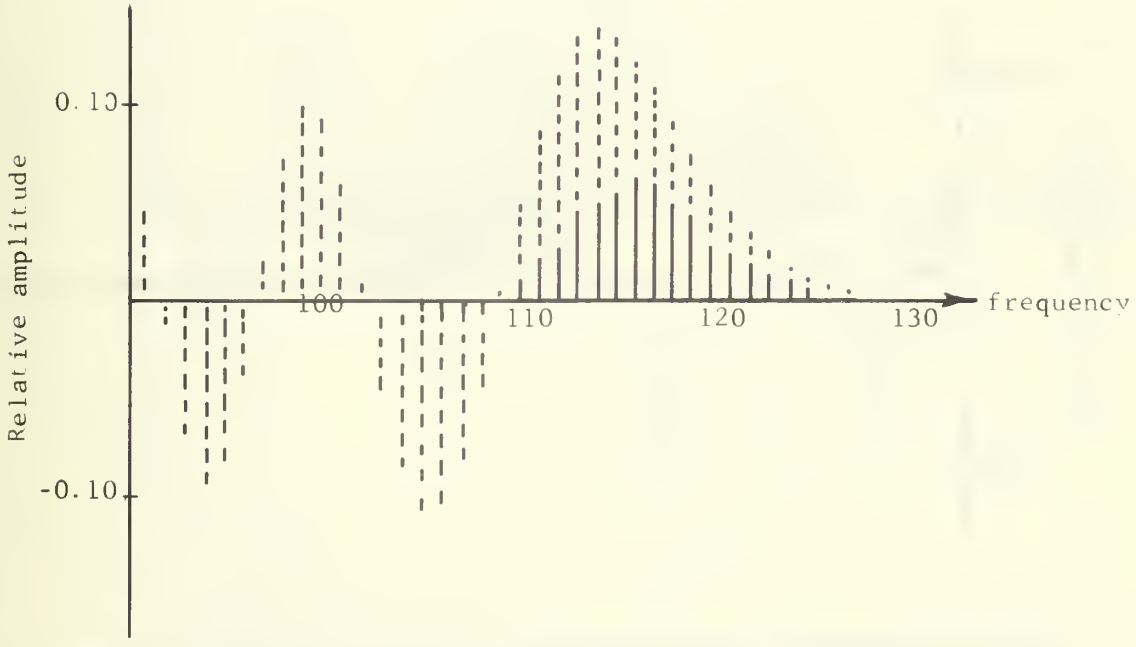

(b) Spectrum of FM by a sinusoid after bandpass filtering. β is 118.

FIG. 31. RESPONSE OF THE EXPERIMENTAL MFD DF SYSTEM AS UNDESIRED FREQUENCY COMPONENTS ARE PROCESSED

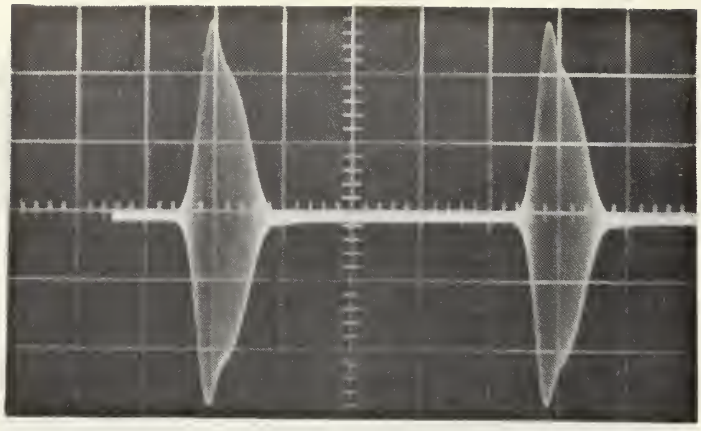

(a) Envelope of the spectrum shown in Fig. 32(b).

(b) Spectrum of FM by a sinusoid after bandpass filtering. β is 118.

FIG. 32. RESPONSE OF THE EXPERIMENTAL MFD DF SYSTEM AS UNDESIRED FREQUENCY COMPONENTS ARE PROCESSED

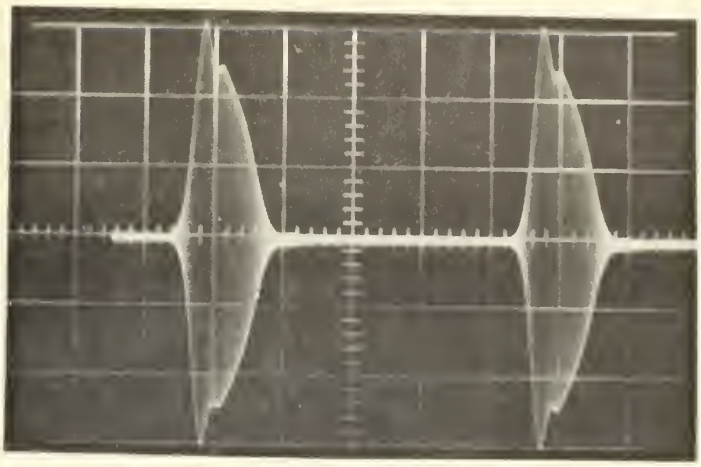

(a) Envelope of the spectrum shown in Fig. 33(b).

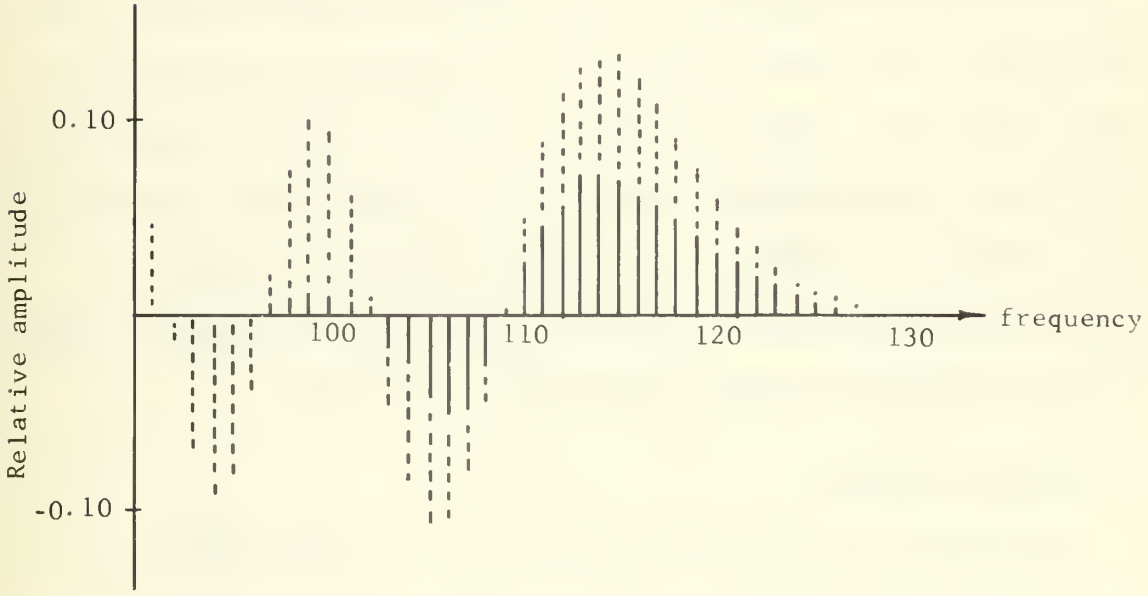

(b) Spectrum of FM by a sinusoid after bandpass filtering. β is 118.

FIG. 33. RESPONSE OF THE EXPERIMENTAL MFD DF SYSTEM AS UNDESIRED FREQUENCY COMPONENTS ARE PROCESSED

graphs shown in Fig. 34 in which in-phase components starting with the 109th harmonic are removed two at a time up to the 114th harmonic. The results are more predictable because the remaining members still form an in-phase group and from Guillemin's frequency-group theory it can be anticipated that as the number of members decreases the principal lobe will broaden proportionately [18]. This general prediction is borne out by Fig. 34 which also suggests that the absence of sidelobes of the envelope is caused by the tapering off in magnitude of $J_n(\beta)$ with n.

Attenuation of the lower-frequency components in the in-phase group reduces the peak level of the envelope and increases the pulse width, but the envelope remains without sidelobes. These analytical results are substantially confirmed experimentally as shown in Figs. 35-37 which show the effect of a non-ideal bandpass filter when the FM spectrum is shifted to exclude or greatly attenuate, some of the desired in-phase components (109-127).

D. NOISE EFFECTS

This section explores the effects of bandlimited gaussian noise on the performance of the experimental MFD DF system. First, the system hardware is described. Next, matched-filter processing without frequency multiplication is considered, theoretically, for a signal-plus-noise input, and an improvement in SNR is predicted. Experimental results for this case are presented. In theory, multiplicative processing is shown to degrade SNR. It is estimated

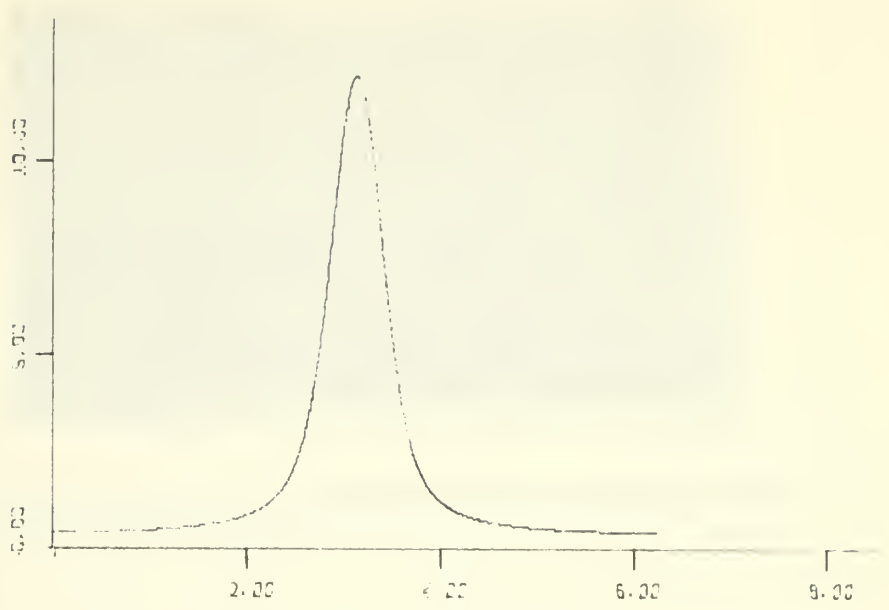

(a) Response when harmonics 111 through 129 are included.

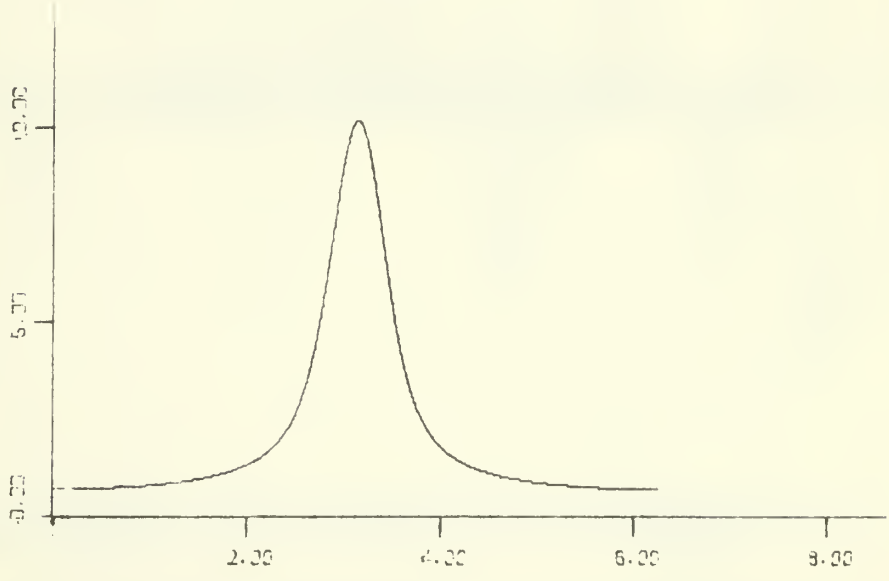

(b) Response when harmonics 113 through 126 are included.

FIG. 34. THEORETICAL RESPONSE OF A MFD DF SYSTEM AS SOME DESIRED FREQUENCY COMPONENTS ARE NOT PROCESSED

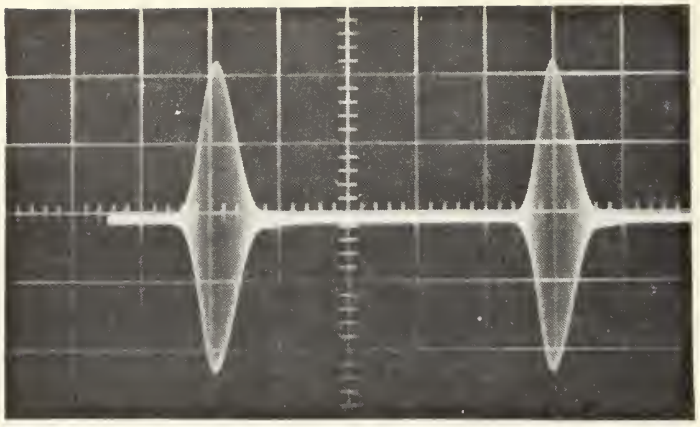

(a) Envelope of the spectrum shown in Fig. 35(b).

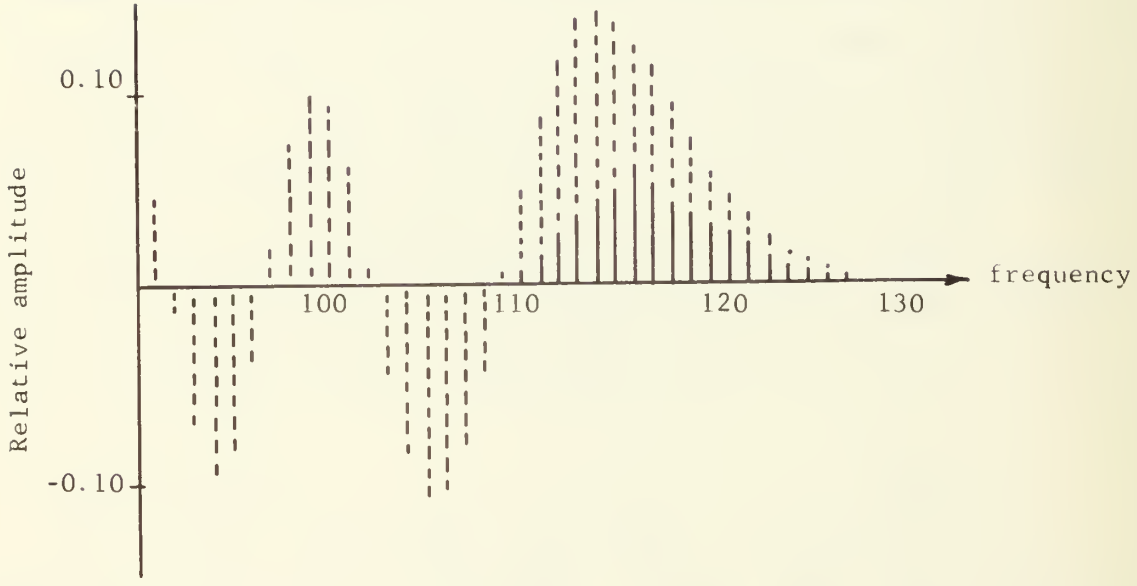

(b) Spectrum of FM by a sinusoid after bandpass filtering. β is 118.

FIG. 35. RESPONSE OF THE EXPERIMENTAL MFD DF SYSTEM AS DESIRED FREQUENCY COMPONENTS ARE NOT PROCESSED

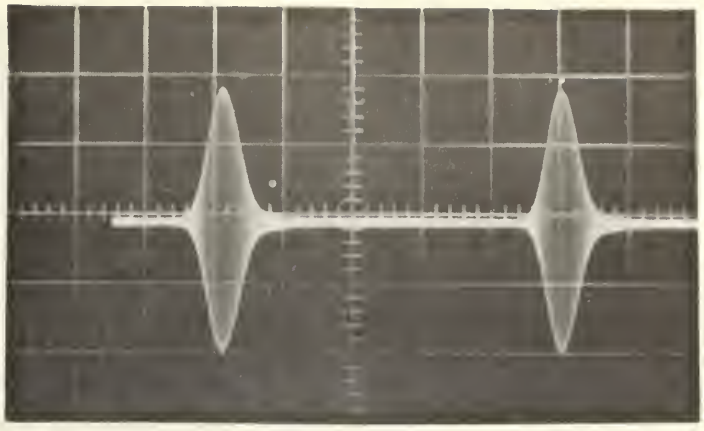

(a) Envelope of the spectrum shown in Fig. 36(b).

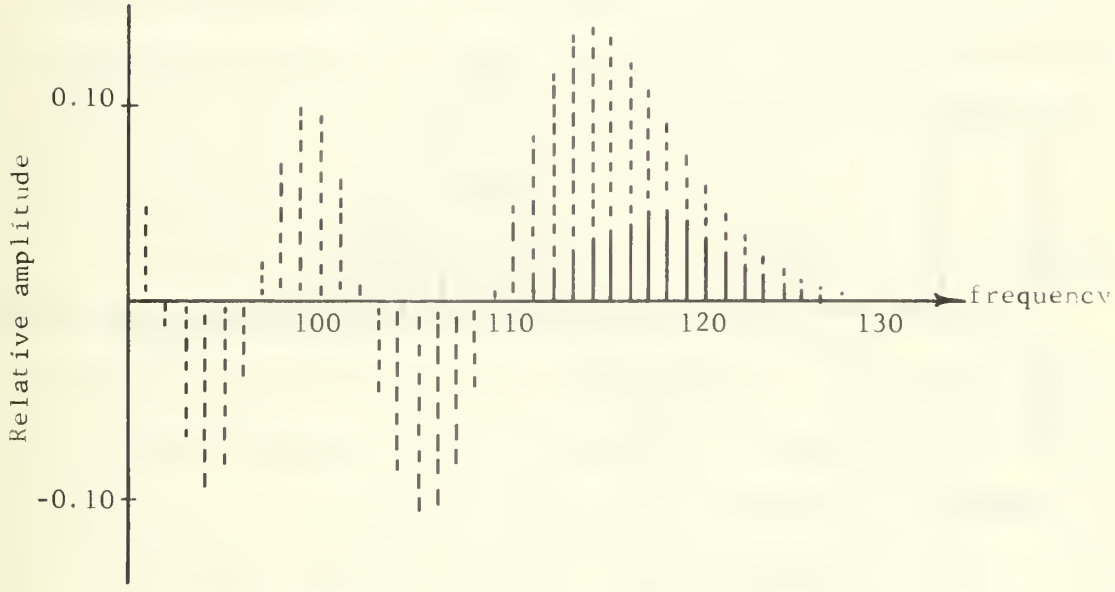

(b) Spectrum of FM by a sinusoid after bandpass filtering. β is 118.

FIG. 36. RESPONSE OF THE EXPERIMENTAL MFD DF SYSTEM AS DESIRED FREQUENCY COMPONENTS ARE NOT PROCESSED

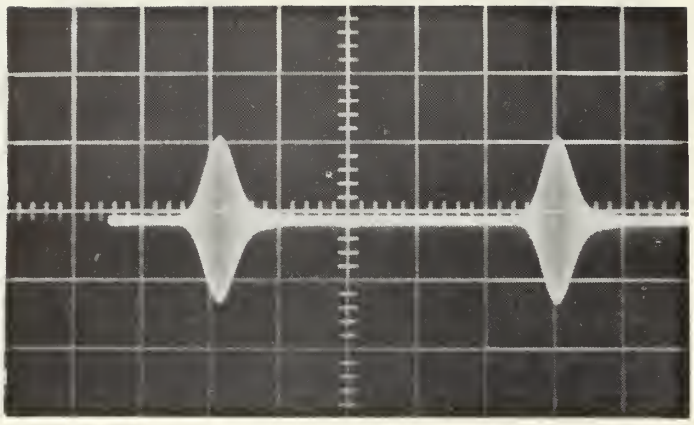

(a) Envelope of the spectrum shown on Fig. 37(b).

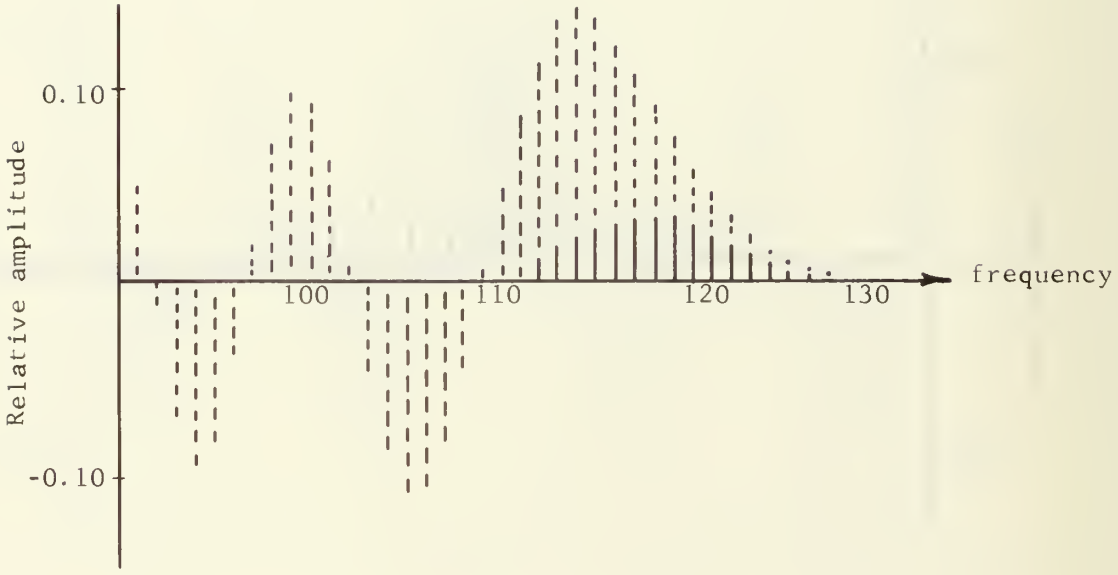

(b) Spectrum of FM by a sinusoid after bandpass filtering. β is 118.

FIG. 37. RESPONSE OF THE EXPERIMENTAL MFD DF SYSTEM AS DESIRED FREQUENCY COMPONENTS ARE NOT PROCESSED

that a 6-dB loss in SNR occurs each time the frequency is doubled. Experimental results confirm this loss in SNR. These data are presented and the performance of a system which uses frequency multiplication is compared with one that does not when the input is signal plus noise.

1. Equipment

The experimental system is shown in Fig. 38. The system is basically the same as that used to demonstrate the MFD DF concept except for the addition of a noise generator and noise bandpass filters.

The output of a wideband gaussian noise generator (Elgenco model 603A) is bandpass filtered to simulate the bandlimited noise in a radio receiver. The VCO output and the noise are combined in a summing network and then applied to the processing hardware.

When the frequency-multiplier section is bypassed, the VCO output is centered at 363 kHz, and the local oscillator is set about 455 kHz higher. A center frequency of 363 kHz ensures that the original signal will not interfere with the difference frequency at the mixer output. The attenuation-vs-frequency characteristics of the circuit used to limit the bandwidth of the output of the noise source (centered at 363 kHz) is shown in Fig. 39-a.

When the frequency multiplier is added, a VCO frequency of 455 kHz poses no problem and permits the use of a ceramic filter (centered at 455 kHz) as an optional

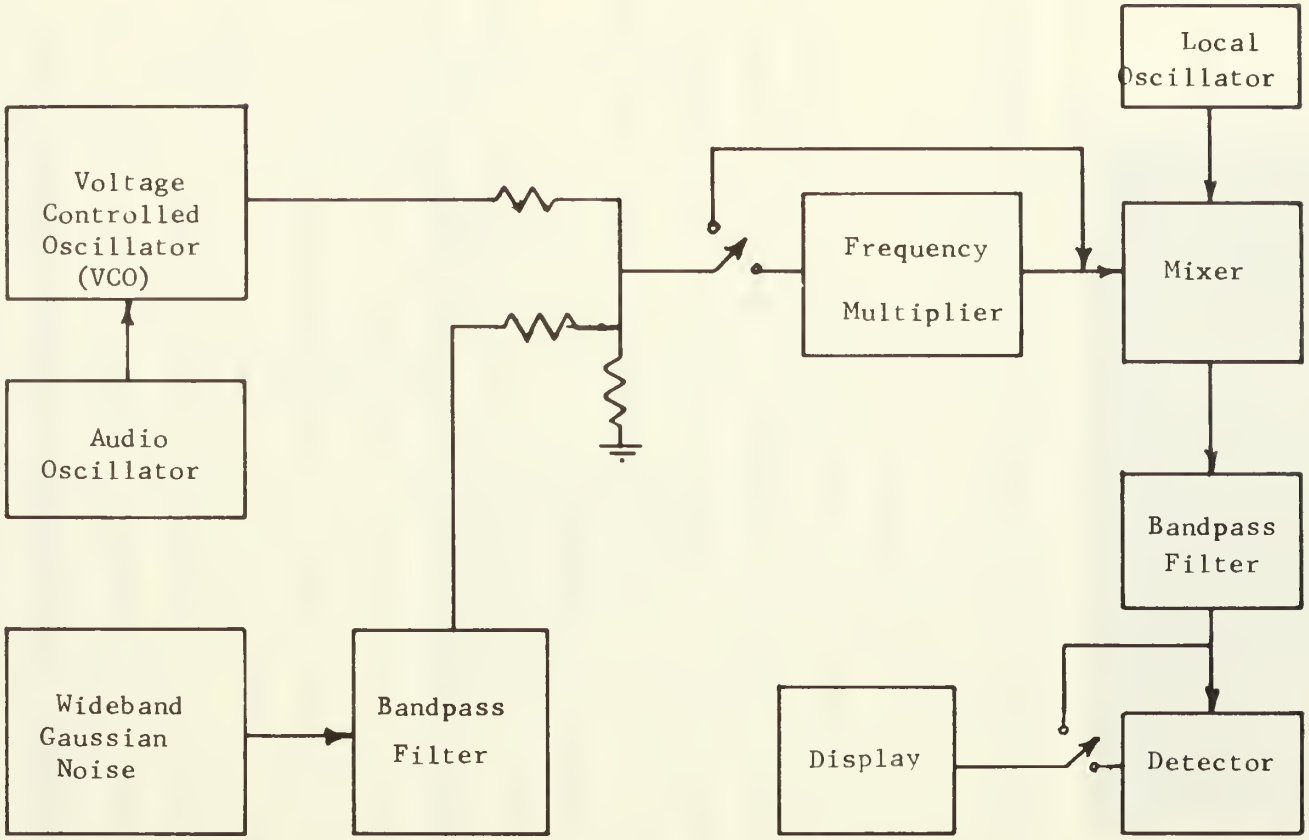

FIG. 38. BLOCK DIAGRAM OF THE EXPERIMENTAL MFD DF SYSTEM USED TO STUDY NOISE EFFECTS

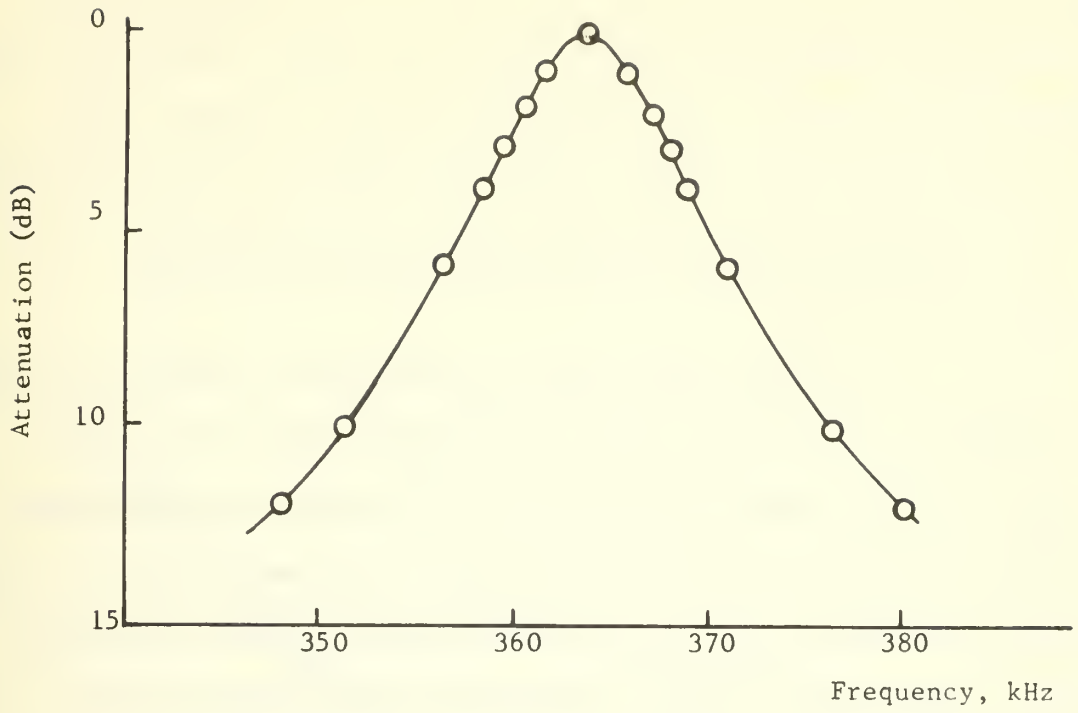

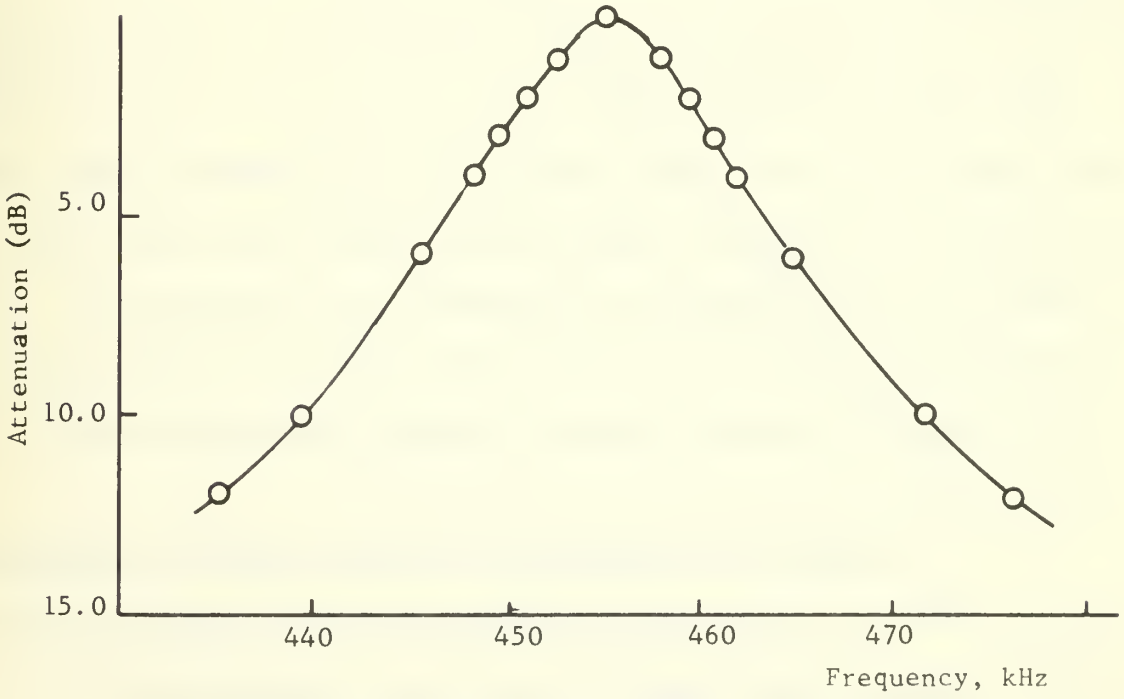

FIG. 39. AMPLITUDE-VS-FREQUENCY CHARACTERISTICS OF BANDPASS NOISE FILTERS

means of obtaining bandlimited noise. The tuned-circuit noise-filter characteristics (455 kHz center frequency) are given in Fig. 39-b. All signal and noise voltages were obtained using a Hewlett-Packard HP 3400A true-RMS voltmeter.

2. Processing Without Frequency Multiplication

a. Theory

Assuming that white, bandlimited, gaussian noise is added to the signal, the theoretical SNR at the output of the system relative to the input SNR can be determined directly from the processing scheme. Assume an ideal filter passes a fraction d of the total bandwidth, and therefore of the total noise power, containing only the desired frequencies which constitute a fraction d' of the total signal power. The change in SNR caused by such filtering is given by

$$I_1 = 10 \log \frac{d'}{d} \tag{46}$$

The value of I_1 increases slowly with β as shown in Fig. 40. This can be understood qualitatively since the total bandwidth of a signal frequency modulated by a sinusoid is approximately equal to 2β, while the number of components in the desired in-phase group increases much more slowly with β.

Since the information on signal AOA is contained in the time of occurrence of the peak of the MFD DF system output, then a useful SNR is the ratio of peak signal voltage to rms noise voltage. This new ratio can be

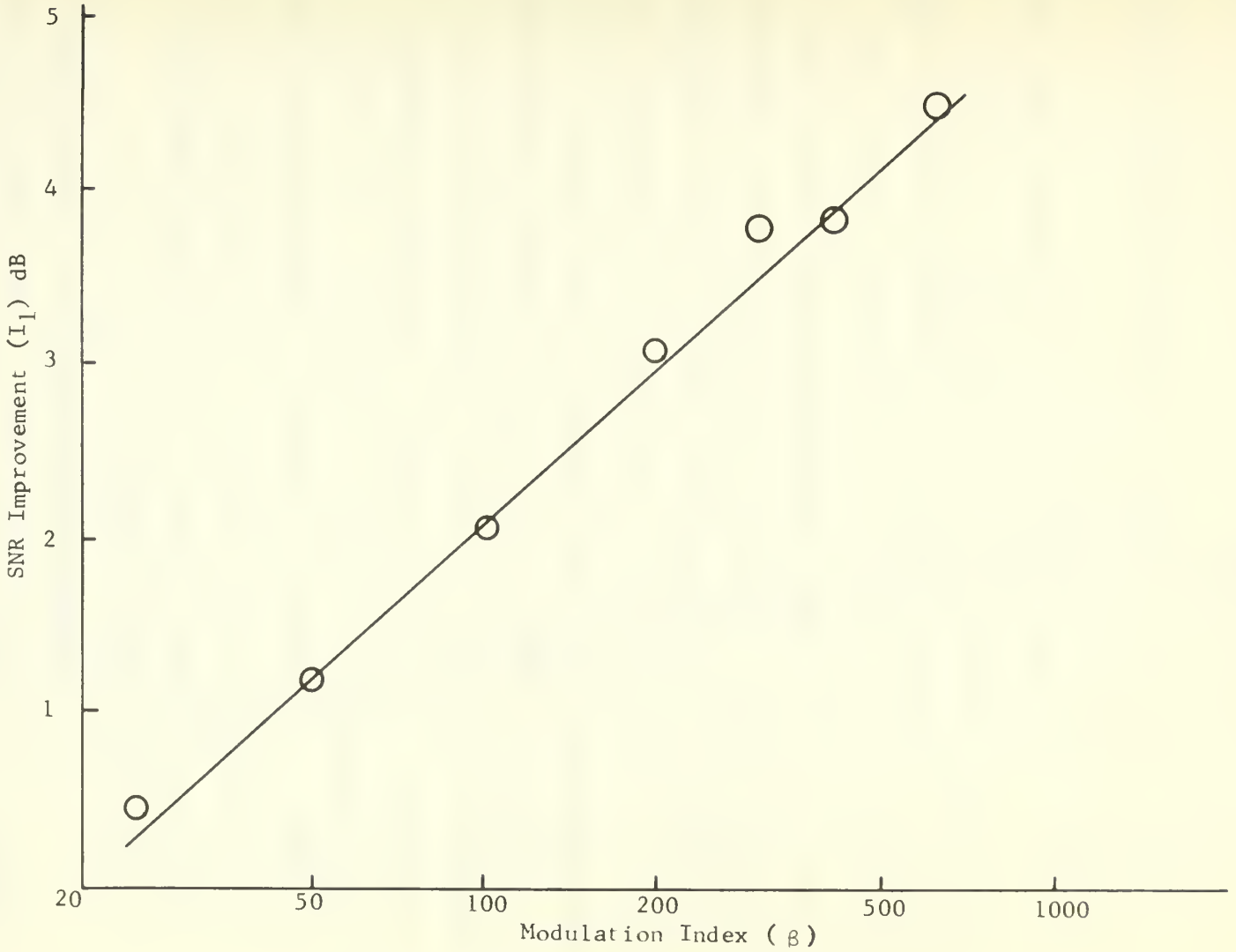

FIG. 40. GRAPH OF THE SNR IMPROVEMENT I_1 VS β

obtained by defining a term which relates the peak envelope voltage to the rms envelope voltage:

$$I_2 = 20 \log \frac{V_{peak}}{V_{rms}} \tag{47}$$

Fig. 41, obtained by computer analysis, shows that I_2 increases as a function of β.

The terms I_1 and I_2 are improvement terms and, as such, are independent of the input SNR. Input SNR depends on receiver bandwidth. We assume a receiver bandwidth which passes all of the significant spectral components of the FM signal appearing at the output of the receiving antenna. Therefore the assumed input bandwidth is a function of the modulation index β and the scanning rate f_r. For any given β, reduction of f_r decreases the spacing between spectral components thus reducing the overall bandwidth. However, f_r cannot be reduced indefinitely because of the need to filter a selected group of side frequencies. If f_r is too small, a desirable bandpass filter characteristic cannot be realized. The optimum bandwidth is determined therefore by engineering considerations, primarily those imposed by the construction state of the art of narrow bandpass filters having acceptable (linear) phase characteristics.

In summary, processing without multiplication produces a theoretical improvement in SNR which is directly related to the modulation index β. In turn, β is directly related to the radius of rotation (aperture) of the

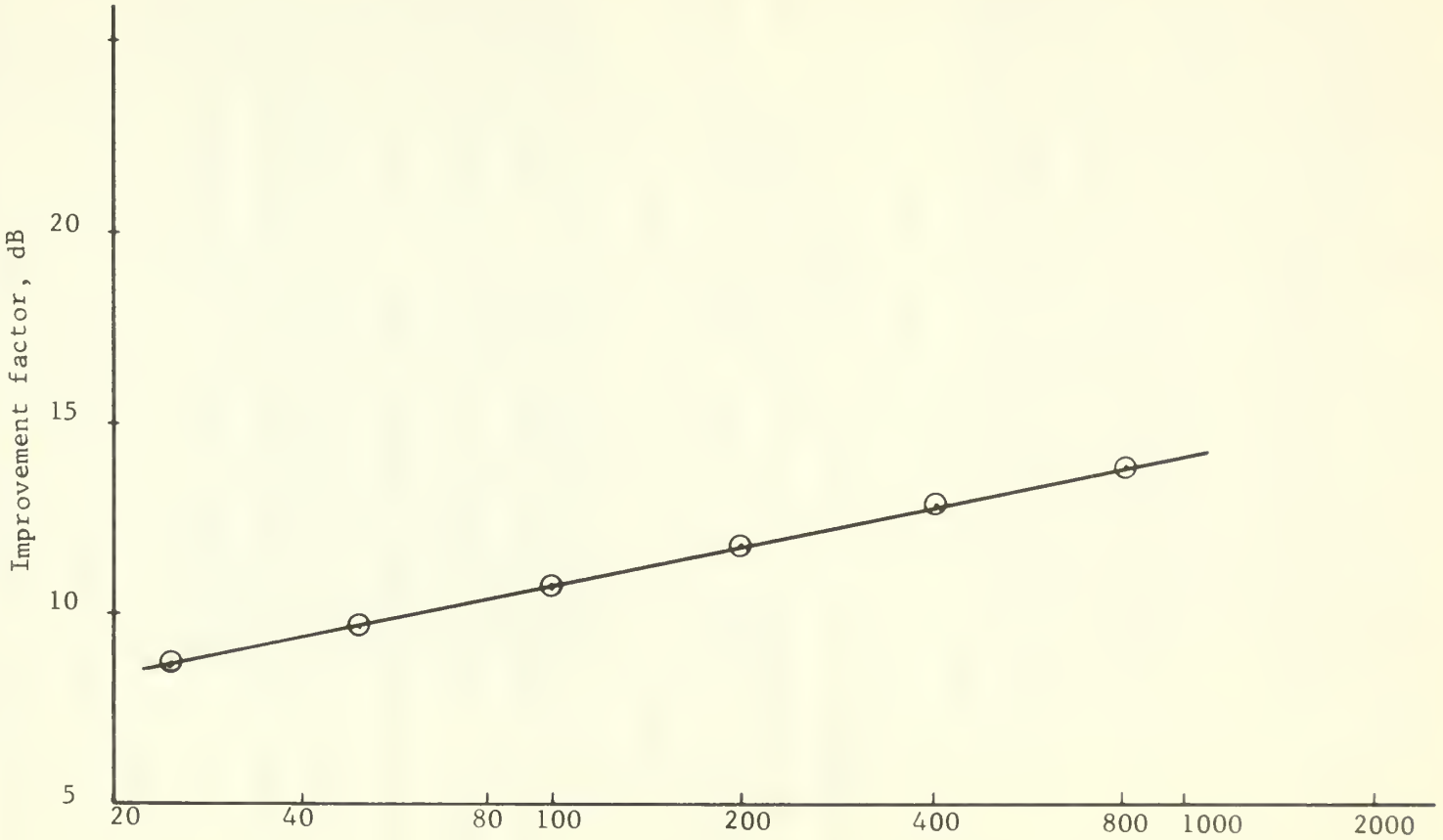

FIG. 41. GRAPH OF THE SNR IMPROVEMENT I_2 VS β

receiving antenna. System SNR varies inversely with f_r. Since system accuracy is proportional to SNR it is desirable to maximize β (increase aperture size) and to minimize f_r consistent with practical considerations such as the availability of suitable bandpass filters.

b. Experimental Results

The effect of bandlimited gaussian noise on the experimental MFD DF system which uses no frequency multiplication is the subject of three experiments. The first experiment uses a FM signal with a β of 25 to which bandlimited noise is added. The mixer output is passed to a 4-kHz bandpass filter (Clevite TL 4D8-A). This filter extracts the desired 12 side frequencies occupying 1.2 kHz of bandwidth. The input SNR is varied from zero to 10 dB. The results are presented as indicated in Table I. The first photograph shows two cycles of the envelope of the output of the bandpass filter; the other photograph indicates this envelope voltage after linear-diode detection and low-pass filtering with an RC filter having a time constant (4.7 ms) comparable with the scanning period (10.0 ms). This large value of time constant provides integration which improves the ability of an operator to determine the time of occurrence of the pulse. The family of photographs associated with Table I is shown in Fig. 42. Because the filter bandpass (4 kHz) is not exactly equal to the bandwidth of the in-phase group of side frequencies,

TABLE I

EFFECT OF NOISE ON THE PERFORMANCE OF
AN EXPERIMENTAL MFD DF SYSTEM

Basic Parameters:

(a) Processing without frequency multiplication

(b) $\beta = 25$

(c) 4-kHz bandpass filter (TL 4D8-A)

Figure	INPUT			OUTPUT		
	Signal (dB)	Noise (dB)	SNR	Signal (dB)	Noise (dB)	SNR
42-a,b	-13.0	$-\infty$	∞	-15.0	$-\infty$	∞
42-c,d	-13.0	-13.0	0	-15.0	-12.0	-3.0
42-e,f	-13.0	-16.0	3.0	-15.0	-14.2	0.8
42-g,h	-13.0	-19.0	6.0	-15.0	-17.0	2.0
42-i,j	-13.0	-23.0	10.0	-15.0	-21.5	6.5

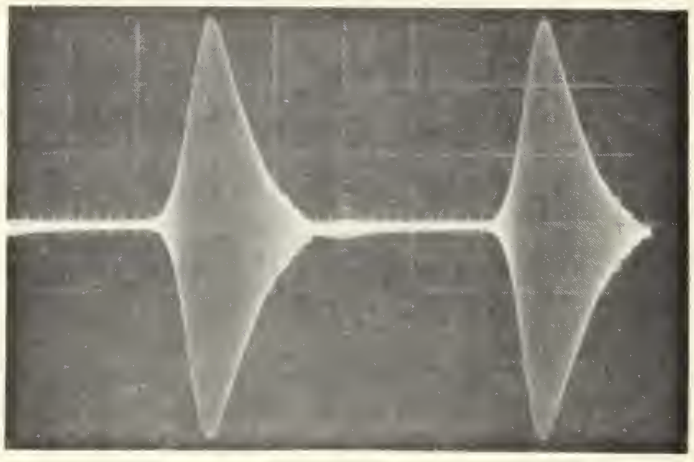

(a)

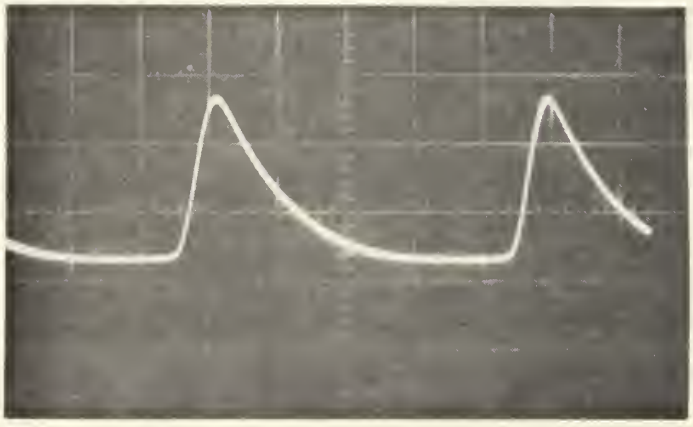

(b)

FIG. 42. PHOTOGRAPHS OF THE RESPONSE OF THE EXPERIMENTAL MFD DF SYSTEM FOR VARIOUS VALUES OF INPUT SNR

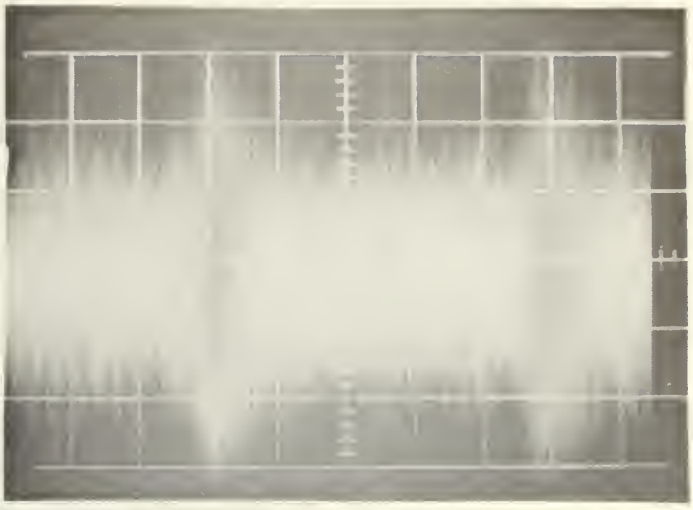

(c)

(d)

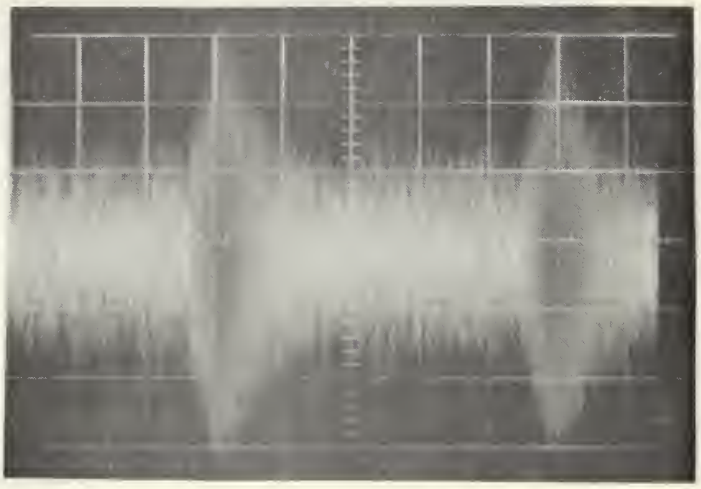

(e)

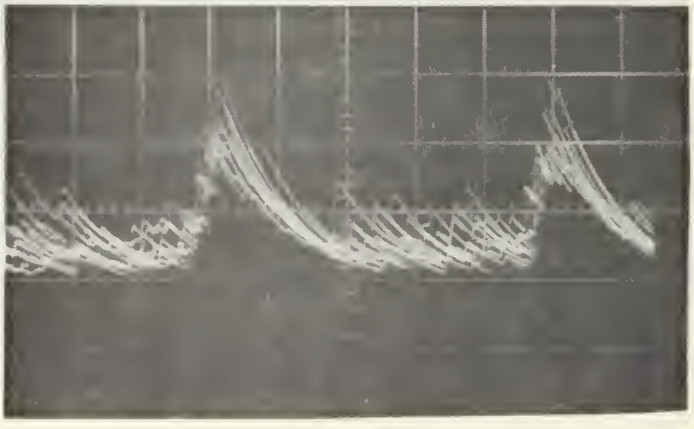

(f)

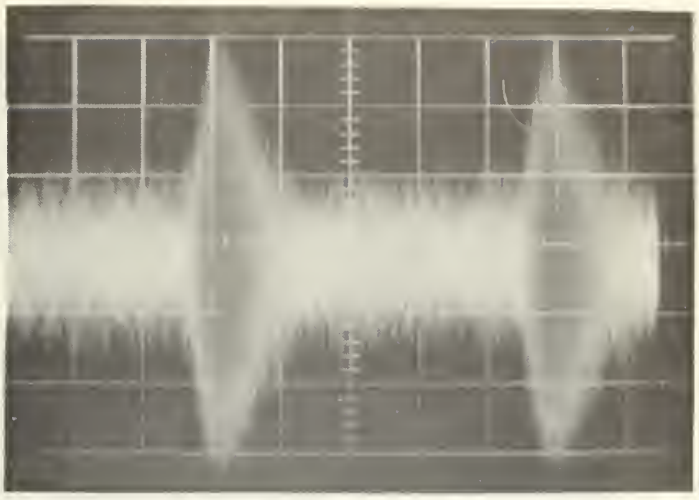

(g)

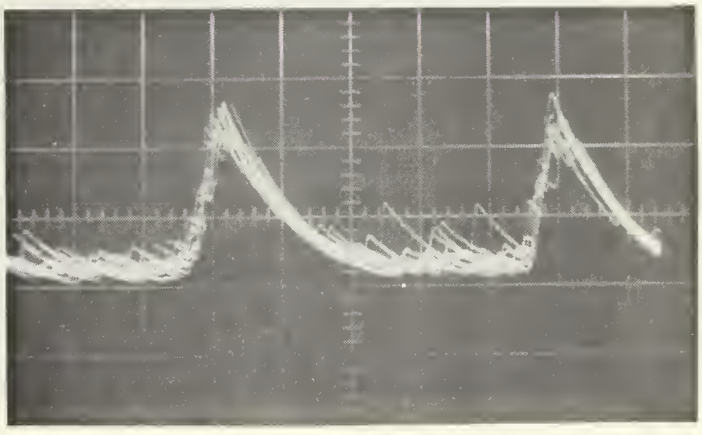

(h)

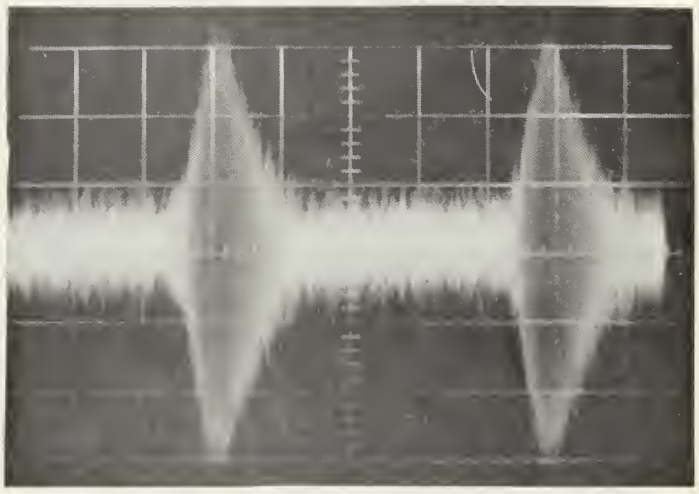

(i)

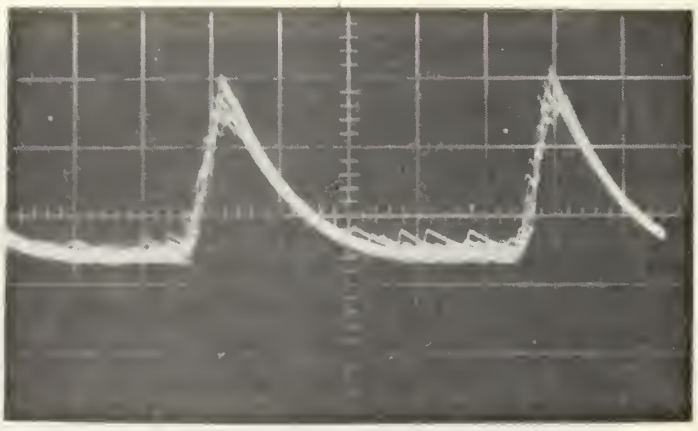

(j)

there is actually a decrease in SNR associated with the filtering operation. (The term I_1 of (46) is negative.)

For the second experiment the modulation index β of the signal is increased to 100. All other system parameters are unchanged. The 4-kHz filter still passes the 18 in-phase side frequencies. Once again the input SNR is varied. The results are presented in Table II and Fig. 43. The effect of the waveform improvement term I_2 due to the higher β can be seen by comparing any two photographs in Figs. 42 and 43 which have approximately equal values of output SNR. For example, compare Fig. 42-g,h with Fig. 43-e,f. Since the 4-kHz bandpass filter is much larger than necessary, the improvement I_1 caused by filtering is about the same for the case $\beta = 25$ as for the case $\beta = 100$; therefore the primary difference in display is due to the larger value of I_2 which is associated with larger values of β.

The use of a detector circuit with a large time constant broadens the peak of the envelope-detected pulse. This broadening destroys a portion of the accuracy improvement which results from an increased value of β. With large values of input SNR such long integration times are not desirable.

The third experiment in this series is similar to the second with the exception that a 10-kHz bandpass filter (Clevite TL 10D9-20A) replaces the 4-kHz filter. The results given in Table III and Fig. 44 provide both visual

TABLE II

EFFECT OF NOISE ON THE PERFORMANCE OF AN EXPERIMENTAL MFD DF SYSTEM

Basic Parameters:

(a) Processing without frequency multiplication

(b) $\beta = 100$

(c) 4-kHz bandpass filter (TL 4D8-A)

Figure	INPUT			OUTPUT		
	Signal (dB)	Noise (dB)	SNR	Signal (dB)	Noise (dB)	SNR
43-a,b	-13.0	$-\infty$	∞	-15.5	$-\infty$	∞
43-c,d	-19.0	-13.0	-6	-18.5	-18.5	0
43-e,f	-13.0	-13.0	0	-15.5	-18.7	3.2
43-g,h	-13.0	-19.0	6	-15.5	-23.7	8.2
43-i.j	-13.0	-23.0	10	-15.5	-28.5	13.0

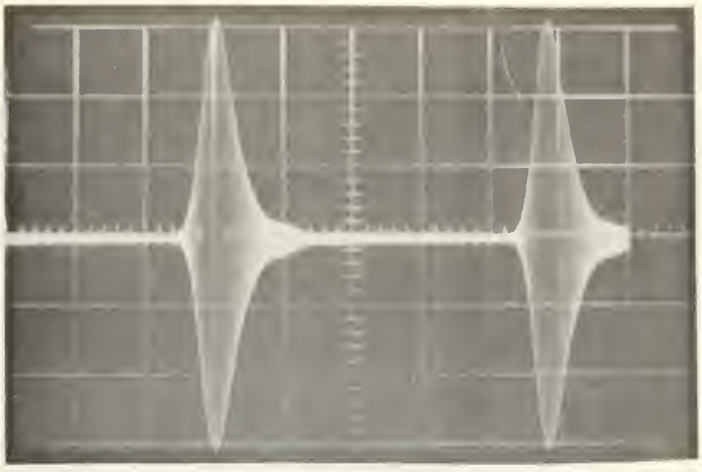

(a)

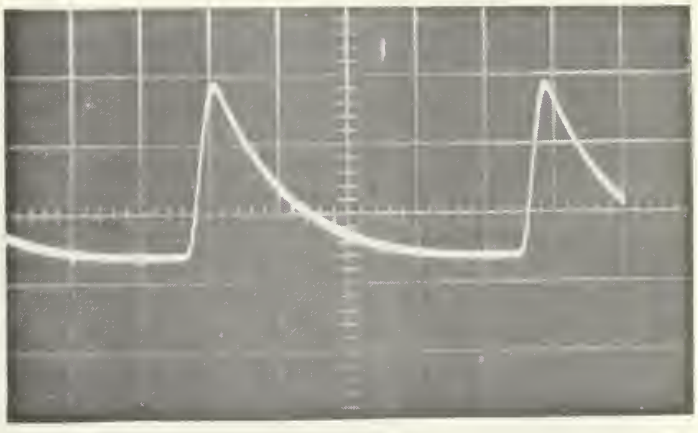

(b)

FIG. 43. PHOTOGRAPHS OF THE RESPONSE OF THE EXPERIMENTAL MFD DF SYSTEM FOR VARIOUS VALUES OF INPUT SNR

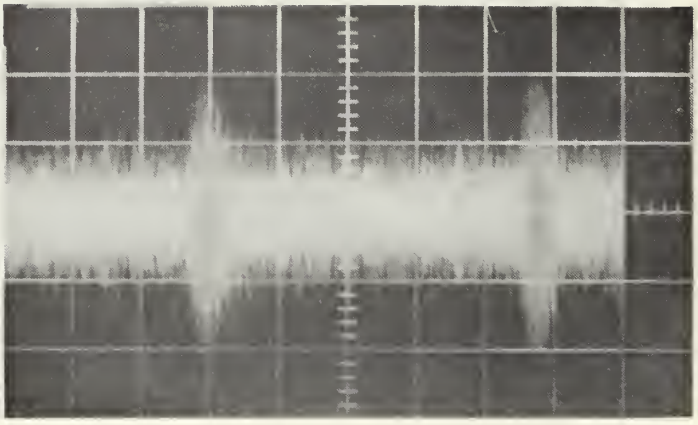

(c)

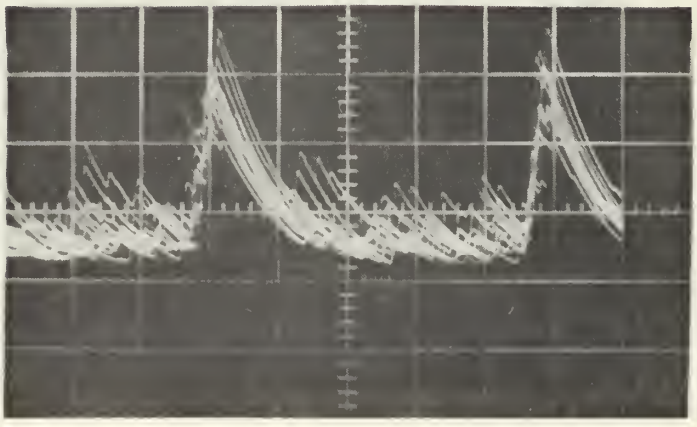

(d)

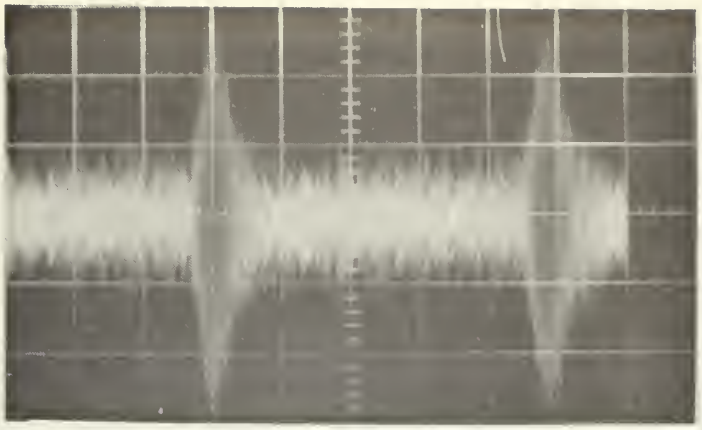

(e)

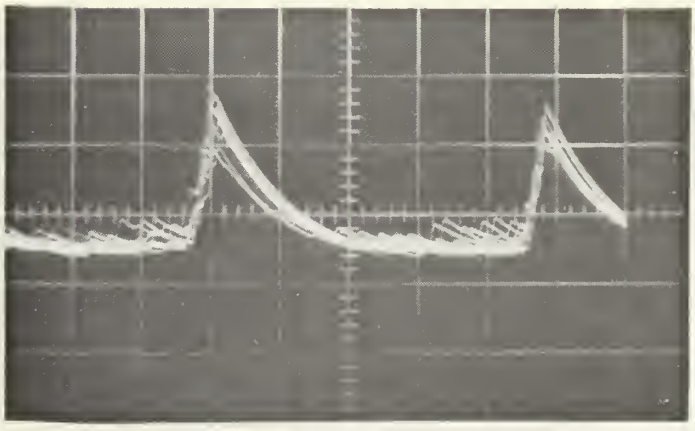

(f)

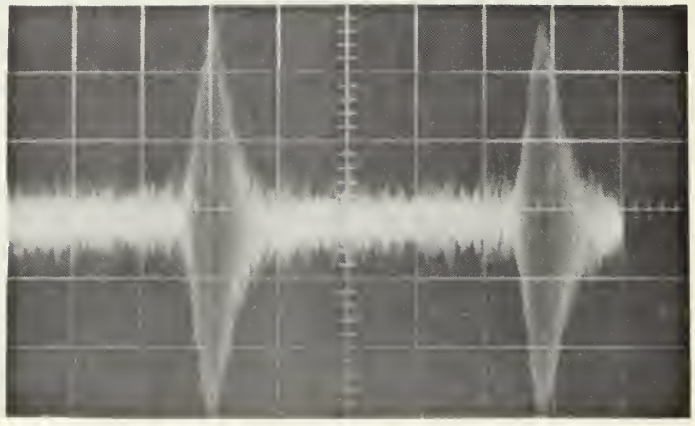

(g)

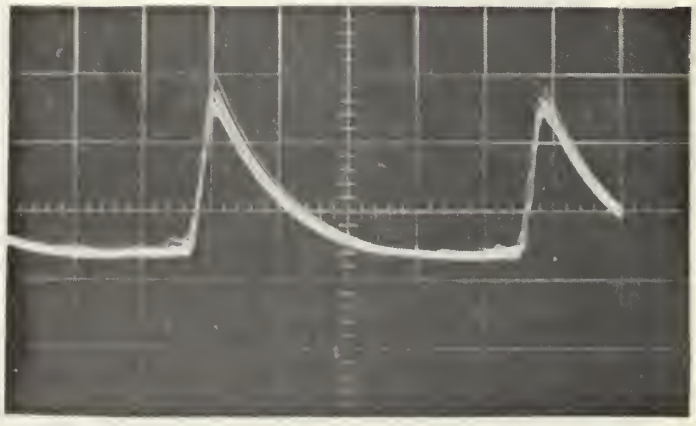

(h)

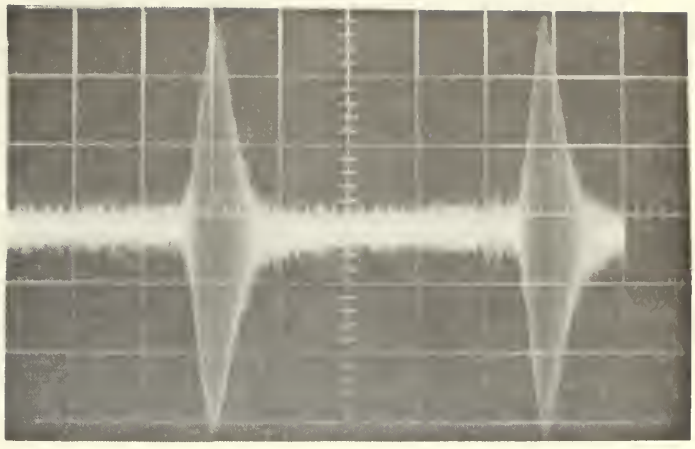

(i)

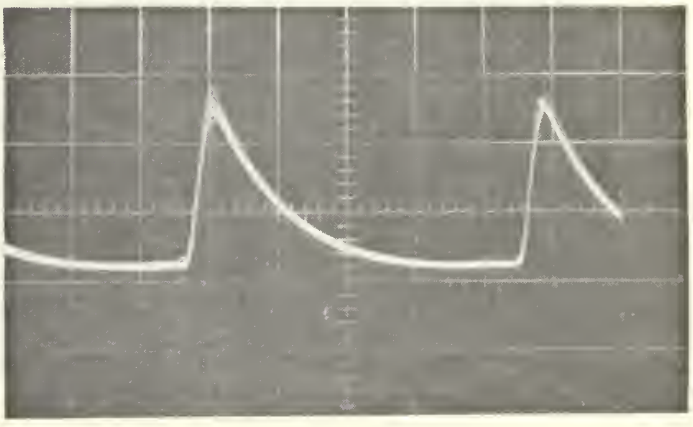

(j)

TABLE III

EFFECT OF NOISE ON THE PERFORMANCE OF AN EXPERIMENTAL MFD DF SYSTEM

Basic Parameters:

(a) Processing without frequency multiplication

(b) $\beta = 100$

(c) 10-kHz bandpass filter (TL10D9-20A)

Figure	INPUT			OUTPUT		
	Signal (dB)	Noise (dB)	SNR	Signal (dB)	Noise (dB)	SNR
44-a,b	-13.0	$-\infty$	∞	-15	$-\infty$	∞
44-c,d	-19.0	-13.0	-6.0	-21.0	-14.5	-5.5
44-e,f	-13.0	-13.0	0	-15.0	-14.5	-0.5
44-g,h	-13.0	-19.0	6.0	-15.0	-20.0	5.0

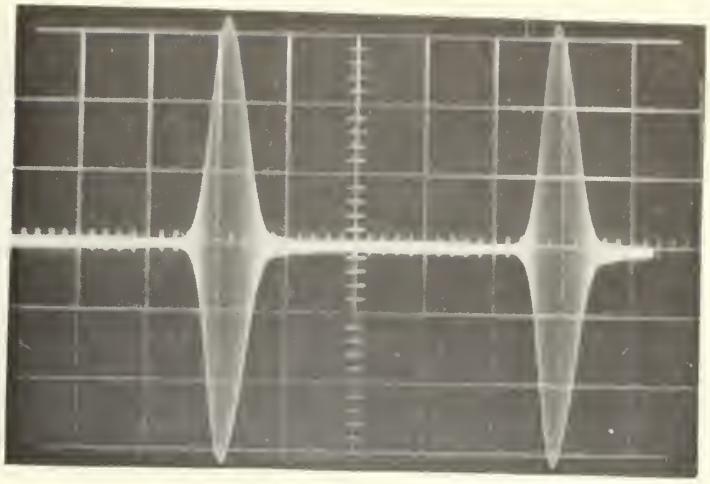

(a)

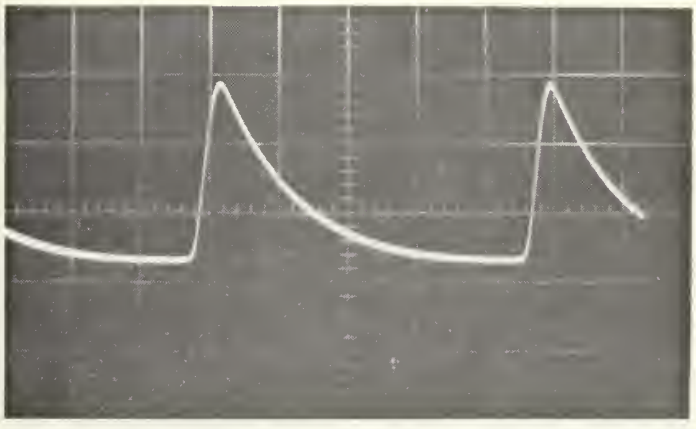

(b)

FIG. 44. PHOTOGRAPHS OF THE RESPONSE OF THE EXPERIMENTAL MFD DF SYSTEM FOR VARIOUS VALUES OF INPUT SNR

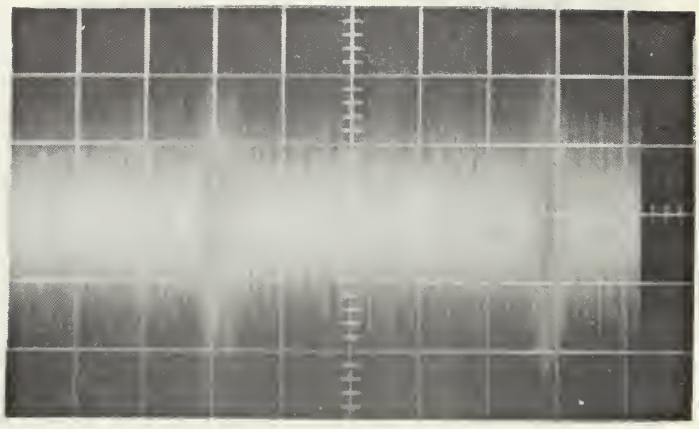

(c)

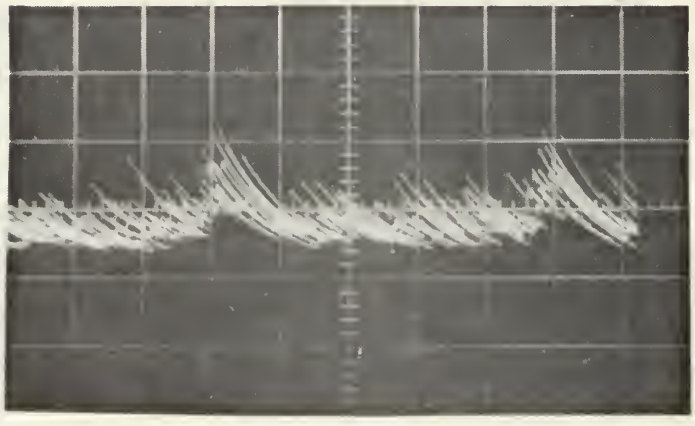

(d)

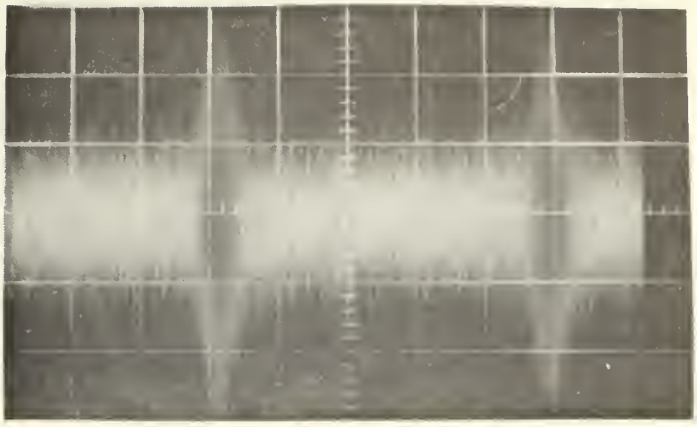

(e)

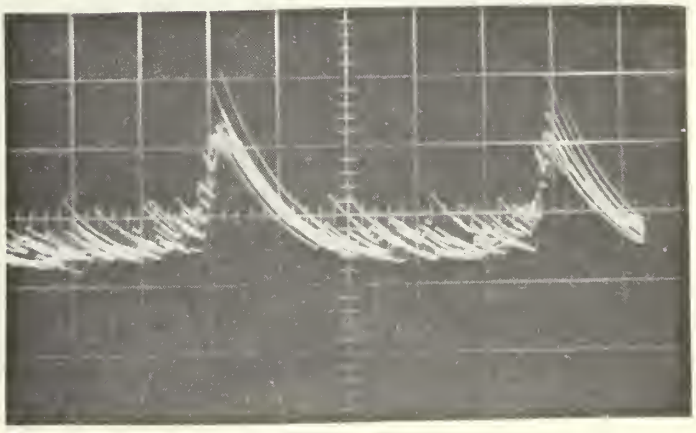

(f)

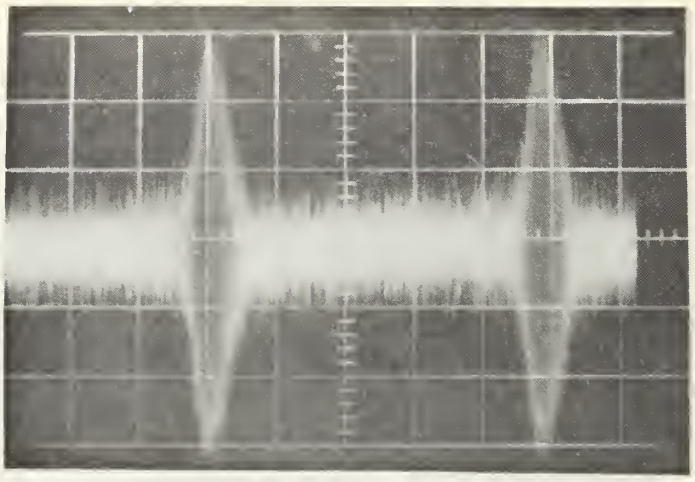

(g)

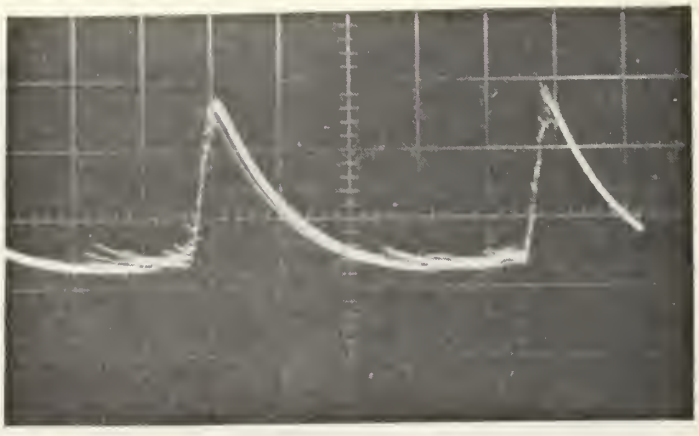

(h)

and experimental evidence of the decrease in SNR and consequent degradation in system accuracy caused by the additional noise power which passes through the increased filter bandpass. The 10-kHz passband contains about 2½ times more noise power than the 4-kHz passband. The effect of this additional noise is seen by comparing any two cases from Tables II and III (Figs. 43 and 44) having the same input SNR. In general there is a 3 to 4 dB decrease in the output SNR when the 10-kHz filter is used.

3. Processing With Frequency Multiplication

Frequency multiplication artificially increases the aperture size of a MFD DF system by increasing the modulation index β of the FM signal produced by the antenna rotation. This section explores the effect of additive, bandlimited gaussian noise when frequency multiplication is employed.

a. Theory

Frequency multiplication is accomplished experimentally by individual frequency-doubler stages consisting of a full-wave linear rectifier followed by a bandpass filter tuned to the second harmonic of the applied signal. Because of the nonlinearity of this process, the output contains the product of signal and noise components. These additional terms reduce the output SNR. An analysis of the SNR reduction for the full-wave linear rectifier is difficult [25]. On the other hand, the noise performance of a full-wave square-law device is well known [26]. Since

it has been shown experimentally that the results obtained using linear and square-law detectors are quite similar [6, p. 432], it is reasonable to use the following analytical results obtained assuming a square-law frequency doubler.

The SNR at the output of each doubler Γ_o as a function of the input SNR Γ_i is given by

$$\Gamma_o = \frac{\Gamma_i^2}{2(1+2\Gamma_i)} \tag{48}$$

For large Γ_i this becomes

$$\Gamma_o \simeq \frac{\Gamma_i}{4}$$

which is equivalent to a 6-dB loss in SNR per stage. This loss factor is only an estimate since it assumes square-law processing of an unmodulated carrier plus noise, whereas the doppler signal is frequency modulated. Further, an increase in SNR may result from bandpass filtering the output of the last frequency-doubler stage. In general, this improvement by filtering arises because the usable signal power tends to be concentrated in the filter passband while in most cases of practical interest the prominent noise terms after frequency multiplication have frequencies which are outside the filter passband.

It is of interest now to consider the effect on the measurement of azimuth angle of the loss in SNR due to frequency multiplication. Based on the results

given by Skolnik [6, p. 462-478] for measurement accuracy under high SNR conditions, the angular error $\varepsilon(\theta)$ which arises is of the form

$$\varepsilon(\theta) = \kappa \frac{\theta_B}{(S/N)^{\frac{1}{2}}} \tag{50}$$

Where θ_B is the half-power width of the output pulse from the MFD DF system with no frequency multiplication and κ is a constant.

Now consider a system consisting of a single frequency doubler preceding the bandpass filter and assume that the 6-dB SNR loss caused by frequency multiplication is reduced to 3 dB by the filtering explained previously. Then at the system output the angular error $\varepsilon'(\theta)$ is given by

$$\varepsilon'(\theta) = \kappa \frac{\theta'_B}{(S'/N')^{\frac{1}{2}}} . \tag{51}$$

Since $S/N = 2(S'/N')$, then

$$\varepsilon'(\theta) = \kappa \frac{\sqrt{2}\theta'_B}{(S/N)^{\frac{1}{2}}} \tag{52}$$

which means that if the new angular error ε' is to be equal to or less than the angular error ε which exists without frequency multiplication, then

$$\theta'_B \leq \frac{\theta_B}{\sqrt{2}} .$$

For a system containing several frequency-doubling stages, the 6-dB loss in SNR per stage requires that the beamwidth be halved with each stage to preserve the same accuracy. Such improvement is not possible as shown in Fig. 15.

The preceding analysis estimates the effect of noise on a system using frequency multiplication. The disadvantages which arise from frequency multiplication may be balanced by other factors such as:

(1) The accuracy obtainable by a human operator is influenced by the width of the pulse which must be "split" by a cursor or other bearing indication device particularly at large values of SNR. An operator can position a cursor more accurately on a narrower pulse thus counteracting some loss in theoretical accuracy due to multiplication.

(2) Integration of a number of sweeps may increase the SNR without increasing the width of the response main lobe.

(3) Additional pulse compression achieved at higher values of β which are obtained by frequency multiplication should offset some of the loss in SNR caused by the multiplication process.

The next section gives a partly qualitative and partly quantitative confirmation of the analyses presented in this section.

b. Experimental Results

This section presents the results of a number of experiments in which signal plus additive bandlimited

noise is applied to an experimental MFD DF system (Fig. 38) using frequency multiplication by a factor of four. Two photographs are generally shown for each input. The first photograph shows two cycles of the output of the final bandpass filter (DF system output). The second photograph shows the system output after envelope detection by a diode followed by an RC lowpass filter having a time constant of 4.7 ms.

In the first experiment, bandlimited gaussian noise having the spectral shape shown in Fig. 39-a is added to the FM signal. The value of β is 25. The signal plus noise is frequency multiplied by a factor of four to produce a signal with a value of β of 100. Mixing and then filtering with a 4-kHz bandpass filter complete the system operations. The results are summarized in Table IV and Fig. 45 for a number of inputs of differing values of SNR. The reduction in SNR by frequency multiplication is seen by comparing these results with the first non-multiplicative case (β = 25) given by Table I and Fig. 42. Because of the interaction of signal with noise in the frequency-multiplication process, measurement of the output signal power (with no input noise), output noise power (with no input signal), and output signal-plus-noise power separately provides no valid indication of the extent to which the signal interacts with the noise. Therefore, systems which use frequency multiplication cannot be compared directly with those that do not on the basis of output SNR.

TABLE IV

EFFECT OF NOISE ON THE PERFORMANCE OF
AN EXPERIMENTAL MFD DF SYSTEM

Basic Parameters:

(a) β (before frequency multiplication) = 25

(b) β (after multiplication in frequency by a factor of four) = 100

(c) 4-kHz bandpass filter (TL 4D8-A)

Figure	INPUT			OUTPUT	
	Signal (dB)	Noise (dB)	SNR	Signal (dB)	Signal plus Noise (dB)
45-a,b	8.0	5.0	3.0	-20.0	-16.7
45-c,d	8.0	-2.0	10.0	-20.0	-17.2
45-e,f	8.0	-12.0	20.0	-20.0	-19.0

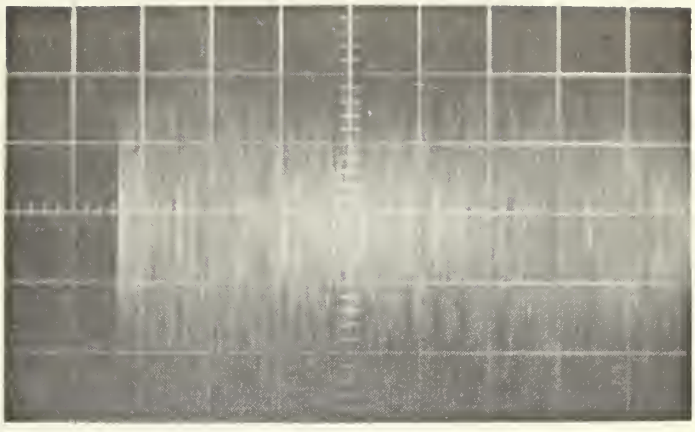

(a)

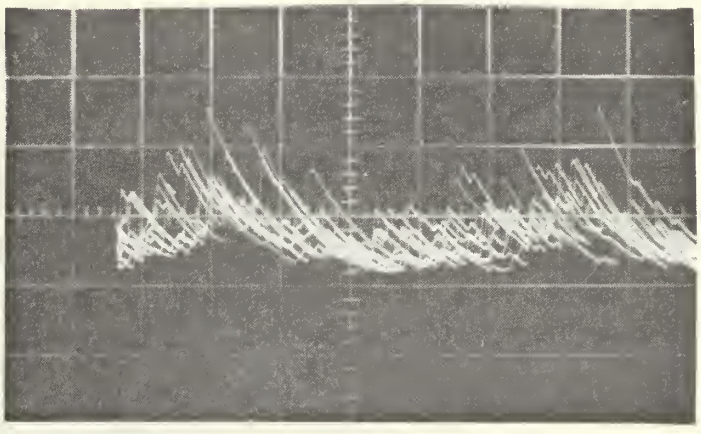

(b)

FIG. 45. PHOTOGRAPHS OF THE RESPONSE OF THE EXPERIMENTAL MFD DF SYSTEM FOR VARIOUS VALUES OF INPUT SNR

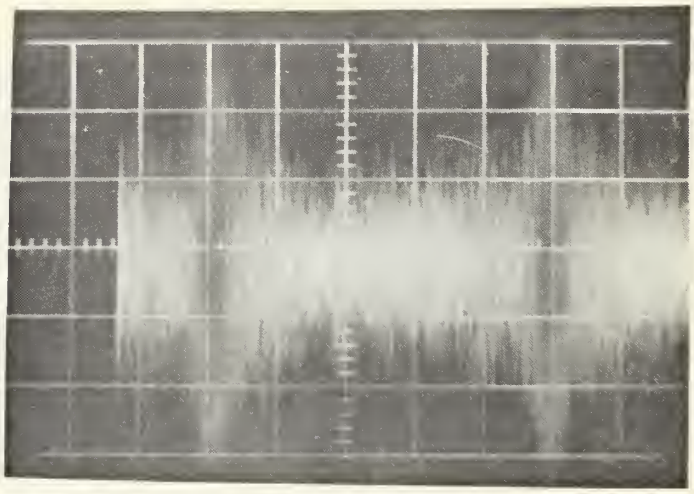

(c)

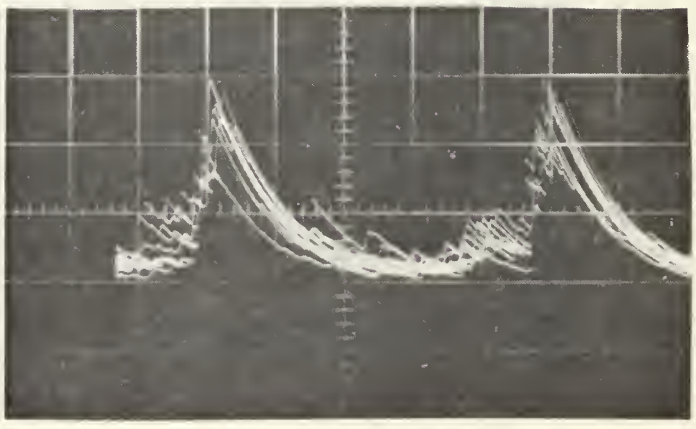

(d)

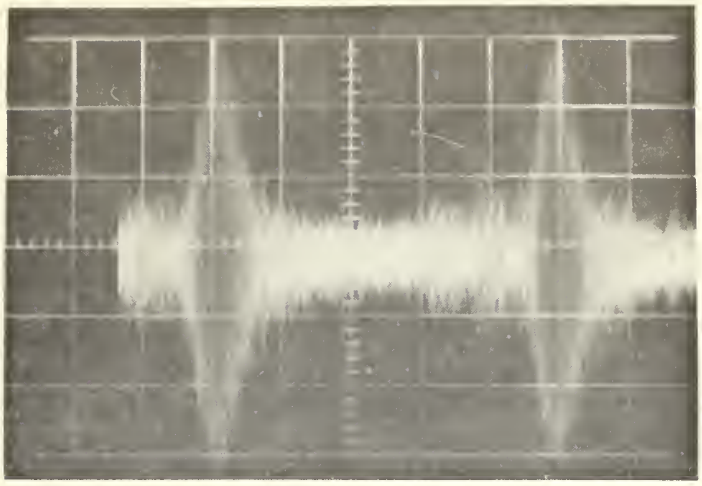

(e)

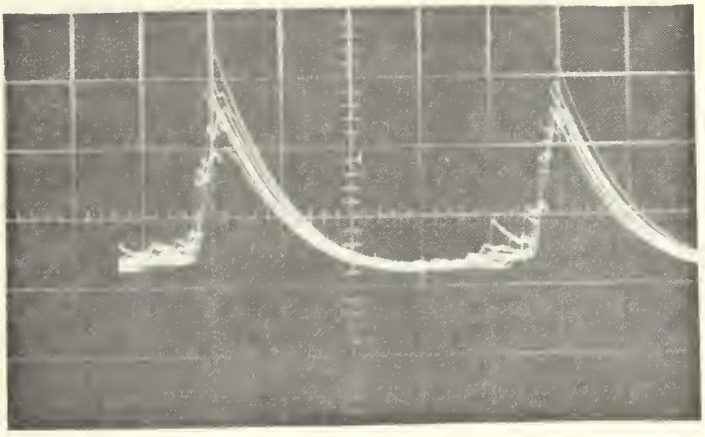

(f)

However, a visual inspection of the photographs for the two cases gives a good indication of the deterioration produced by frequency multiplication. For example, Fig. 42-e,f, the 3-dB input SNR case, is visually comparable to the 10-dB input SNR case in Fig. 45-c,d. This comparison indicates that the presentation obtained using a system without frequency multiplication is comparable to that obtained with a times-four frequency-multiplying system having a 7-dB larger value of input SNR. Comparisons of other photographs generally confirm the 7-dB figure.

The second experiment of interest is identical to the first except a 10-kHz bandpass filter is used instead of the 4-kHz bandpass filter. The disadvantage of the increased bandwidth is evidenced by the results given in Table V and shown in Fig. 46 which show on the average a 3-to 4-dB loss in the SNR of the system output relative to the results given in Table IV.

In a third experiment, the tuned circuit which filters the wideband noise spectrum at the output of the noise generator, is replaced by a 10-kHz ceramic bandpass filter and the 4-kHz ceramic filter is used to select the desired frequency group. The results, summarized in Table VI and Fig. 47, are surprising because the noise tended to concentrate around the output pulses much more than when tuned LC circuits are used to limit the noise bandwidth. There is no obvious explanation for this phenomenon.

TABLE V

EFFECT OF NOISE ON THE PERFORMANCE OF
AN EXPERIMENTAL MFD DF SYSTEM

Basic Parameters:

(a) β (before frequency multiplication) = 25

(b) β (after multiplication in frequency by a factor of four) = 100

(c) 10-kHz bandpass filter (TL 10D9-20A)

Figure	INPUT			OUTPUT	
	Signal (dB)	Noise (dB)	SNR (dB)	Signal (dB)	Signal plus Noise (dB)
46-a,b	8.0	5.0	3.0	-18.0	-10.7
46-c,d	8.0	-2.0	10.0	-18.0	-12.7
46-e,f	8.0	-12.0	20.0	-18.0	-15.9

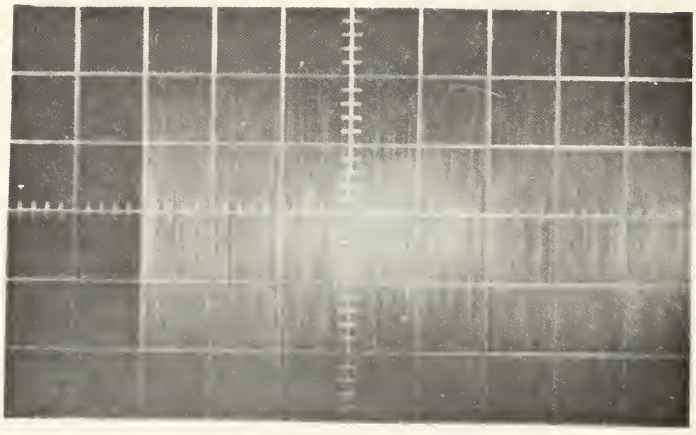

(a)

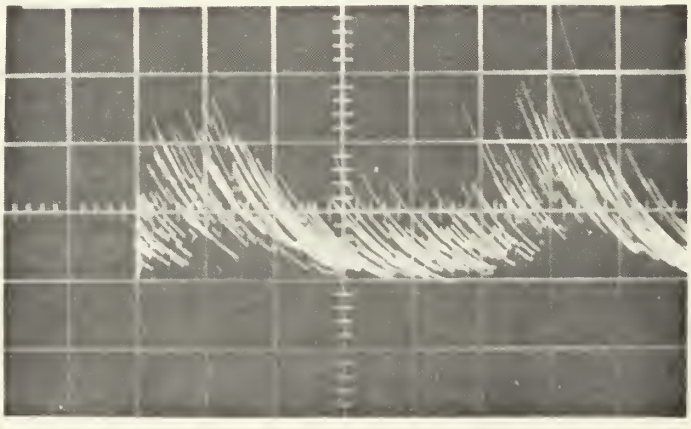

(b)

FIG. 46. PHOTOGRAPHS OF THE RESPONSE OF THE EXPERIMENTAL MFD DF SYSTEM FOR VARIOUS VALUES OF INPUT SNR

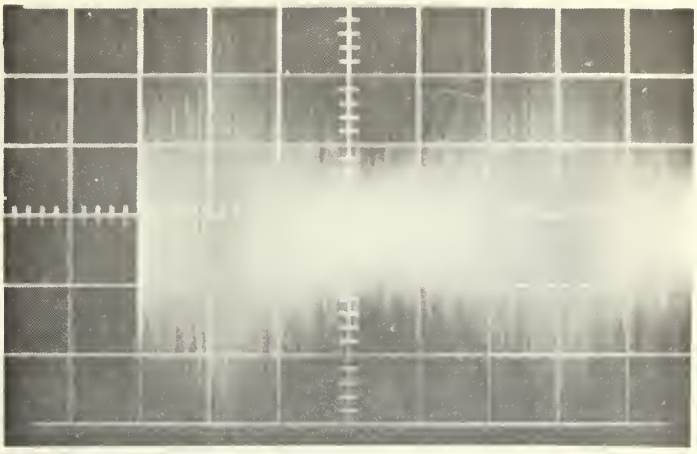

(c)

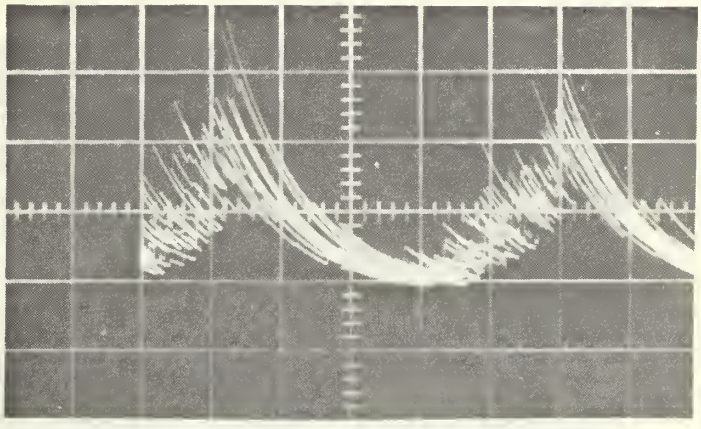

(d)

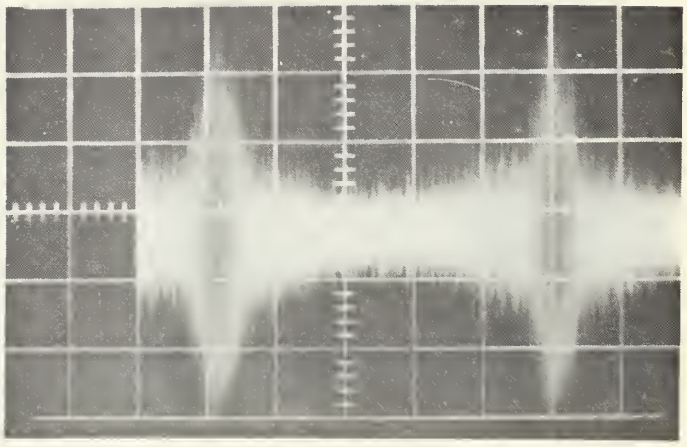

(e)

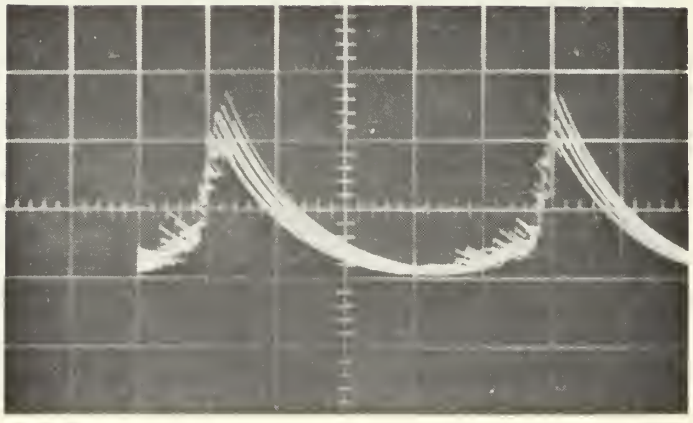

(f)

TABLE VI

EFFECT OF NOISE ON THE PERFORMANCE OF
AN EXPERIMENTAL MFD DF SYSTEM

Basic Parameters:

(a) β (before frequency multiplication) = 25

(b) β (after frequency multiplication by a factor of four) = 100

(c) 4-kHz bandpass filter (TL 4D8-A)

(d) 10-kHz bandpass noise filter (TL 10D9-20A)

Figure	INPUT			OUTPUT	
	Signal (dB)	Noise (dB)	SNR (dB)	Signal (dB)	Signal plus Noise (dB)
47-a,b	8.0	5.0	3.0	-20.0	-18.0
47-c,d	8.0	-2.0	10.0	-20.0	-19.0
47-e,f	8.0	-12.0	20.0	-20.0	-19.7

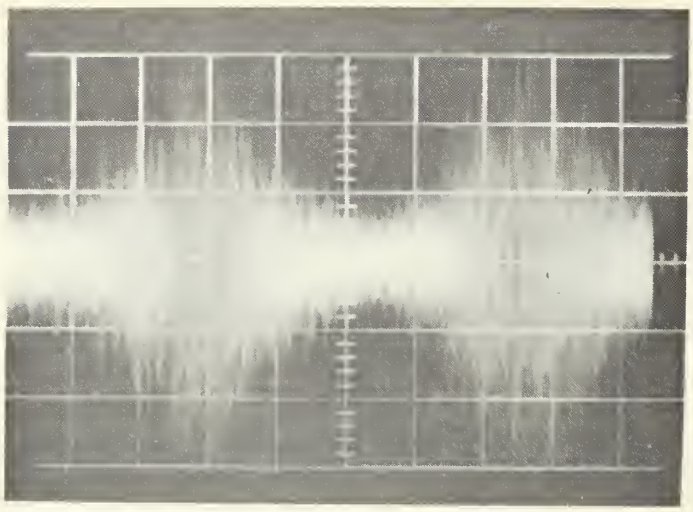

(a)

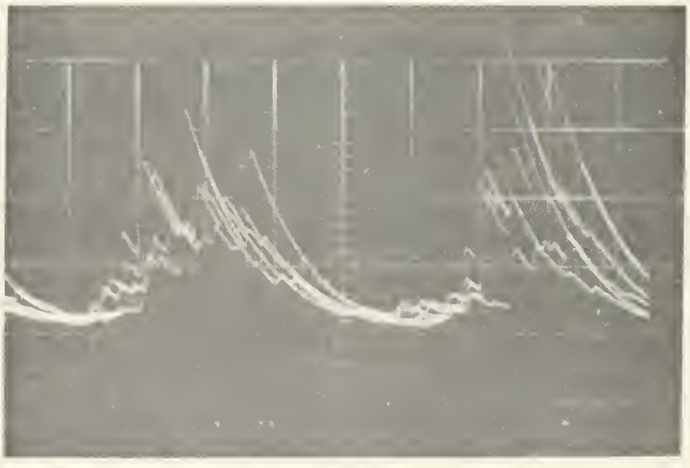

(b)

FIG. 47. PHOTOGRAPHS OF THE RESPONSE OF THE EXPERIMENTAL MFD DF SYSTEM FOR VARIOUS VALUES OF INPUT SNR

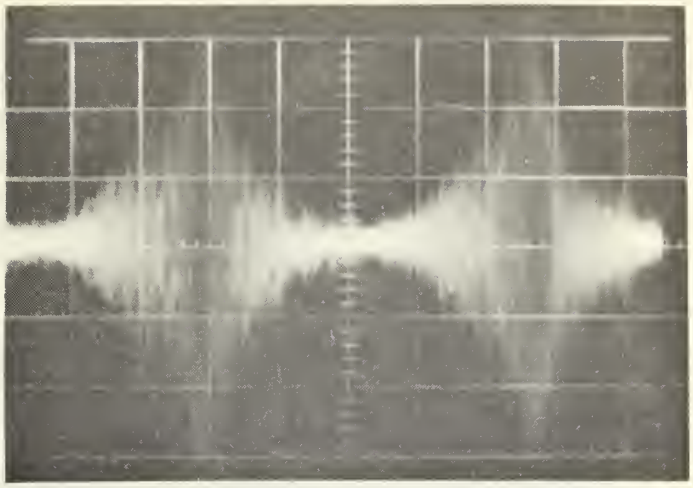

(c)

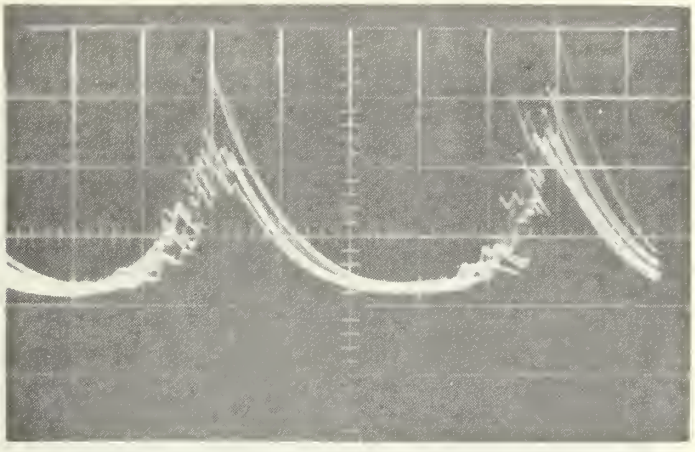

(d)

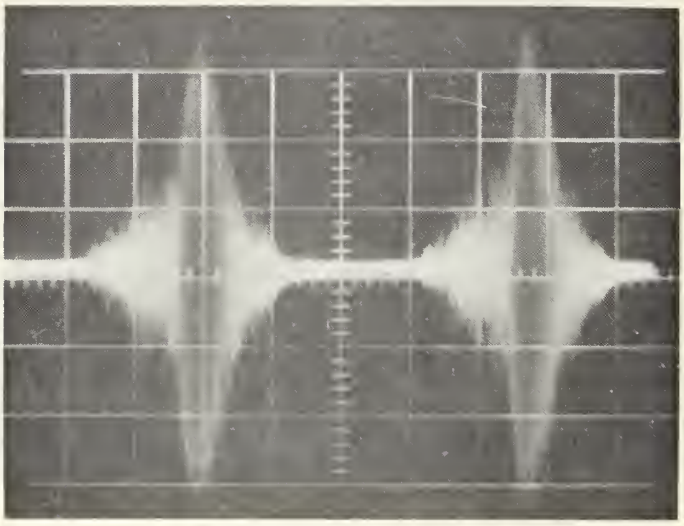

(e)

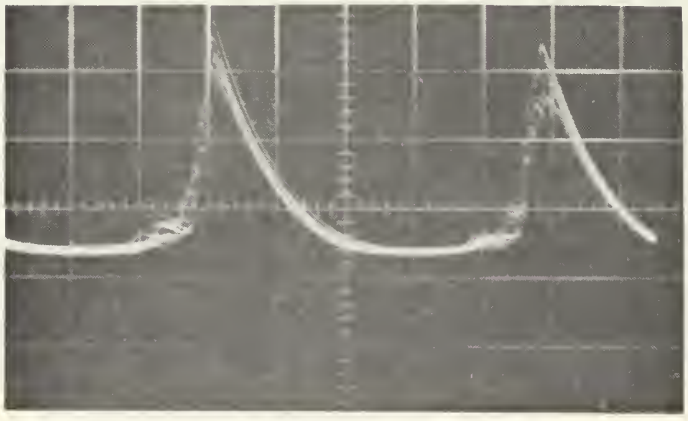

(f)

E. EXPERIMENT USING A CONVENTIONAL DOPPLER DF SYSTEM

This section describes the equipment, procedures and results of an experiment in which a MFD DF system was assembled by interfacing the hardware constructed for the laboratory experiments with a conventional doppler DF set. The experimental system was tested both with controlled target transmitters and distant targets of opportunity. Despite the discrepancies between the theoretical and experimental results, the experiment shows the MFD DF system can be used with existing commutated circular arrays to provide information on signal AOA.

1. Description of Equipment

An AN/TRD-15 DF set [27] is used to provide live signals to test the MFD DF principle. The particular set used consists of an array of 25 monopoles equally spaced around a circle of 150 ft diameter. A matched cable from each antenna is connected to a stator of an RF rotary coupler physically situated in a hut at the center of the array. The effective point of reception is made to travel around the array by rotating at a 50 Hz rate a pickup-winding commutator located on the rotor of the coupler. The commutator rotation simulates the rotation of a single antenna around the circle.

The rotor output is applied to a superheterodyne receiver and converted to an IF of 455 kHz. In the conventional set, the IF is processed and eventually sent to a display unit. For this experiment, a parallel connection

was made from the last limiter stage of the receiver to the MFD DF experimental hardware. This allows both DF systems to function simultaneously.

The experimental hardware consists of frequency multipliers, a balanced mixer, a ceramic bandpass filter, and optionally, an envelope detector (see Fig. 48).

By varying the local-oscillator frequency, the difference frequency in the mixer output is shifted at will and any portion of the FM spectrum can be placed in the filter passband. The filtered output can be viewed on an oscilloscope, either before or after envelope detection.

2. Results

During the course of the experiment several signals in the HF region were examined. They included controlled target transmitters, as well as targets of opportunity such as WWV. Because circuitry to remove modulation from incoming signals was not used, primary emphasis was on unmodulated or slowly modulated carriers.

The results presented in Table VII and Figs. 49-53 confirm some of the important characteristics of the MFD DF technique including

(1) Filtering of the appropriate side frequencies of the output of a commutated circular array which operates in an equivalent manner to a single rotating element yields an output having an envelope consisting of a periodic pulse. The relative time of occurrence of the pulse is linearly related to the AOA of the received signal.

TABLE VII

PERFORMANCE OF AN EXPERIMENTAL MFD DF SYSTEM
USED WITH A CONVENTIONAL DOPPLER DF SET

Fig	Signal NR	Freq mHz	Transmitter	Modulation	Freq Mult by	Estimated MFD DF Bearing	Modulation Index (β)	Horizontal Scale, $\frac{ms}{cm}$	Comments
49-a	1	9.960	Local target at 90°	None	2	100°	10	5	RF envelope
49-b	1	"	"	"	"	"	"	2.5	"
50-a	2	10.902	Unknown	Intermittent FSK	2	210°	10	5	"
50-b	2	"	"	"	4	"	20	5	"
51	3	20.600	"	None	"	40°	40	5	Detected envelope
52-a	4	21.740	Local target at 90°	"	"	90°	"	5	
52-b	4	"	"	"	"	"	"	5	
53-a	4	"	Local target at 190°	"	"	200°	"	5	
53-b	5	29.951	"	"	"	"	60	5	

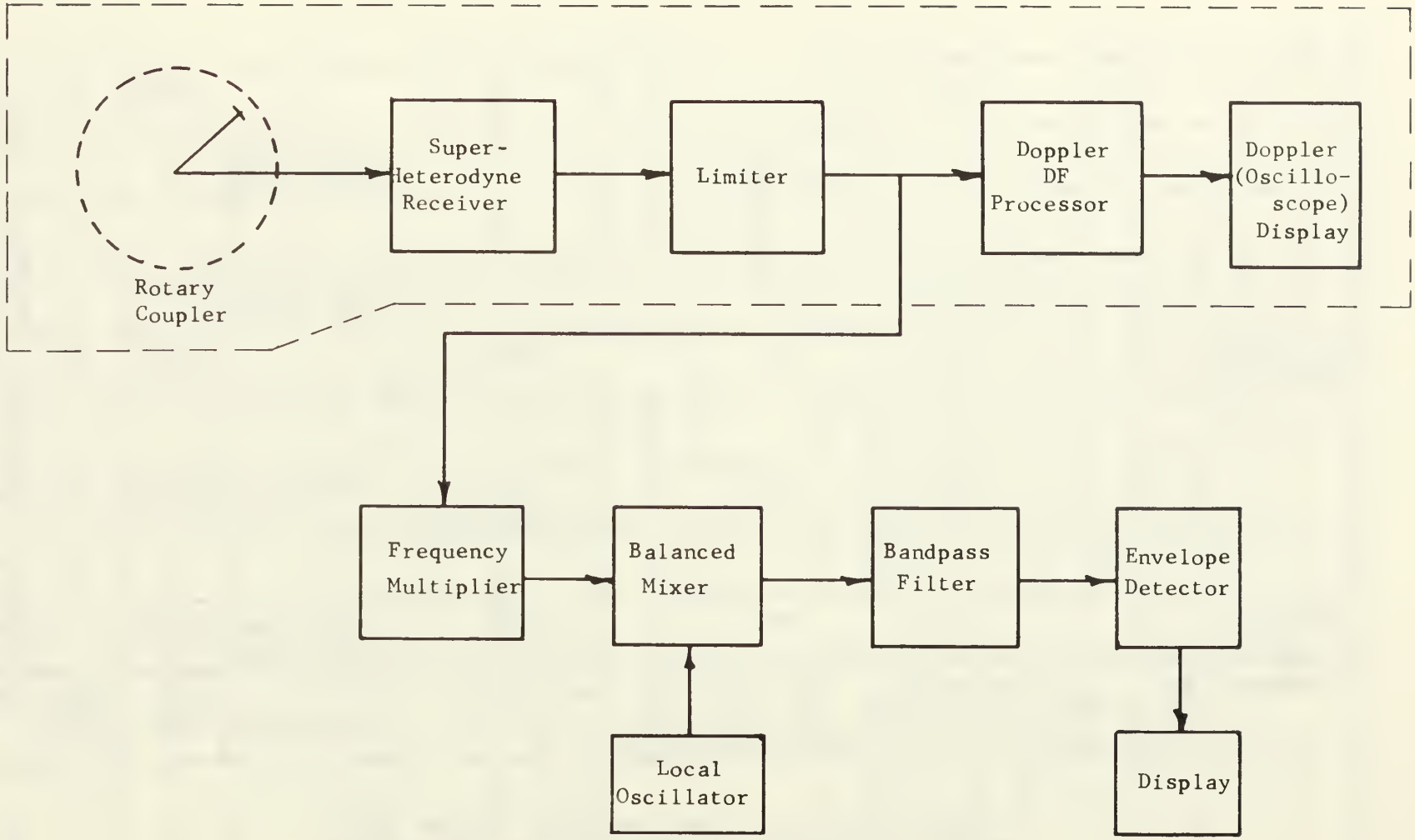

FIG. 48. BLOCK DIAGRAM OF THE EXPERIMENTAL MFD DF SYSTEM INTERFACED WITH A CONVENTIONAL DOPPLER DF SYSTEM

(2) The 180° shift in apparent bearing which occurs when the group of in-phase frequency components below the carrier frequency is selected is demonstrated.

(3) The relative time of occurrence of the pulse (bearing) is shown to be independent of transmitter frequency.

The system output for signal 1 of Table VII is shown in Fig. 49 for approximately three cycles of scanning. The second pulse is weaker than the first and third because of incidental amplitude modulation of the envelope at twice the rotor revolution rate. The oscilloscope from which the photographs were taken was set to trigger at a north reference; hence by relating the distance between pulses to one revolution of the rotor, approximate bearings can be derived from the position of the pulse along the horizontal axis. For example, in Fig. 49-a the pulse appears at a point slightly more than one-quarter of a cycle from the triggering point; thus the signal bearing is estimated to be about 100 degrees. Figure 49-b is an expanded version (horizontal trace) of Fig. 49-a showing the structure of the pulse in more detail.

Signal 2 of Table VII (Fig. 50) shows the system response (three cycles) to an unidentified target of opportunity. The main pulses in Fig. 50-b are narrower than those in Fig. 50-a since multiplication by a factor of four is used in the former case and by a factor of two in the latter.

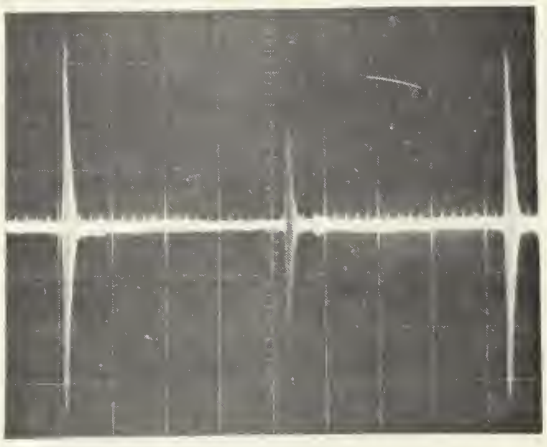

(a) Response of experimental MFD DF system to signal #1. (Table VII). Three cycles of scan.

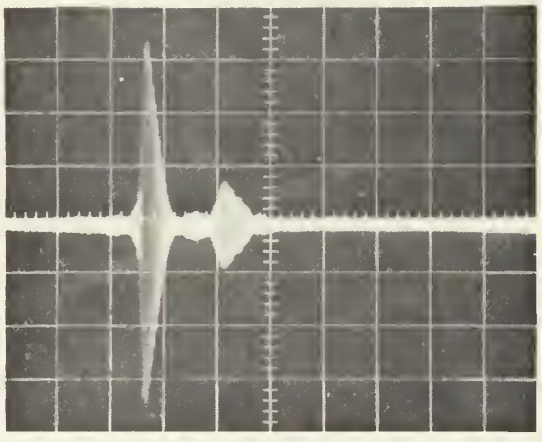

(b) Response of experimental MFD DF system to signal #1. (Table VII). Part of one scan.

FIG. 49. PHOTOGRAPHS OF THE RESPONSE OF THE MFD-AN/TRD-15 DF SYSTEM

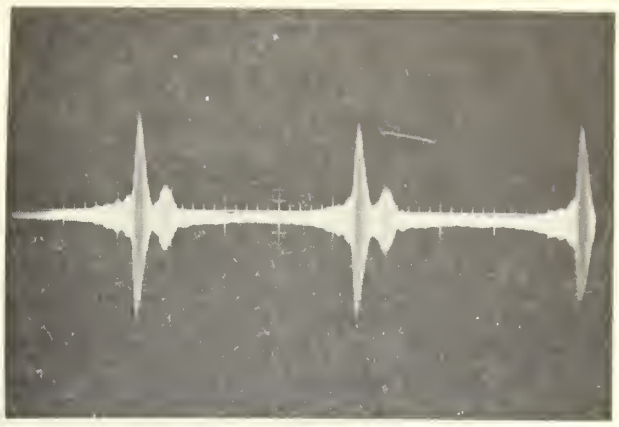

(a) Response of experimental MFD DF system to signal #2 (Table VII).

(b) Response of experimental MFD DF system to signal #2 (Table VII).

FIG. 50. PHOTOGRAPHS OF THE RESPONSE OF THE MFD-AN/TRD-15 DF SYSTEM

Figs. 51-53 are photographs of detected voltages. For example, Fig. 51 shows the envelope of the system output for an unidentified signal (number 3 of Table VII).

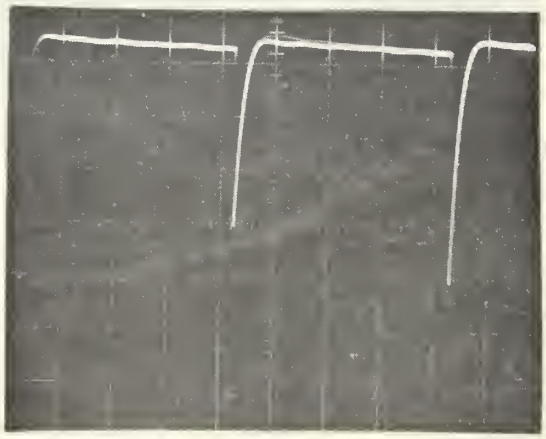

FIG. 51. PHOTOGRAPH OF THE ENVELOPE OF THE RESPONSE OF THE MFD-AN/TRD-15 DF SYSTEM

As discussed previously in Chapter II, the frequency components of the spectrum of a carrier frequency modulated by a sinusoid are symmetrical with respect to magnitude, though not phase, about the carrier frequency f_c. Filtering the in-phase group of frequency components below f_c was shown to produce a pattern identical in shape to that obtained by selecting the corresponding group above f_c. The only difference in the outputs is a time delay corresponding to a half period of rotation of the rotor, or in terms of AOA measurement, a bearing shift of 180 degrees. Despite the poor quality of the pulses, Fig. 52 illustrates this result.

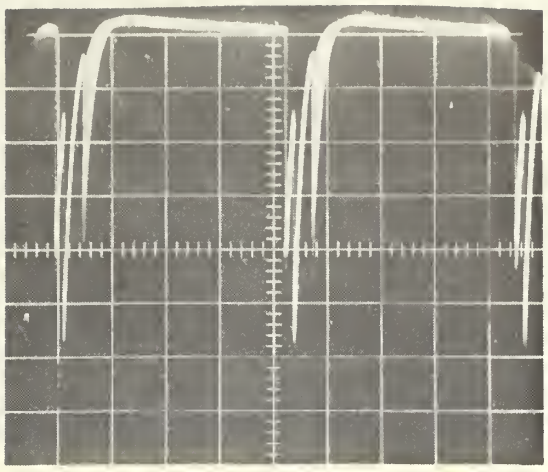

(a) Detected response of experimental MFD DF system to signal #4 (Table VII). In-phase group above the carrier frequency.

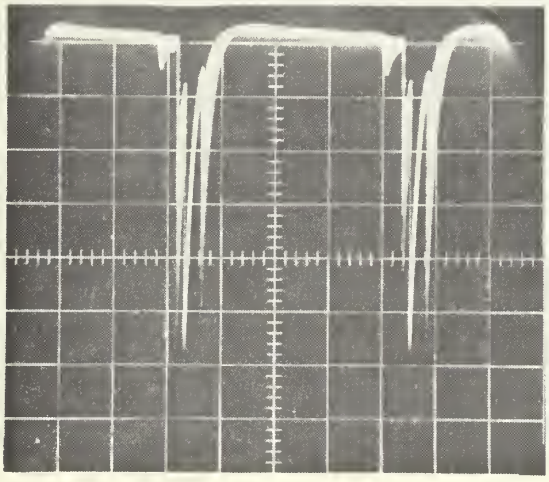

(b) Detected response of experimental MFD DF system to signal #4 (Table VII). In-phase group below the carrier frequency.

FIG. 52. PHOTOGRAPHS OF THE ENVELOPE OF THE RESPONSE OF THE MFD-AN/TRD-15 DF SYSTEM

Fig. 52-a shows the transmitter bearing to be about 100 degrees when the in-phase frequency components above f_c are filtered, while Fig. 52-b shows the same signal at an apparent bearing of about 280 degrees when the in-phase group below f_c is filtered.

Fig. 53 is intended to show that the presentation obtained with a target transmitter at a fixed bearing is unchanged as the frequency changes from 21.74 MHz to 29.95 MHz.

Discrepancies between the results just presented, the results obtained from laboratory experiments, and the computer results can in part be attributed to the following:

(1) The inductive sampling of RF energy from 25 discrete antennas instead of a continuous output from a single rotating antenna.

(2) Incidental FM caused by the limiter.

(3) Non-ideal amplitude- and phase-vs-frequency characteristics of the RF and IF portions of the superheterodyne receiver.

(4) Lack of knowledge of the position of the received signal in the passband of the receiver. The local oscillator was tuned until an optimal or near optimal MFD DF system output was observed on the oscilloscope. Use of a spectrum analyzer would have permitted more precise tuning.

(a) Detected response of experimental MFD DF system to signal #4 (Table VII). Transmitter at 21.74 MHz.

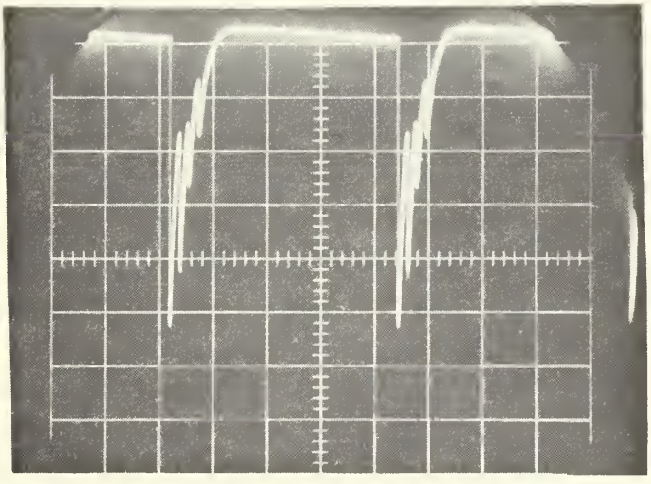

(b) Detected response of experimental MFD DF system to signal #5 (Table VII). Transmitter at 29.95 MHz.

FIG. 53. PHOTOGRAPHS OF THE ENVELOPE OF THE RESPONSE OF THE MFD-AN/TRD-15 DF SYSTEM

Particular discrepancies which appear in Figs. 49-53 are

a. pulses narrower than anticipated.

b. undesired secondary pulses

c. irregular pulse shapes.

V. THE TWO SIGNAL CASE

A common occurrence in the propagation of radio waves is the arrival of a signal at a receiver by two different paths. This phenomenon is particularly troublesome in DF when the multipath signal arrives from two different azimuth angles. This chapter explores analytically the theoretical performance of a MFD DF system under multipath conditions. The effect of angle of elevation is briefly considered.

A. THEORY

When two signals of the same frequency with angles of arrival θ_1 and θ_2 are received by an element (or equivalent array) oriented initially as shown in Fig. 54 and rotated (or sampled) counterclockwise, the response of the system is

$$p(t) = C_1\cos[\omega_c t + \beta\sin(\omega_r t - \theta_1)] + C_2\cos[\omega_c t + \beta\sin(\omega_r t - \theta_2) + \psi_1] \qquad (53)$$

where ψ_1 is the phase difference between the incoming signals when received at the center of rotation and C_1 and C_2 are constants.

To simplify (53) let

$$C_1 > C_2\ ,\quad C_1 = 1\ ,\quad b = C_2/C_1\ ,\quad \text{and}\quad \theta_1 = 0.$$

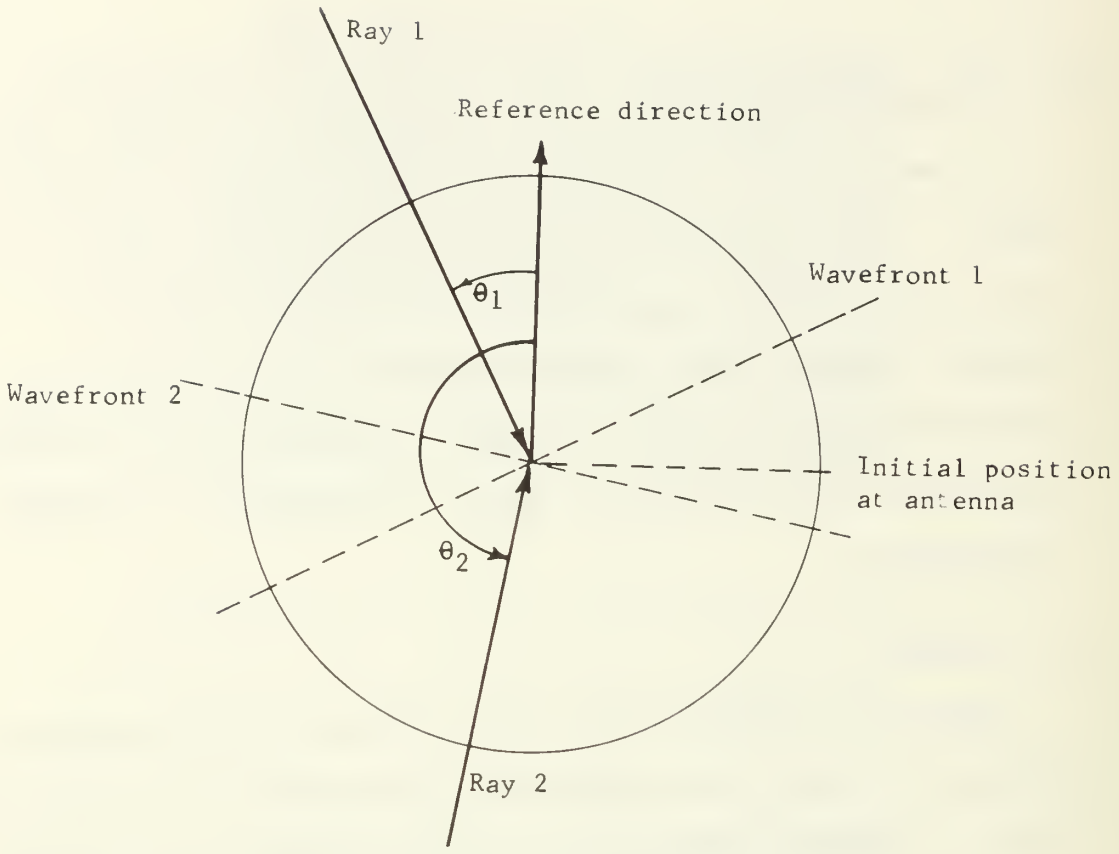

FIG. 54. PLAN VIEW OF A ROTATING ANTENNA ELEMENT SHOWING THE RECEPTION OF TWO LIKE-FREQUENCY SIMULTANEOUS SIGNALS

Under these conditions (53) becomes

$$p(t) = \cos[\omega_c t + \beta \sin\omega_r t] + b\cos[\omega_c t + \psi_1 + \beta \sin(\omega_r t - \theta_2)] \quad (54)$$

Because of the symmetry in the spectrum of sinusoidal FM, no generality is lost by considering only the frequencies above the carrier. Following a development similar to the single-signal case in Chapter II, and shown in detail in Appendix B, two groups of in-phase harmonics, one from each term in (54), can be isolated and expressed in the form of a carrier and a modulating envelope as

$$p_1(t) = F(t)\cos[\omega_c t + \Phi(t)] \qquad (55)$$

where F(t) is the amplitude-modulation factor and $\Phi(t)$ is the phase-modulation term.

Concerning MFD DF processing of multipath signals it is of interest to determine whether the envelope F(t) at the output will have two main pulses corresponding in time to the azimuth angles of the two incoming signals, assuming that the azimuth separation is sufficient for resolution. From (55) and Appendix B it appears that there are two terms which may correspond to two separate pulses. The only uncertainty is the effect of the phase difference ψ_1.

Figure 55 confirms the existence of two separate pulses in the case of two equal-amplitude signals, one at

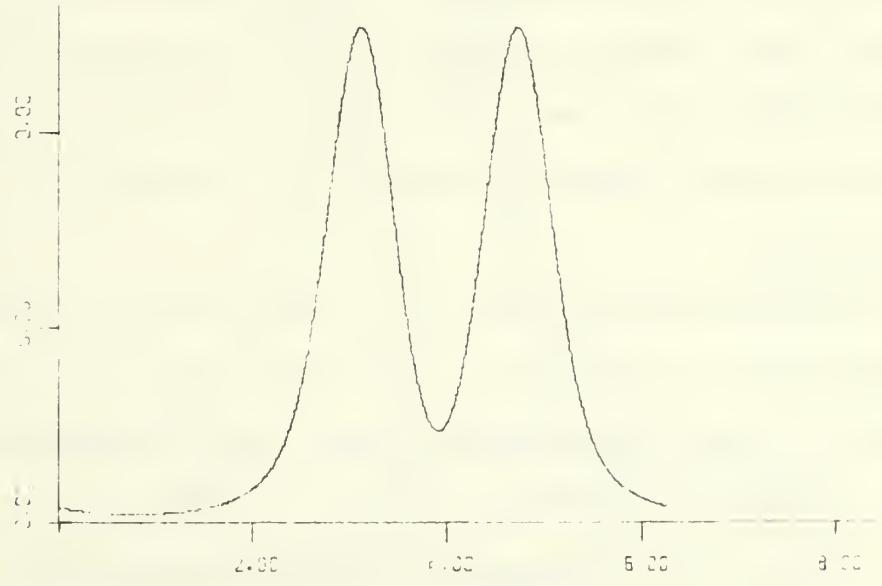

FIG. 55. COMPUTED ENVELOPE OF THE RESPONSE OF AN IDEAL MFD DF SYSTEM TO TWO SIMULTANEOUS SIGNALS

180 degrees of azimuth and the other at 270 degrees, with a relative carrier phase difference ψ_1 of zero. In this example, a value of β of 50 is assumed as well as ideal filtering of the in-phase group of frequencies (44th through 58th harmonics of f_r above f_c).

The effect of the phase difference can be seen by varying ψ_1 from zero to 360 degrees. Calculated results show that ψ_1 causes the peak-to-dip ratio to vary slowly from 9.6 dB when ψ_1 = 253 degrees to 51.4 dB when ψ_1 = 70 degrees. However, variations in the location of the two maxima, corresponding to errors in bearing measurements are less than 1.6 degrees for all values of ψ_1. Figure 56 shows the "best" and "worst" cases for this example corresponding to the two extremes in peak-to-dip ratio mentioned above.

The MFD DF system response to two signals of the same frequency thus consists basically of the superposition of each individual response. The phase difference ψ_1 between the two arriving signals may affect the interaction of the two responses.

The relative amplitudes of the two received signals can reasonably be expected to directly affect the relative amplitudes of the two pulses at the output of the MFD DF system. This is exemplified in Fig. 57 which shows computed output envelopes from a system having a value of β of 50 for the case of two signals separated 90 degrees in azimuth. Four different relative amplitudes are shown in Fig. 57 ranging from b = 0.9 to b = 0.1. The error in the derived

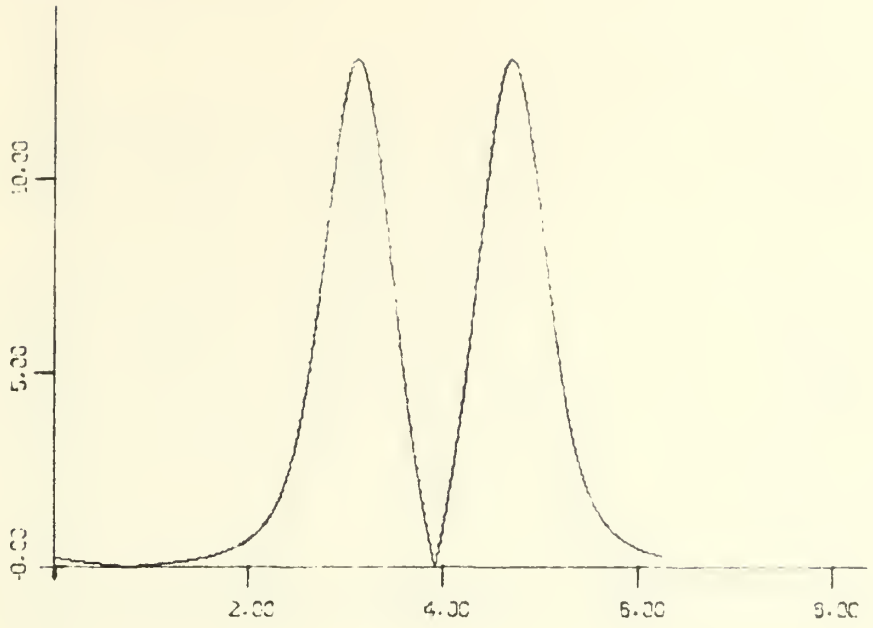

(a) Phase difference is 70 degrees.

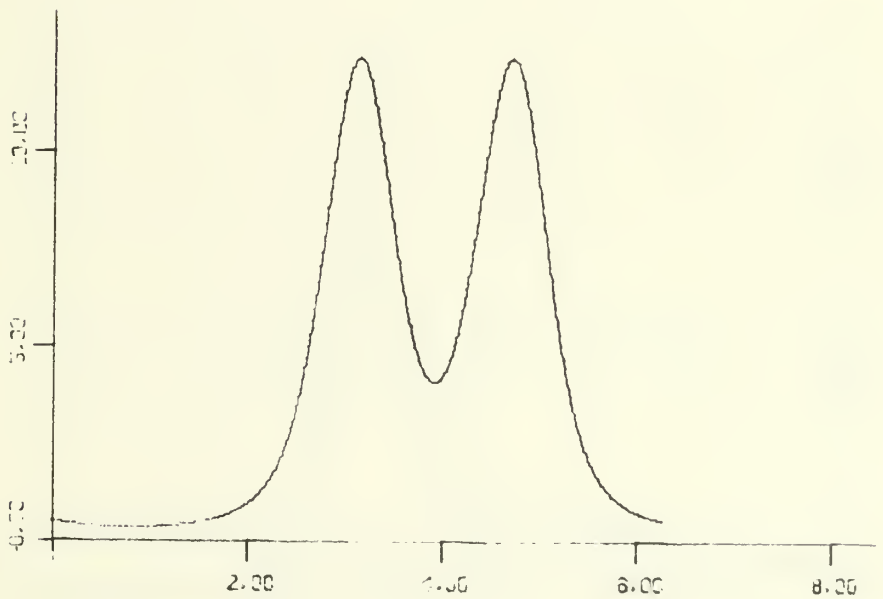

(b) Phase difference is 253 degrees.

FIG. 56. COMPUTED ENVELOPES OF THE RESPONSE OF AN IDEAL MFD DF SYSTEM TO TWO SIMULTANEOUS SIGNALS

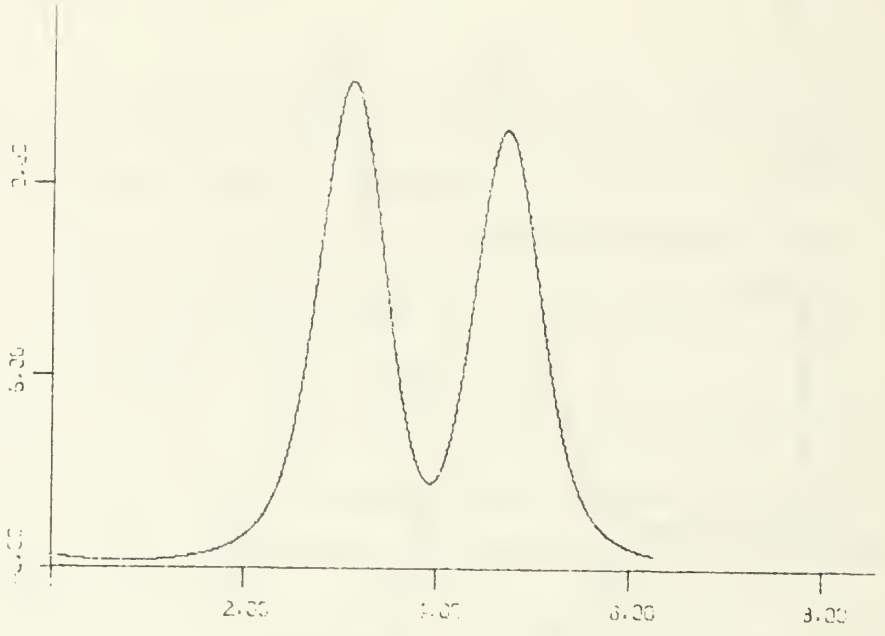

(a) b = 0.9

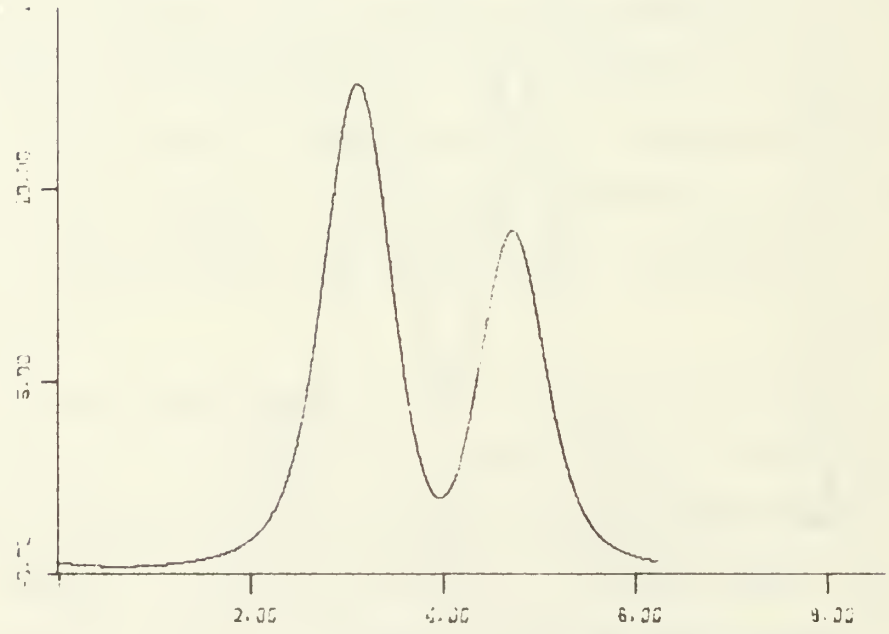

(b) b = 0.7

FIG. 57. COMPUTED ENVELOPES OF THE RESPONSE OF AN IDEAL MFD DF SYSTEM TO TWO SIMULTANEOUS SIGNALS

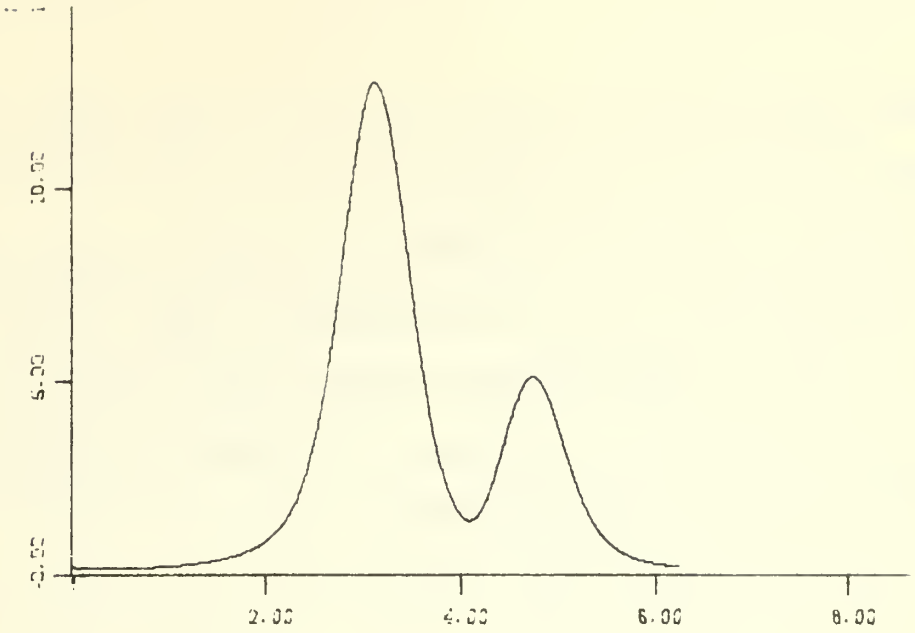

(c) b = 0.4

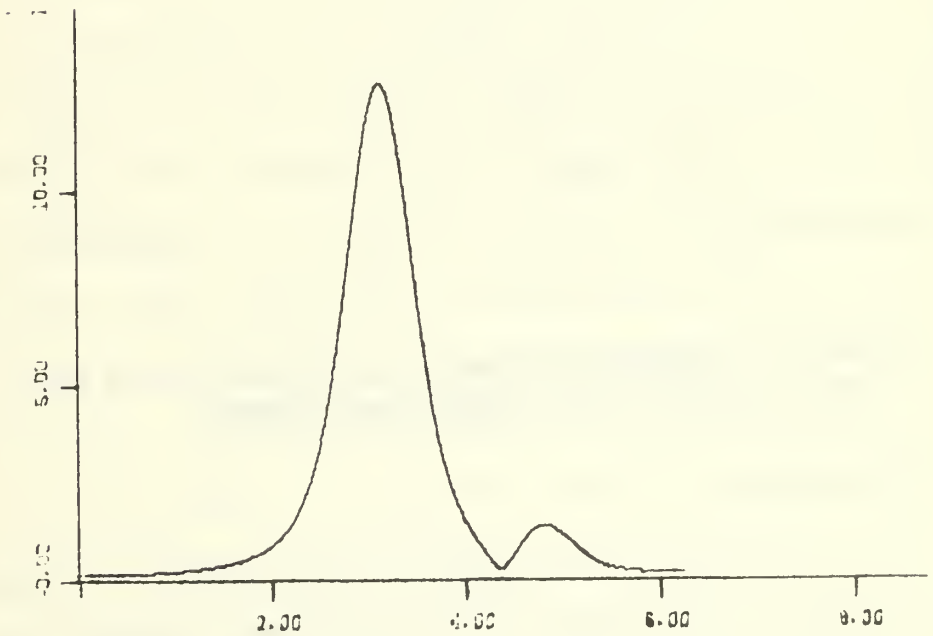

(d) b = 0.1

azimuth angle of the weaker of the two varies from 1.0 degree (b = 0.9) to 12.5 degrees (b = 0.1).

As the value of β increases the system output pulses which indicate the AOA of the received signals become narrower. This is exemplified by Fig. 58 which shows the response produced by two signals 90 degrees separated in AOA when the value of β is 200.

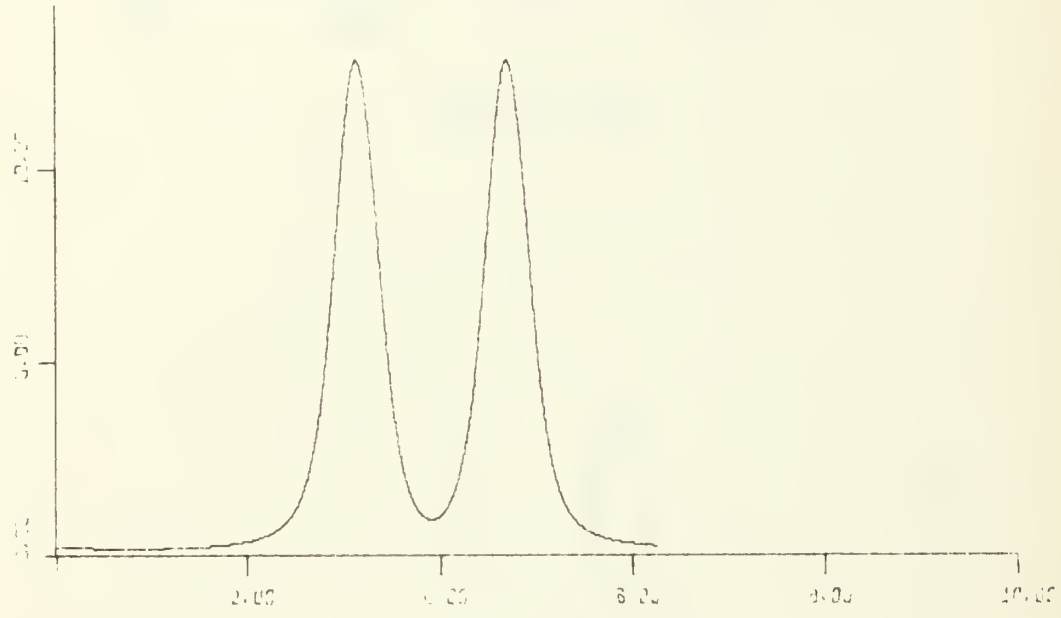

FIG. 58. COMPUTED ENVELOPE OF THE RESPONSE OF AN IDEAL MFD DF SYSTEM TO TWO SIMULTANEOUS SIGNALS

B. RESOLUTION

The theoretical resolution of a DF system is a measure of the smallest difference in AOA between two arriving signals at which each can be separately distinguished. For the output of the MFD DF system, this corresponds to some measure of the distinguishability between the two pulses corresponding to the AOA of the two received signals. The

measure taken here is the smallest interval (expressed in degrees of azimuth) for which the dip between the two pulses is at least 3 dB below the smaller of the two.

The most important parameters affecting resolution are relative signal amplitude b, carrier phase difference ψ_1, and modulation index β.

The effect of the relative amplitude b is to decrease the resolution as b decreases. Thus, as shown in Fig. 59 for $\beta = 50.0$ and $\psi_1 = 0$ the resolution angle varies from 60.7 degrees when the two signals are of equal amplitude, to 102 degrees when the amplitude of the weaker signal is 0.1 that of the stronger (20-dB level difference).

The effect of the carrier phase difference ψ_1 is seen in Fig. 60 obtained at a constant value of $\beta = 50$ for equal-amplitude signals, which shows the resolution angle varying from 55.5 degrees to 61.5 degrees as ψ_1 goes from 0 to 2π radians.

Finally, the effect of β on resolution is presented in Fig. 61 as the other two pertinent parameters b and ψ_1 are held constant. As might be expected from previous discussions the resolution improves directly with β.

C. INFLUENCE OF ELEVATION ANGLE

The effect of the angle of elevation α of the received signal on the FM signal produced by a rotating antenna 13 can be taken into account by rewriting (54) as

$$p(t)=\cos[\omega_c t+\beta\cos\alpha_1\sin(\omega_r t)]+b\cos[\omega_c t+\psi_1+\beta\cos\alpha_2\sin(\omega_r t-\theta_2)] \quad (56)$$

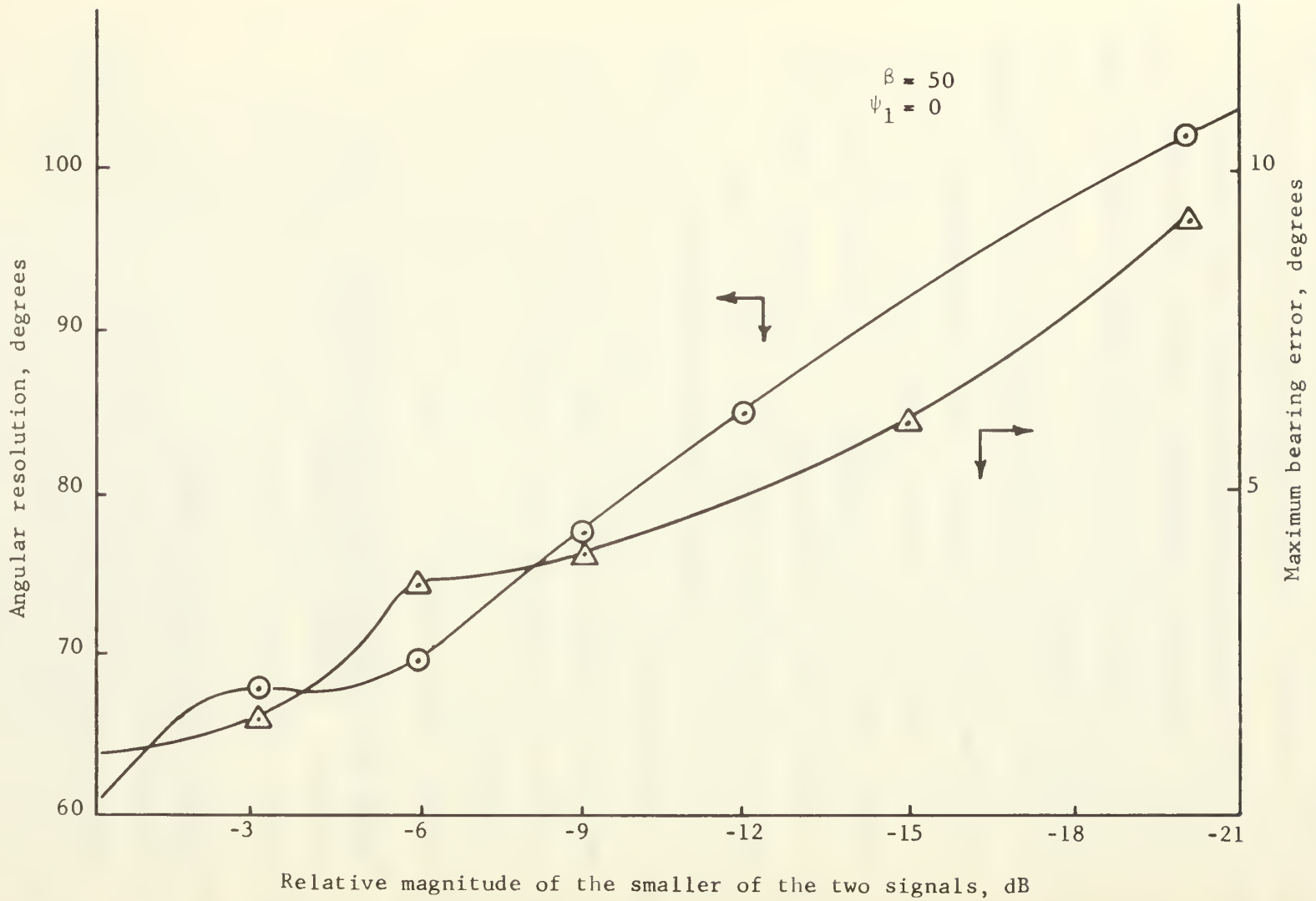

FIG. 59. GRAPH OF THE THEORETICAL R SOLUTION AND BEARING ERROR OF THE MFD DF SYSTEM VS THE RATIO OF THE AMPLITUDES OF TWO LIKE-FREQUENCY SIMULTANEOUS SIGNALS

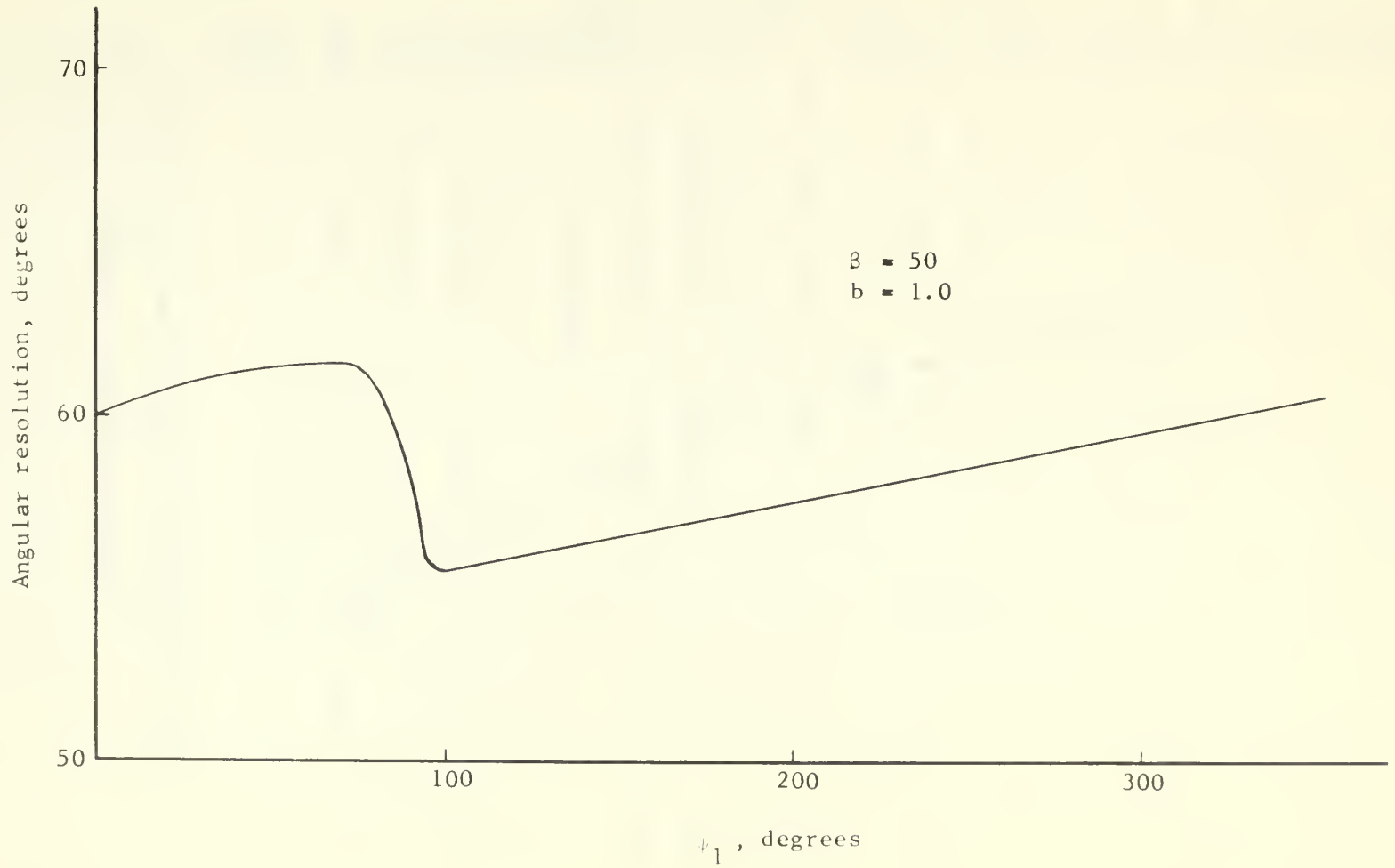

FIG. 60. GRAPH OF THE THEORETICAL RESOLUTION OF THE MED DF SYSTEM VS THE DIFFERENCE ψ_1 IN PHASE OF THE TWO LIKE-FREQUENCY SIMULTANEOUS SIGNALS

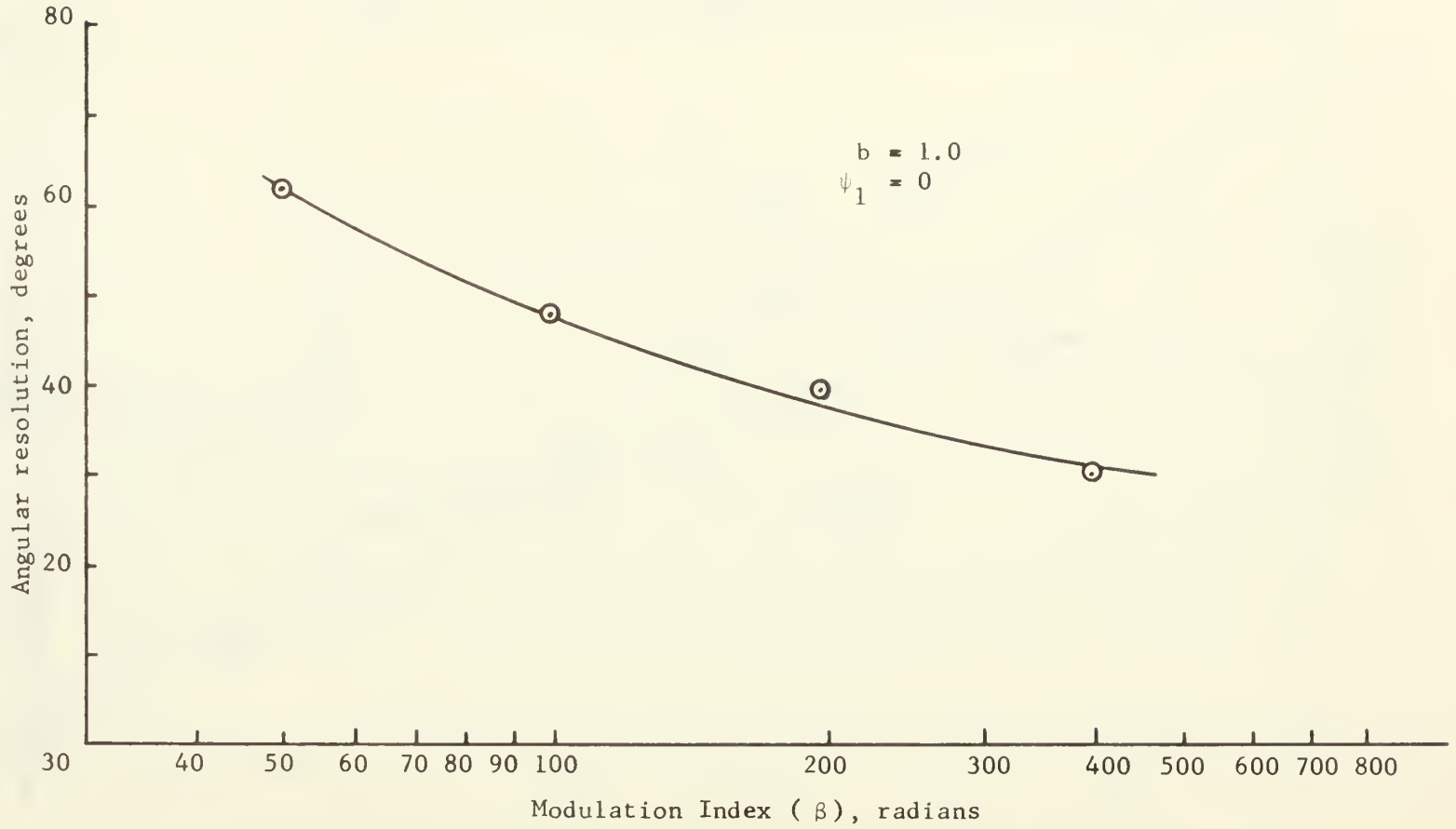

FIG. 61. GRAPH OF THE THEORETICAL RESOLUTION OF THE MFD DF SYSTEM VS THE MODULATION INDEX β

The effect of elevation angle can be equated to a reduction in the modulation index β. As long as α_1 and α_2 are approximately equal, the effect is a decrease in the effective aperture of the antenna since a lower value of β can be associated with a smaller radius of rotation. However if α_1 and α_2 differ significantly, there will be a considerable difference in the overall bandwidths of the two FM signals at the output of the antenna. This means that a bandpass filter which selects the in-phase group of frequency components from the signal having the larger value of β (smaller α) will have fewer or none of the desired spectral components of the signal having the lower value of β (larger α) in its passband. The MFD DF system output under these circumstances de-emphasizes the effect of the signal having the largest elevation angle or would provide no indication of its presence.

On the other hand, to attempt to bandpass filter the in-phase group of frequency components associated with the signal having the smaller value of β would necessarily admit undesired frequency components of the signal having the larger value of β, so this procedure may not be acceptable.

VI. SUMMARY AND RECOMMENDATIONS

A. SUMMARY

The problem of determining the direction of arrival of a radio wave has been approached from a different point of view, namely, that of applying matched-filter processing to the output of a rotating antenna.

Chapter II presents the principal results of this research which are the development of the theory and an indication of the performance of a matched-filter doppler DF system which is simple to realize and completely linear. When a radio wave impinges upon an antenna element omni-directional in the plane of propagation and which rotates in a circle (also in the plane of propagation) the output of the antenna is modulated sinusoidally in frequency due to the doppler effect. If this modulated signal is applied to a bandpass filter which allows only a particular group of frequency components to pass, the output is a periodic train of short duration pulses having no sidelobes. The time of occurrence of each output pulse relative to one rotation period is directly related to the AOA of the radio wave.

This technique evolves as a practical compromise after recognizing the difficulty in realizing a filter matched to the entire spectrum of a signal frequency modulated by a sinusoid. The bandpass filter isolates a group of frequency components which by themselves satisfy without

processing of any kind the condition of in-phase frequency components normally obtained with a matched filter.

To improve system accuracy it is desirable that the duration of the pulse used to measure AOA be small. Pulse duration is inversely related to the value of the modulation index β of the FM signal. In turn, at any given frequency, the value of β is directly proportional to the radius of the circle of rotation (or of an equivalent circular array). It appears, therefore, that a reduced pulse duration results only from an increase in the size of the receiving aperture. However, it is shown that the technique of frequency multiplication can be used to increase the value of β without increasing the aperture size.

To apply signal-processing techniques, such as matched filtering, to obtain spatial information, such as direction of arrival, the receiving antenna must convert spatial information to temporal form. As shown in Chapter III this is exactly what occurs when a linear antenna (or array) is rotated about a central point. This chapter also includes a Fourier transform representation of an antenna and reveiving system.

The physical realizability of the MFD DF technique, including the frequency-multiplication scheme, is demonstrated by presenting results obtained with a hardware simulation system. A critical component is found to be the bandpass filter since imperfect filtering of the desired

frequency components is found to produce undesireable results such as generation of double maxima in the output.

The effect of bandlimited gaussian noise on the MFD DF system is considered. When processing without frequency multiplication the system improves SNR due to the difference in spectral distribution of the noise power and the signal power. There is also an increase in the ratio of peak signal to average-noise power because the output signal power is concentrated in a fraction of the cycle (pulse compression) while the noise power is distributed over the entire cycle. When the processing of the signal includes frequency multiplication (a nonlinear step), the SNR is reduced by about 6 dB each time the frequency is doubled. This loss in SNR tends to degrade system accuracy whenever the input SNR is less than about 20 dB. Therefore, frequency multiplication may be a useful option in system operation only if the input SNR exceeds about 20 dB.

An experiment in which the experimental MFD DF circuitry is interfaced with a conventional doppler DF set confirms under field-operating conditions the basic characteristics of the MFD DF technique.

The theoretical response of the system to two signals of the same frequency at different angles of arrival consists basically of the superposition of the two individual responses.

B. RECOMMENDATIONS

1. To further evaluate the merits and limitations of the MFD DF technique an operational system should be constructed and tested.

2. A tactical DF system based on the MFD technique may be possible by installing an antenna in the end of a helicopter rotor.

3. A study should be made of the spectrum of various types of frequency or phase modulation with the object of finding signal spectra which are amenable to matched-filter processing using simple conventional filters.

4. Other methods of direction finding should be studied to determine if various means of increasing signal bandwidth can be used advantageously in conjunction with these DF techniques.

APPENDIX A

COMPUTATION OF THE RESPONSE OF AN IDEAL MATCHED-FILTER DOPPLER DF SYSTEM

The response of an ideal doppler DF array of radius ℓ to an unmodulated signal at frequency f_c and azimuth θ_o is given by (1) as

$$s(t) = C\cos[\omega_c t + \frac{2\pi\ell}{\lambda_c} \sin(\omega_r t - \theta_o)] \qquad \text{(A-1)}$$

Expanding the above in a Fourier series yields (when $C = 1$),

$$s(t) = [J_o(\beta)\cos\omega_c t + \sum_{k=1}^{\infty} J_k(\beta)\cos[(\omega_c+k\omega_r)t-k\theta_o]$$

$$+ \sum_{k=1}^{\infty} (-1)^k J_k(\beta)\cos[(\omega_c - k\omega_r)t+k\theta_o] \qquad (6)$$

Because $J_k(\beta)\rightarrow o$ as $k>>\beta$ the above series may be truncated at some integer n_1 for which $J_{n_1}(\beta)$ has decreased to some small factor of the largest $J_k(\beta)$. The effect of an idealized bandpass filter is simulated by omitting all terms in the series except those which correspond to the frequencies which are passed by the filter. This yields

$$s_1(t) = \sum_{k=n_o}^{n_1} J_k(\beta)\cos[(\omega_c + k\omega_r)t - k\theta_o] \qquad \text{(A-2)}$$

To study the envelope $E(t)$ of (A-1), a conversion is made, using trigonometric identities, as follows

$$s_1(t) = A_1(t)\cos\omega_c t - B_1(t)\sin\omega_c t \qquad \text{(A-3)}$$

where

$$A_1(t) = \sum_{k=n_o}^{n_1} J_k(\beta)[\cos k(\omega_r t - \theta_o)] \qquad \text{(A-4)}$$

$$B_1(t) = \sum_{k=n_o}^{n_1} J_k(\beta)[\sin k(\omega_r t - \theta_o)] \; . \qquad \text{(A-5)}$$

Finally,

$$s_1(t) = E(t)\cos[\omega_c t + \phi(t)] \qquad \text{(A-6)}$$

where

$$E(t) = \sqrt{[A_1(t)]^2 + [B_1(t)]^2} \qquad \text{(A-7)}$$

and

$$\phi(t) = \tan^{-1}\frac{B_1(t)}{A_1(t)} \; . \qquad \text{(A-8)}$$

Values of E(t) are obtained with the aid of a digital computer.

APPENDIX B

COMPUTATION OF IDEAL MFD DF SYSTEM TWO-SIGNAL RESPONSE

The response of an ideal doppler array to two signals at the same frequency but different azimuth angles is given by

$$p(t) = C_1\cos[\omega_c t + \beta\sin(\omega_r t - \theta_1)] + C_2\cos[\omega_c t + \beta\sin(\omega_r t - \theta_2) + \psi_1] \qquad (53)$$

This expression can be simplified by assuming

$$C_1 = 1, \quad C_2 < C_1, \quad b = C_2/C_1, \quad \text{and} \quad \theta_1 = 0.$$

Under these conditions,

$$p(t) = \cos[\omega_c t + \beta\sin\omega_r t] + b\cos[\omega_c t + \psi_1 + \beta\sin(\omega_r t - \theta_2)] \qquad (B\text{-}1a)$$

from which

$$p(t) = \cos[\omega_c t + \beta\sin\omega_r t] + b\cos\psi_1\cos[\omega_c t + \beta\sin(\omega_r t - \theta_2)] - b\sin\psi_1\sin[\omega_c t + \beta\sin(\omega_r t - \theta_2)]. \qquad (B\text{-}1b)$$

Expanding (B-1b) in a Fourier series yields

$$p(t) \simeq J_o(\beta)\cos\omega_c t + \sum_{k=1}^{n_1} J_k(\beta)\cos(\omega_c+k\omega_r)t + \sum_{k=1}^{n_1} J_k(\beta)\cos(\omega_c-k\omega_r)t$$

$$+ b\cos\psi_1 \left[J_o(\beta)\cos\omega_c t + \sum_{k=1}^{n_1} J_k(\beta)\cos[(\omega_c+k\omega_r)t - k\theta_2] \right.$$

$$\left. + \sum_{k=1}^{n_1} (-1)^k J_k(\beta)\cos[(\omega_c-k\omega_r)t + k\theta_2] \right]$$

$$-b\sin\psi_1 \left[J_o(\beta)\sin\omega_c t + \sum_{k=1}^{n_1} J_k(\beta)\sin[(\omega_c+k\omega_r)t - k\theta_2] \right.$$

$$\left. + \sum_{k=1}^{n_1} (-1)^k J_k(\beta)\sin[(\omega_c-k\omega_r)t + k\theta_2] \right] \qquad \text{(B-2)}$$

The effect of a bandpass filter is simulated as in Appendix A by omitting all terms in the series except those which correspond to the frequencies which are passed by the filter. This yields

$$p_1(t) = \sum_{k=n_o}^{n_1} J_k(\beta)\cos(\omega_c + k\omega_r)t$$

$$+ b\cos\psi_1 \sum_{k=n_o}^{n_1} J_k(\beta)\cos[(\omega_c+k\omega_r)t - k\theta_2]$$

$$- b\sin\psi_1 \sum_{k=n_o}^{n_1} J_k(\beta)\sin[(\omega_c+k\omega_r)t - k\theta_2] \qquad \text{(B-3)}$$

To study the envelope $F(t)$ of $p_1(t)$ (B-3) is put into a more useful form as follows

$$p_1(t) = A_2(t)\cos\omega_c t - B_2(t)\sin\omega_c t \qquad \text{(B-4)}$$

where

$$A_2(t) = \sum_{k=n_o}^{n_1} J_k(\beta)\{\cos(k\omega_r t) + b\cos[k(\omega_r t - \theta_2) + \psi_1]\} \quad \text{(B-5)}$$

$$B_2(t) = \sum_{k=n_o}^{n_1} J_k(\beta)\{\sin(k\omega_r t) + b\sin[k(\omega_r t - \theta_2) + \psi_2]\} \quad \text{(B-6)}$$

Finally

$$p_1(t) = F(t)\cos[\omega_c t + \Phi(t)] \quad \text{(B-7)}$$

where

$$F(t) = \sqrt{[A_2(t)]^2 + [B_2(t)]^2} \quad \text{(B-8)}$$

and

$$\Phi(t) = \arctan \frac{B_2(t)}{A_2(t)} \quad \text{(B-9)}$$

APPENDIX C

MODIFICATION OF MFD DF TO PROCESS MODULATED SIGNALS

The following is a summary of known means of removing modulation from a received carrier.

A. AMPLITUDE MODULATION

A limiter is sufficient to remove envelope variations of an AM signal

B. ANGLE MODULATION

For FM or PM signals the process consists of using an auxiliary receiver at the center of the array. The IF output of this receiver is

$$s_a(t) = K_a \cos[\omega_1 t + \Lambda(t)] \qquad \text{(C-1)}$$

where $\Lambda(t)$ is the carrier angle modulation generated by the transmitter.

The receiver associated with the doppler DF system yields an IF output given by

$$s_b(t) = K_b \cos[\omega_2 t + \Lambda(t) + \beta \sin(\omega_r t - \theta_o)] \ . \qquad \text{(C-2)}$$

If $s_a(t)$ and $s_b(t)$ are applied to a mixer, the difference-frequency output signal is given by

$$s_c(t) = K_c \cos[(\omega_2 - \omega_1)t + \beta \sin(\omega_r t - \theta_o)] \qquad \text{(C-3)}$$

which contains only the doppler modulation. The signal $s_c(t)$ is then processed for DF purposes in the usual manner. This technique of removing carrier angle modulation is used in conventional doppler DF systems [27].

LIST OF REFERENCES

1. Travers, D. N., and Hixon, S. M., Abstracts of Available Literature on Radio Direction Finding 1899-1965, Southwest Research Institute, 1966.

2. Keen, R., Wireless Direction Finding, p. 6-10, Illife and Sons, Third edition, 1938.

3. Benoit, R. C., Jr., and Coughlin, F., Jr., "Designing RDF Antennas," Electronic Industries, v. 18, p. 77-83, April 1959.

4. Gething, P. J. D., "High-Frequency Direction Finding," Proceedings of the IEE, v. 113, p. 49-61, January 1966.

5. Rhodes, D. R., Introduction to Monopulse, McGraw-Hill, 1959.

6. Skolnik, M. I., Introduction to Radar Systems, McGraw-Hill, 1962.

7. Papoulis, A., The Fourier Integral and Its Applications, p. 62-67, McGraw-Hill, 1962.

8. Iehrukimovich, Iu. A., "The Principles Involved in the Construction of an Automatic Radio Direction Finder," Radiotekhnika, v. 14, p. 62-68, June 1959.

9. Ksienski, A., "Signal Processing Antennas," Microwave Journal, v. 4, nrs 10 and 11, p. 77-85 and 87-94, October and November 1961.

10. Budenbom, H. T., Direction Finder, U.S. Patent 2,414,798, 28 January 1947.

11. Boulet, J. L. L., Investigation of Doppler Effect on Determining Direction of Arrival of Radio Waves, Master's Thesis, University of Illinois, 1947.

12. Earp, C. W., and Godfrey, R. M., "Radio Direction Finding by the Cyclical Differential Measurement of Phase," Journal of the IEE, v. 94, part III-A, p. 705-721, 1947.

13. Stanford Electronics Laboratories, Radio Propagation Laboratory Technical Report 32, The Use of Doppler Shift for the Directional Resolution of Received Signals, by E. Gehrels, p. 4-10, April 1958.

14. Baghdady, E. J., Lectures on Communication System Theory, p. 490-508, McGraw-Hill, 1961.

15. Turin, G. L., "An Introduction to Matched Filters," Transactions of the IRE(Information Theory), v. IT-6, p. 311-329, June 1960.

16. Schwartz, M., Information Transmission Modulation and Noise, McGraw-Hill, 1959.

17. Corrington, M. S., "Variation of Bandwidth with Modulation Index," Proceedings of the IRE, v. 35, p. 1013-1016, October 1947.

18. Guillemin, E. A., The Mathematics of Circuit Analysis, p. 512-517, Wiley, 1949.

19. Tucker, D. G., "Superdirective Arrays: The Use of Decoupling between Elements to Ease Design and Increase Bandwidth," The Radio and Electronic Engineer, v. 34, p. 251-255, October 1967.

20. Bracewell, R. N., and Roberts, J. A., "Aerial Smoothing in Radio Astronomy," Australian Journal of Physics, v. 7, p. 615-640, December 1954.

21. Ksienski, A., "Spatial Frequency Characteristics of Finite Aperture Antennas," Electromagnetic Theory and Antennas, v. 2, edited by E. C. Jordan, p.1249-1265, Macmillan, 1963.

22. Bracewell, R. N., The Fourier Transform and Its Applications, p. 275-286, McGraw-Hill, 1965.

23. Davies, D. E. N., and Longstaff, I. D., "Some New Studies of Angular Resolution for Linear Arrays," The Radio and Electronic Engineer, v. 32, p. 341-350, December 1966.

24. Jordan, E. C., Electromagnetic Waves and Radiating Systems, p. 445-451, Prentice-Hall, 1950.

25. Davenport, W. B., and Root, W. L., Random Signals and Noise, p. 277-278, McGraw-Hill, 1950.

26. Harman, W. W., Principles of Statistical Theory of Communications, p. 194-202, McGraw-Hill, 1963.

27. Department of the Army Technical Manual TM 11-5825-231-25, Direction Finder Set AN/TRD-15, May 1966.

DISTRIBUTION LIST

Defense Documentation Center
Cameron Station
Alexandria, Virginia
Attn: IRS (20 copies)

Library
Naval Postgraduate School
Monterey, California 93940
(2 copies)

Naval Security Group Hdq.
3801 Nebraska Ave., N. W.
Washington, D. C. 20390
Attn: G-40 (3 copies)

Naval Ship Systems Command
Navy Department
Washington, D. C. 20360
Attn: W. Steed, Code 6050C

Commanding Officer and Director
Naval Electronics Laboratory Center
San Diego, California 92152

Commander
Naval Electronics Systems Command
Navy Department
Washington, D. C. 20360

Director
Naval Research Laboratory
Washington, D. C. 20390

Office of Naval Research
Navy Department
Washington, D. C. 20305
Attn: Code 427

Librarian
Naval Weapons Center
China Lake, California 93555
Attn: Joseph J. Kovar
Code 3012

Dr. E. O. Brigham, N1
National Security Agency
Fort Meade, Maryland 20755

Argo Systems
1069 E. Meadow Circle
Palo Alto, California
Attn: Dr. B. B. May

Dr. R. C. Cumming
Stanford Research Institute
Building 320
333 Ravenswood Avenue
Menlo Park, California 94025

Dr. Steve Jauregui
Dept. of Electrical Engineering
Naval Postgraduate School
Monterey, California 93940

Prof. C. E. Menneken
Dean of Research Administration
Naval Postgraduate School
Monterey, California 93940

Prof. Glen A. Myers
Department of Electrical
Engineering
Naval Postgraduate School
Monterey, California 93940
(10 copies)

Lt. Cmdr. Henry Orejuela
Naval Security Group Hdq.
3801 Nebraska Ave., N.W.
Washington, D. C. 20390

DOCUMENT CONTROL DATA - R & D

(Security classification of title, body of abstract and indexing annotation must be entered when the overall report is classified)

1. ORIGINATING ACTIVITY *(Corporate author)*

Naval Postgraduate School
Monterey, California 93940

2a. REPORT SECURITY CLASSIFICATION

Unclassified

2b. GROUP

3. REPORT TITLE

Theory and Performance of a Matched-Filter Doppler Direction-Finding System

4. DESCRIPTIVE NOTES *(Type of report and inclusive dates)*

Technical Report - September, 1970

5. AUTHOR(S) *(First name, middle initial, last name)*

Henry Orejuela — Lt. Cmdr., U. S. Navy
Glen A. Myers — Assoc. Prof., Naval Postgraduate School

6. REPORT DATE	7a. TOTAL NO. OF PAGES	7b. NO. OF REFS
September 1970	183	27

8a. CONTRACT OR GRANT NO.	9a. ORIGINATOR'S REPORT NUMBER(S)
b. PROJECT NO.	NPS-52MV70091A
c.	9b. OTHER REPORT NO(S) *(Any other numbers that may be assigned this report)*
d.	None

10. DISTRIBUTION STATEMENT

This document has been approved for public release and sale; its distribution is unlimited.

11. SUPPLEMENTARY NOTES	12. SPONSORING MILITARY ACTIVITY
	Naval Ship Systems Command Code 6050

13. ABSTRACT

A new radio direction-finding (DF) technique which applies matched-filter theory to the DF problem is presented. The new technique, called Matched-Filter Doppler Direction Finding (MFD DF) is based on the doppler DF principle in which a rotating antenna, or its equivalent, superimposes periodic frequency modulation on the received carrier. The phase of the induced modulation contains information on the angle of arrival. It is shown that a bandpass filtering operation, which satisfies the phase-matching requirement of a matched filter, converts the frequency-modulated signal to an amplitude-modulated signal whose envelope is a periodic narrow pulse with no sidelobes. The relative time of occurrence of the pulse is a measure of angle of arrival.

Included is the description of and results obtained with an experimental system used to confirm the analytical results, to study the effects of noise, and to explore alternatives available in the design of an operating system. Encouraging results were obtained using this same experimental system with a conventional operating doppler DF set.

14 KEY WORDS	LINK A		LINK B		LINK C	
	ROLE	WT	ROLE	WT	ROLE	WT
DIRECTION FINDING						
MATCHED FILTER PROCESSING						
DOPPLER DIRECTION FINDING						
CIRCULAR ARRAYS						
SIGNAL PROCESSING ANTENNAS						

U137269

DUDLEY KNOX LIBRARY - RESEARCH REPORTS
5 6853 01058009 5